Probing Bulk Flows With Spiral Galaxy Rotation Curves and the Tully-Fisher Relation

Joshua Simon
Stanford University
Advisor: Jeffrey Willick

June 10, 1998

Acknowledgments

I have many people to thank for their contributions to this thesis. First, the project and data belong to my advisor, Jeff Willick, from whom I have received tremendous guidance over the past four quarters as well. I would like to thank Roger Romani for being my second reader. Stéphane Courteau was kind enough to send me all of his reduced data, allowing the extensive comparisons that I have made. He also offered helpful information and suggestions along the way. David Schlegel and Doug Finkbeiner helped me with their dust map. I am very grateful to the URO office and my donor, Thomas A. Wheeler, Jr., who supported my research in the summer of 1997. Denis Barkats and Seth Hoedl have helped me solve innumerable small problems along the way. Marcos Lopez, Denis, and Felicia Tam did much of the photometry work that I used. Steve Shih and Wendy Ellis also deserve thanks for reading and offering comments on the first two chapters.

Contents

Chapter 1

Introduction

The work on this thesis has covered many stages of analyzing, processing, and interpreting data. It falls under the auspices of the Shellflow project, a collaborative effort between Jeffrey Willick, Michael Strauss, Stéphane Courteau, Marc Postman, and David Schlegel. The goal of the project is to produce an all-sky Tully-Fisher survey that can be used to determine the bulk flow of matter in a shell of $cz = 5000$ to 7000 km/s centered on the Local Group of galaxies. My research addresses the issues involved in the preparation of that data as well as assessing the value of a parameterization of rotation curves comprised of a two-parameter arctangent function. I also provide a preliminary result of the bulk flow analysis.

1.1 Background

1.1.1 Spiral Galaxies

Spiral galaxies as a class of astronomical objects were first noticed by Messier in the eighteenth century [1]. The existence of M31, the Andromeda Galaxy, had been obvious earlier, but as there are no other naked-eye spirals, it remained alone until after Galileo's invention of the telescope in the seventeenth century. In 1924, Edwin Hubble identified the so-called "spiral nebulae" as lying outside of our own galaxy based on the period-luminosity relation of Cepheids in Andromeda [1]. Five years later, Hubble made another seminal discovery: many of the spiral nebulae had large observed recession velocities of these objects away from the earth. Hubble correctly attributed this fact to the expansion of the universe, and although his data were inaccurate he was the first person to realize the significance of the redshift of distant objects [1]. Seventy years later, we are still using related techniques to investigate many aspects of the nature of galaxies.

Spirals are currently thought to be composed of a central bulge (a few kiloparsecs in diameter) that is roughly spherical in shape surrounded by a luminous flat disk (about 25 kpc across) of stars, gas, and dust that slowly orbits in a nonrigid fashion about the center. In the 1960s, astronomers measuring the rotation velocity as a function of radius (the rotation curve, often abbreviated RC) in spiral galaxies found that in most cases, this velocity quickly reaches a peak (within a few kpc of the center of the galaxy) and then remains constant or slowly increasing out as far as it can be reliably observed. The significance of these results was not realized for a decade, when observations of a high enough quality were obtained that it became obvious that the RCs were inconsistent with earlier models of the mechanics of spirals [2, 3]. This highly puzzling discovery led to the prediction that dark matter is a crucial component of spiral galaxies — and the rest of the universe.

1.1.2 RCs and Dark Matter

The reasoning behind the dark matter hypothesis goes as follows: the orbital velocity of an object (a star, for example) gravitationally bound in a central potential produced by a symmetric mass distribution (a spiral galaxy) depends only on the total mass contained in the potential that is closer to the center than the object is, and on the distance the object is from this center. This is a consequence of Newton's Law of Gravitation,

$$F = \frac{GM_1M_2}{R^2} \tag{1.1}$$

Equating this force with the centripetal force felt by an object in circular motion, we see that

$$v_{rot} = \sqrt{\frac{GM_{enclosed}}{R}} \tag{1.2}$$

Outside of the mass distribution, $M_{enclosed}$ is a constant — just as for a point mass — so that the velocity falls off as $R^{-1/2}$. This velocity distribution is known as a Keplerian dropoff. For many years astronomers assumed that near the visible edge of a spiral galaxy, the rotation curve would have a Keplerian region where the velocity followed this general form. The earliest observed RCs (from the 1950s) were produced using relatively small telescopes and showed no evidence of a Keplerian region in any spiral. Over the next two decades, though, increasingly extended RCs were gathered and the predicted Keplerian dropoff had yet to materialize - spiral galaxies had flat RCs as far out as they could be observed [2].

From Equation 1.2, we see that to produce a flat RC, the mass enclosed inside a particular radius R must increase linearly with R. The mass distribution of a galaxy is impossible to measure directly due to the great size and distance of galaxies, but there are certainly ways to accurately estimate the amount of mass contained in stars within a galaxy. One would expect that, since there are a tremendous number ($\sim 10^{11}$) of stars in an average spiral, statistical fluctuations will be minimal and the mass distribution will trace the light distribution (which comes almost entirely from the stars). Light profiles are directly and easily observable, and it is well-established that they fall off exponentially with radius: $I(R) = I_o e^{-R/R_d}$ [4]. Therefore, if mass traces light, at radii $R \gg R_d$ the mass $M(R)$ is constant. But we just noted that the overall mass distribution must be proportional to R! Thus, there is a significant inconsistency between the observed and predicted distributions of mass in spiral galaxies. There are two conceivable explanations for the discrepancy: 1) Equation 1.1 is *not* a universal law of nature, as postulated, or 2) there is mass in these galaxies that we cannot see; that is, dark matter. Some scientists have proposed and investigated a theory in which gravity does in fact deviate from the inverse-square law on extremely large (galaxy-size) scales [5]. Nevertheless, the evidence in favor of this point of view is weak, and the most reasonable conclusion is that dark matter is indeed present in large quantities in spiral galaxies [2].

The composition of dark matter has proved to be one of the more enduring mysteries in astronomy. The various theories can basically be narrowed down into two categories, MAssive Compact Halo Objects (Machos) and Weakly Interacting Massive Particles (Wimps). Searches for Machos - brown dwarfs and other substellar objects - have turned up significant evidence that they exist, but not in numbers nearly large enough to explain dark matter phenomena like flat RCs [6]. Wimps are somewhat more theoretical at this point, although there are experiments currently underway to detect the axion (one postulated Wimp) and to observe neutrino oscillations (which were recently detected, proving that neutrinos have at least a small mass and thus could make up dark matter) [7]. In addition, simulations of structure formation in the early universe are used to model the effect of different amounts and types of dark matter on how the universe appears today. Most of these - including the most popular model, Cold Dark Matter (CDM) - fail to adequately replicate our universe. Even though we do not yet know with confidence what form dark matter takes, we can take advantage of its presence to study related phenomena, such as RCs and the Tully-Fisher relation.

There is an intimate connection between dark matter in spiral galaxies and rotation curves, as well as to the Tully-Fisher relation. Detailed study of rotation curves can, through sophisticated modeling, reveal information about the structure and content of dark matter in spirals; however, that is not the focus of my research. We are proceeding with the ultimate goal of investigating concentrations of mass (both dark and light) on far larger scales. Specifically, Shellflow is designed to settle an ongoing controversy about the motion of the local portion of the universe. First, though, an accurate and well-calibrated Tully-Fisher survey must be carried out.

1.2 The Tully-Fisher Relation

One of the consequences of flat RCs in spiral galaxies is the Tully-Fisher (TF) relation. The TF relation is an empirical connection between the intrinsic luminosity and asymptotic rotation velocity of spirals that was first noticed by Tully and Fisher in 1977. They found that the expression

$$L = Cv_{rot}^{\alpha} \tag{1.3}$$

holds fairly tightly for all spirals [8]. There is as yet no firm theoretical explanation for the TF relation. Some relationship between luminosity and rotation velocity is expected because both quantities depend on the mass of the galaxy [9]. Still, why it takes the form that it does seems to depend on details of the dark halo composition and distribution and hence to the galaxy formation process, which is currently not well understood.

Despite the lack of a theoretical underpinning, the TF relation is extremely useful. Any correspondence between absolute luminosity and some other property that can be observed independent of distance provides the basis for a distance indicator. Since it is usually not possible in astronomy to reach out and touch the objects that are being studied, often the biggest challenge faced by astronomers is to accurately determine the distances to faraway heavenly bodies. Ordinary spiral galaxies are both bright (visible across the entire universe) and extremely numerous, which makes them ideal distance indicators.

Distance indicators can be used in two related ways. One, as a standard candle, allows absolute distances to be measured. The other, rather than determining the actual distance to an object, instead measures its velocity with respect to some standard frame (the solar system, the Local Group, or the Cosmic Microwave Background radiation, for example) [10]. Velocities are useful because they are directly related to distance via the Hubble expansion of the universe (see Section 1.1). In addition to the Hubble flow, though, galaxies are acted on by the gravity of other nearby galaxies. Because galaxies and clusters of galaxies are so massive, they are able to attract each other even over the vast intergalactic distances. Therefore, superimposed on its Hubble velocity, every galaxy also has a *peculiar velocity*, which represents its net attraction to all the other matter in the nearby universe. By separating peculiar velocities from Hubble flow we can learn about the distribution of dark matter on very large scales.

The TF relation gives us a straightforward way of performing this separation. Since the apparent magnitude m of a spiral is dependent only on its absolute magnitude M and its distance d,

$$m = M + 5\log d \tag{1.4}$$

we can use its predicted TF magnitude to solve for the distance. Given the distance, we know what portion of its total velocity (redshift) is attributable to Hubble flow, and thus the remainder must be the peculiar velocity. With a large enough collection of galaxies with peculiar velocities, it is possible to analyze whether the velocities are randomly directed or whether everything is moving toward some distant mass. Such correlated motions are called bulk flows, and they are key to understanding the distribution of mass in the universe on scales in the range of tens of megaparsecs.

It turns out that it is generally more convenient for astronomers to use Equation 1.3 in log space, because the magnitudes of astronomical objects are computed as the log of the luminosity. Since M = const - $2.5\log L$, we can define a quantity $\eta = \log(2v_{rot}) - 2.5$ that serves as an effective velocity width. Then,

$$M = A - b\eta \tag{1.5}$$

A cursory examination of Equation 1.3 reveals that the TF relation does nothing more than specify a unique correspondence between luminosity and rotation velocity; there is no intrinsic reason for writing it to solve for luminosity as a function of rotation velocity as opposed to rotation velocity as a function of luminosity. It is simple to formulate the inverse Tully-Fisher relation,

$$\eta = \eta_o - \gamma M \tag{1.6}$$

In this form, TF is much more impervious to the statistical biases (such as Malmquist bias) that are virtually unavoidable in observational astronomy. This effect is the result of the fact that Equation 1.6 uses the predictive power of a distance-independent quantity (the velocity width) rather than a distance-dependent quantity (the luminosity) and thus removes the bias that is acquired by analyzing a magnitude-limited sample [11].

Although the TF relation has become one of the most widely-used distance indicators in astronomy today, it is neither completely understood nor extremely accurate. The TF slope (the exponent α in Equation 1.3) has never been agreed upon to particularly high accuracy. It tends to vary significantly with different choices of the velocity width and with the bandpass used, and thus may only be well-defined within a particular data set [11]. There are widely-varying estimates of the intrinsic scatter of the TF relation, ranging from about 0.25 mag up to almost 1 mag. Because a similar relation (the Fundamental Plane or D_n-σ relation) involving three parameters has been found for elliptical galaxies [12, 13], there has been a long search for a third parameter that would narrow the TF scatter [14, 15, 16].

This mysterious third parameter has eluded investigators, who have thoroughly examined nearly all possible photometric properties of spirals for any correlation with TF residuals. Such efforts have yielded minimal results, and recently, more attention has been given to physical properties of spirals and RC shape as potential third parameters. In his PhD thesis, Schlegel asserts that the third parameter is the radius at which the velocity width is measured, which of course has been used by astronomers all along [16]. If this is true, it still leaves open the question of what radius to use in order to minimize the scatter. There have been claims made by some astronomers that a third parameter would not help the TF relation because it is already a nearly edge-on projection of the Fundamental Plane of elliptical galaxies and thus the scatter cannot be further reduced [12]. This is at best unproven, and even if it turns out to be correct, does not lessen the importance of finding the fiducial radius that best defines the TF relation.

My research focuses on this third parameter and how it relates to both the definition of velocity widths and the best TF radius. Tully and Fisher's original work was carried out using observations of velocity widths derived from the 21 cm hyperfine transition in hydrogen. It has since been found that actual rotation velocities from visible and infrared spectral lines (optical rotation curves) can be used just as accurately to define η. These ORCs are usually derived from Doppler-shifted Hα spectral lines. However, no consensus exists on what the velocity width of an ORC is. There are several possible approaches to defining this velocity width. Some authors use the distance between the last point on either side of the RC [18], some choose a set radius and evaluate the velocity difference there [9, 16], and others take the average of several points. We will study these choices, picking the one that minimizes TF scatter. We will pay special attention to defining a fiducial radius, possibly based on the RC shape parameter that comes out of our arctangent fits.

1.3 Overview

Chapter 2 describes the process of reducing and analyzing the data. The techniques of spectroscopic and photometric analysis are discussed, along with the issues involved in rotation curve extraction. In Chapter 3, the data itself and the results of the TF research are presented. I introduce the methods and results of our bulk flow analysis and review our overall conclusions in Chapter 4. Much of the machinery I produced and used for this thesis during the past year, along with a graphical representation of the data set, is in the appendices.

Chapter 2

Data Processing and Reduction

In this chapter, we describe the data set used in the thesis. We discuss in detail the mechanics of data reduction and RC extraction, and the other steps leading up to the final goal of establishing a TF relation.

2.1 Galaxy Sample

The data for this project consist primarily of long-slit spectra of the 6000-7000 Å region of spiral galaxies. Spectra have been collected by the aforementioned collaborators over the past two years using the 4-meter telescope at Kitt Peak National Observatory in Arizona, the 4-meter telescope at Cerro Tololo Interamerican Observatory in Chile, and the 2.7-meter telescope at McDonald Observatory in Texas.

Approximately 300 spiral galaxies have been observed, and all but a handful yielded useful rotation curve data. These galaxies were selected from the Optical Redshift Survey of Santiago et al. on the basis of their redshift (between 5000 and 7000 km/s) and magnitude [17]. They are all late-type spirals (Sb and Sc) with $m_B \leq 14.5$. The sample is uniformly distributed throughout the sky (the zone of exclusion, $|b| \leq 20^o$, is avoided). Raw spectra for 240 of the galaxies were reduced and analyzed as part of my thesis.

For each galaxy, a spectrum was taken, using exposure times of 20 to 30 minutes, depending on the strength of the galaxy's Hα emission. Many of the galaxies were observed several times for cross-checking purposes or to obtain a sufficient signal-to-noise ratio. Either for each galaxy or for each observing night (depending on the observer), a set of helium and/or neon comparison lamp frames was taken. V and I band CCD photometry was also obtained for each object, because the Tully-Fisher relation is a predictor of absolute luminosity.

The spectra are centered around the Hα emission line of each galaxy, which is always at roughly the same wavelength — 6700 Å — because of the similar redshifts. Hα was chosen because it is one of the strongest emission lines of spiral galaxies, it is easily identifiable due to the proximity of strong sulfur and nitrogen emission lines, and it is conveniently located near the red end of the visible spectrum. Hα results from the $n = 3$ to $n = 2$ transition in neutral hydrogen gas and has a rest-frame wavelength of 6563 Å. In spiral galaxies, it is associated with star-forming regions (i.e. the spiral arms). Therefore, the motion of the gas giving off Hα radiation accurately traces the rotation of the entire galaxy.

2.2 Reduction and Processing Techniques

At the beginning of this project, the data were available only in raw spectroscopic frames that were recorded directly from the telescope instrumentation. Many of these images were backwards, sideways, or upside-down (necessitating rotations of the entire images) and some were overly large, creating disk space problems on our computers (necessitating cropping). More importantly, they suffered from geometric distortions and were not spatially or wavelength-calibrated. All of the spectroscopic data reductions were performed with the Image Reduction and Analysis Facility (IRAF), a commonly-used tool of professional astronomers. A description of the more detailed elements of processing follows.

2.2.1 Spectroscopic Reductions

The first step in preparing the spectra for analysis was to correct the unwanted distortions and imperfections that inevitably occur during astronomical observations. As with all CCD images, flat-fielding and bias-subtraction were necessary. Each image contained a number of columns along one side that were not exposed along with the rest of the CCD chip when the light was gathered, so the signal in that section represents the average number of electrons gathered as a result of the bias voltage that is applied to the CCD. In addition, a set of dome flatfield frames was recorded during each night of observing. The pixel-by-pixel division of a spectrum by these images corrects for sensitivity variations over the area of the chip. Dark frames were also prepared to check whether dark current had any effect over and above the contribution of the bias voltage, but in most cases the further subtraction of these dark frames made no noticeable difference in the quality of the data, so this correction was not applied.

Most of the spectra showed a systematic curvature of the night-sky emission lines across the frame. In order to rescale the spectra onto a coordinate system that was regular, rectangular, and with a known and useful scale, an IRAF script was written (see Appendix B for details) and each image was passed through it. The script began with the IDENTIFY routine, which asks the user to identify spectral lines on a helium or neon comparison lamp image. After marking three of the included lines with their known wavelengths, the routine performs a polynomial fit to the rest of the line positions using a list of the relevant lines and their actual wavelengths. A third- to fifth-order Chebyshev polynomial was used in the fit (starting at third-order and raising the degree as necessary until the residuals were small and random, as examined by eye). In some cases it was necessary to remove one or more of the lines from the fit because the routine could not accomodate them at any reasonable order (for polynomials of greater than fifth order the solutions often became nonmonotonic and therefore unusable).

Using the information gathered in IDENTIFY, the REIDENTIFY routine then duplicates IDENTIFY at every tenth column across the image, creating a widely-spaced grid of wavelength values across the spectrum. FITCOORDS takes the grid from REIDENTIFY and interpolates from it a full two-dimensional set of coordinates that has a value for every point in

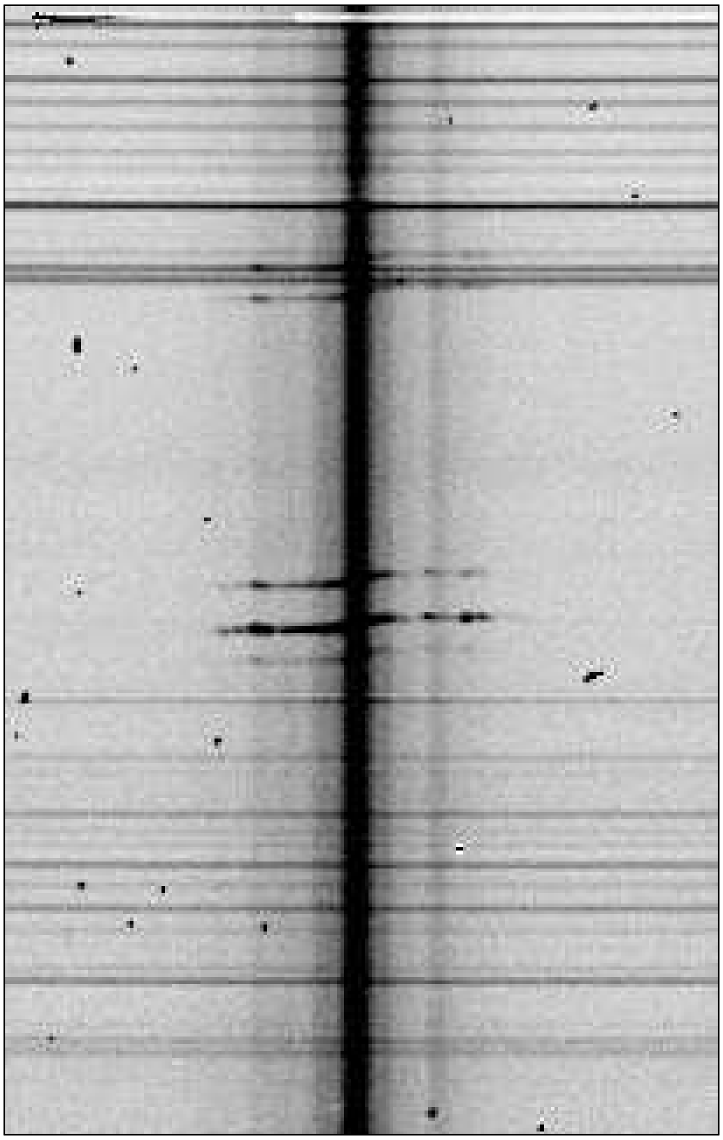

Figure 2.1: A typical example of one of our spectra. This is of the galaxy g063. Horizontal lines across the spectra are emission lines from the night sky and the galaxy. Vertical lines represent the galaxy's broadband emission, and bright spots are cosmic rays. The S-shape of the galaxy lines results from the Doppler shift as one side of the galaxy rotates toward us and the other away from us. The bright galaxy line slightly below the center of the spectrum is Hα.

the image. This routine also uses Chebyshev polynomials to perform its fits, although in two dimensions rather than one. The polynomials selected were usually between fifth and ninth order, and were again chosen after examining the residuals by eye. Finally, the TRANSFORM routine applies this derived coordinate fit to the galaxy spectrum.

Having undergone these operations, a spectrum should be in a position-wavelength space that is both uniform and properly calibrated (along the wavelength axis). The next imperfection to correct in the images is the presence of cosmic rays. CCDs are sensitive to all energetic particles, not just photons, so when muons, protons, and other high-speed particles go through the detector, they deposit large amounts of energy that show up as clusters of "hot" pixels. When cosmic rays hit the detector near the Hα emission line or other parts of the image that are needed for our analysis, they must be digitally erased so as not to obscure or distort any actual data. The IRAF routine COSMICRAYS performs this task. The script allows the user to proceed interactively through the routine and input the boundaries of regions containing offending cosmic rays. The routine calculates the average background signal in a 5×5 or 7×7 box around each cosmic ray it detects and replaces the pixels affected by the cosmic ray with the average of the surrounding pixels. Experiment showed that this process destroys some of the Hα signal in cases where the cosmic ray is directly on top of (or very close to) the emission line, so all such points were left out of the final rotation curves.

2.2.2 Rotation Curve Extraction

After these initial reductions, the rotation curves can be extracted from the spectra. I wrote a Fortran program outlined by Professor Willick for this purpose (see Appendix B). This programs was created in IRAF's IMFORT environment so that it could take advantage of IRAF's image processing capabilities. The user inputs the approximate position and shape of the Hα emission line of a particular galaxy to the programs by specifying a number of "pieces" — straight lines, which, when put together, trace out the path followed by the rotation curve. Each of these pieces contains an x- and y-starting point (in pixels) and an x- and y-ending point, which represents a segment of Hα that is more or less continuous. A classic RC would probably be made up of three pieces: one for the flat portion of the curve on each side of the galaxy and one for the sloping inner region of the RC. In actuality, most of the galaxies in our data set needed between 5 and 25 pieces to accurately trace their RCs. This discrepancy is a result not only of the bumps and wiggles in real RCs, but also of the inherent patchiness of Hα emission.

In each column of pixels, the program begins at the point where that column intersects the appropriate user-defined piece of Hα, and reads in the photon fluxes registered by the CCD for a few pixels surrounding that point (see Figure 2.2). Theoretically, this profile should be a gaussian, although with noise and the systematic limitations of telescopes, it turns out to be not exactly gaussian (the higher the signal-to-noise ratio, the more gaussian it is).

The program finds the highest value in the column and fits a centroid to this peak, which should lessen the impact of random errors. Then, the natural log of the flux in each pixel is used to fit a parabola to the data, with the centroid used to define the fitting region for the parabola. A parabolic fit to a natural log is mathematically equivalent to fitting a gaussian to the original data. Such a fit defines three coefficients that can be manipulated into providing the center of the flux distribution, which yields the wavelength of Hα in that column, and the error in measuring that center. We make allowances for several columns to be summed together in low signal-to-noise regions, in effect smoothing the RC somewhat in

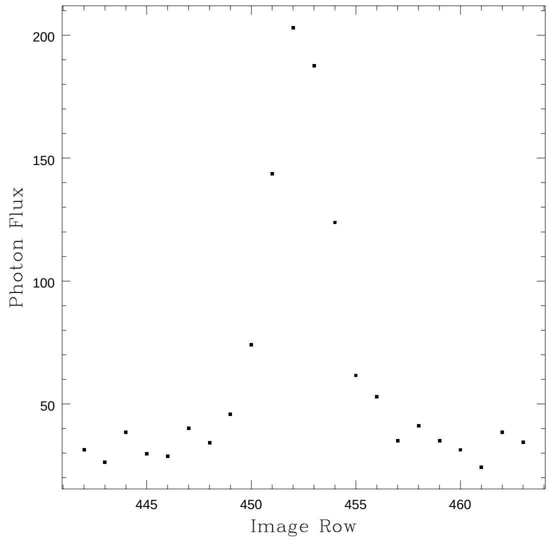

Figure 2.2: A plot of one column of the Hα line profile for g063.

these areas. The resulting set of Hα line centers comprises the rotation curve of the galaxy. The size of the errorbars on each point of the RC was typically on the order of 0.01 pixels in high signal-to-noise regions and up to a pixel or more in areas with lower signal quality. The largest errorbars were often reduced as I gained a better understanding of the proper way to choose pieces for the program to analyze.

The rotation curve next needs to be transformed from a function in pixel-wavelength space to one in arcsecond-velocity space. This conversion is made with a C program that takes into account the pixel scale of the spectrograph (0.68 "/pixel at KPNO, 0.50 "/pixel at CTIO), the apparent wavelength of the Hα line at the center of the galaxy (where its rotation speed is zero), and the known wavelength of Hα in the rest frame.

$$V = c\left(\frac{\lambda}{\lambda_o} - 1\right) \tag{2.1}$$

This velocity must then be divided by $(1 + z)$ in order to eliminate the redshift broadening of the emission line (redshifts are derived from our spectra). The calibrated plot is inputted to another program that performs the final major task of the data reduction stage: fitting a known functional form to the data.

Rotation curves bear an obvious resemblance to the arctangent function (see Figure 2.3). They are both S-shaped curves that pass through the origin and asymptotically approach the same value on either side. Apart from zero-point shifts, there are only two parameters that affect the appearance of a particular arctangent - its amplitude (asymptotic value) and the point at which it begins to turn over from the central portion to the flat outer region. Accordingly, our RCs can be modeled by arctangents of the form

$$V(R) = \frac{2V_a}{\pi}\arctan\left[\frac{(R-\delta R)}{R_t}\right] + \delta V \tag{2.2}$$

where δR corrects for a zero-point offset in the spatial direction which could be caused by inaccurate calculation of the continuum position (this is a problem for weakly emitting galaxies) and δV allows for a similar offset in velocity.

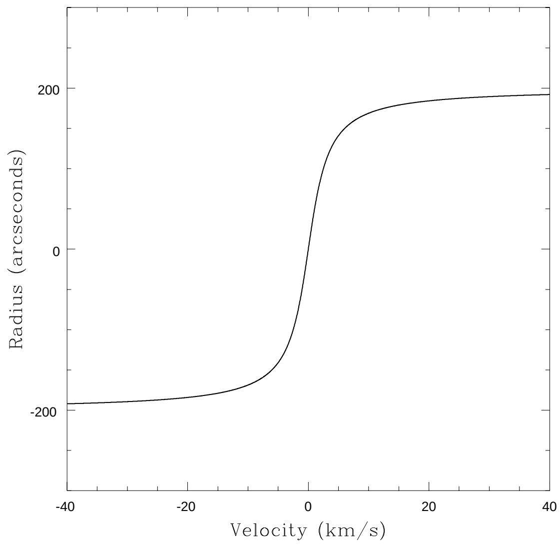

Figure 2.3: An arctangent with $V_a = 200$ and $R_t = 2.5$.

Clearly, no one-parameter function can hope to approximate the shape of an RC (one that reaches the turnover radius, at least), so a two-parameter function is the simplest possible choice. Among these, the arctangent is the most logical. We know that such a function cannot offer a complete description of the RC, but the TF relation does not require that we trace RCs perfectly at every point. Rather, we need to have a function that describes the approximate behavior of the RCs, expecially in the flat outer regions, which the arctangent accomplishes. Adding more variables would lead to an even better fit, but we maintain not only that this fit has the least covariance between its parameters, but also that it yields as good a TF relation as any other form that is presently used.

This fitting program uses the Powell routine from *Numerical Recipes* to find the best set of parameters for the chosen function. Powell is a multidimensional direction set minimization method [19]. The program was first written by Daniel Kasen for his honors thesis, *The Rotation Curves of Spiral Galaxies* (see Appendix B) [20]. It was modified in order to improve estimation of errors and to use a slightly different function as the fitting model.

The Powell routine in the program evaluates and minimizes a goodness-of-fit parameter that is defined by the user. In this case, we calculated

$$\chi^2 = \sum \frac{(V_{calc}^2 - V_{obs}^2)|R|}{(\sigma_v)^2} \tag{2.3}$$

where V_{calc} is the velocity according to the fitting function, V_{obs} is the observed velocity, R is the position, and σ_v is the size of the errorbar on V_{obs}, at each point of the RC. This function does not represent a true χ^2 because it is neither normalized nor dimensionless, but it can still accurately characterize the quality of the fits. Several similar weighting schemes were considered, in which various powers of R between 0 and 2 were tested. The reason for experimenting with different weights is that the error bars on points in the middle of the RCs (the linear part) tended to be smaller than those in the outer regions. But we are most interested in the behavior of RCs in their flat portions where the velocity width will be evaluated. Hence, putting R into the χ^2 function allows us to deemphasize the inner parts of the galaxy in the fit somewhat. A weighting proportional to R seemed to be the best compromise, fitting both the data and multi-parameter RC fits most closely.

A serious attempt was made to quantify both the uncertainties in the fits for each parameter and the covariance between the two parameters. For the following procedures we employed the χ^2 function defined above without the R weighting. This effort ultimately proved futile, for reasons which are not completely understood. The strategy employed was to evaluate the χ^2 function at incremental steps away from the actual values of V_a and R_t, evenly spaced in a logarithmic sense (the method was taken from Kasen's thesis, where it was applied incorrectly). Theoretically, this approach should define the curvature of χ^2 in the $V_a - R_t$ plane. Some linear algebra yields the expected dependence of χ^2 on changes in V_a and R_t. Near the minimum of $\chi^2(V_a,R_t)$ at χ^2_o, χ^2 should be quadratic in both variables. We take a first-order Taylor expansion around the minimum,

$$\chi^2 = \chi^2_o + C_{11}\Delta V_a^2 + C_{22}\Delta R_t^2 + 2C_{12}\Delta V_a \Delta R_t \tag{2.4}$$

where the Cs are partial derivatives: $C_{11} = \frac{\partial\chi^2}{\partial V_a^2}$, $C_{22} = \frac{\partial\chi^2}{\partial R_t^2}$, and $C_{12} = \frac{\partial\chi^2}{\partial V_a \partial R_t}$. Then, we define a function to measure the quality of our fits to the coefficients C.

$$S = \sum_i [\chi_i^2 - (\chi_o^2 + C_{11}\Delta V_{a,i}^2 + C_{22}\Delta R_{t,i}^2 + 2C_{12}\Delta V_{a,i}\Delta R_{t,i})]^2 \tag{2.5}$$

Simplifying and taking derivatives of S with respect to C_{11}, C_{22}, and C_{12}, we can combine the result into the following matrix equation:

$$\begin{bmatrix} \Delta V_{a,i}^4 & \Delta V_{a,i}^2\Delta R_{t,i}^2 & 2\Delta V_{a,i}^3\Delta R_{t,i} \\ \Delta V_{a,i}^2\Delta R_{t,i}^2 & \Delta R_{t,i}^4 & 2\Delta V_{a,i}\Delta R_{t,i}^3 \\ \Delta V_{a,i}^3\Delta R_{t,i} & \Delta V_{a,i}\Delta R_{t,i}^3 & 2\Delta V_{a,i}^2\Delta R_{t,i}^2 \end{bmatrix} \begin{bmatrix} C_{11} \\ C_{22} \\ C_{12} \end{bmatrix} = \begin{bmatrix} \Delta\chi_i^2\Delta V_{a,i}^2 \\ \Delta\chi_i^2\Delta R_{t,i}^2 \\ \Delta\chi_i^2\Delta V_{a,i}\Delta R_{t,i} \end{bmatrix} \tag{2.6}$$

where $\Delta\chi_i^2 = \chi_i^2 - \chi_o^2$.

From these quantities, the individual variances of the parameters and their covariance should be calculable. However, the algorithm never yielded physically reasonable numbers for both the variances and the covariance at the same time. Typical values for the variances were on the order of 0.1 km/s in V_a and 1 in R_t. Since V_a is always at least 100 km/s and the data were of good, but not spectacular, quality, there is no basis for believing that the rotation velocities were well-defined to better than 1 km/s. Likewise, if the errors for R_t were to be accepted, the actual value of R_t would often be meaningless because it was usually of similar size. Additionally, no means were found to force the covariance to have an absolute value less than 1 for every fit, even though this must be true mathematically by the definition of a covariance coefficient. After a substantial amount of effort with little visible progress made, it was decided that none of these numbers were crucial to the success of the analysis (because reasonable guesses should be possible visually) and the attempt was abandoned.

After the fits were completed, they were compared to higher-dimensional fits to the same raw data reduced independently by Stéphane Courteau (see Section 3.2). Because the Courteau fits include three and sometimes four parameters, they will by design do a better job of precisely following the RCs. Still, large features at the turnover radius, multiple wiggles in the flat portion of the RCs, and RCs that substantially increase or decline again after leveling out cannot be completely accounted for in these fits. Therefore, we believe (and shall investigate in the sections that follow) that the arctangent fit is a sufficiently good approximation to RCs for Tully-Fisher work and that our two parameters are a more physically meaningful description of spiral galaxies than are fits with many parameters.

2.2.3 Photometric Reductions and Analysis

While one side of the TF relation requires spectroscopic information, the other needs photometry. The photometric observations took place over roughly the same period as the spectroscopic ones, at 1-meter class telescopes in Arizona and Chile. Much of the photometric data reduction was performed by Marcos Lopez-Caniego in 1997, with significant contributions by Denis Barkats and Felicia Tam over the past year. The photometric calibration, described as follows, I performed myself.

The photometric data reduction consists of running the same preliminary corrections as were enumerated in Section 2.2.1 for the spectra and then extracting information in the form of a surface brightness profile. The isophotes of the galaxy are modeled and their ellipticity is calculated (see Figure 2.4). An exponential function is then fit to the isophotes, yielding the central surface brightness and the scale radius.

For each galaxy that had a spectrum taken of it, there were also accompanying digital images in both V and I bands. On the photometry runs, images were taken of fields containing standard stars with well-known magnitudes and colors (tabulated by Landolt) [21]. These standard star frames can be used to compare actual magnitudes with the instrumental ones, which depend on the telescope and instrument used to make the observation.

The data manipulation was again based in IRAF. The approximate positions of the desired standard stars were located with IMEXAM. This information was fed into the task QPHOT, which calculates the actual positions and converts the total flux for each object into an instrumental magnitude. With an IRAF script, the results of this processing were placed (along with the Landolt data) into organized files. Using a program written by Professor Willick, the true and instrumental magnitudes of each star and the airmass at the time of the observation were compared and compiled into the following function,

$$V = m_v + C_v + f_v(V - I) + g_v a_v \tag{2.7}$$

where V is the actual apparent magnitude, m_v is the instrumental magnitude, C_v is a constant offset, f_v describes the color dependence, g_v describes the airmass dependence, and a_v = airmass - 1. The I-band function was of an identical form. These fits were examined for systematic residuals, and saturated stars and obviously non-photometric frames were eliminated from consideration. Such imperfections were identifiable because the fit was designed to leave them with large negative residuals. In general, residuals less than -0.1 mag and greater than 0.1 mag were thrown out, leaving an overall scatter in the photometric fits of less than .025 mag.

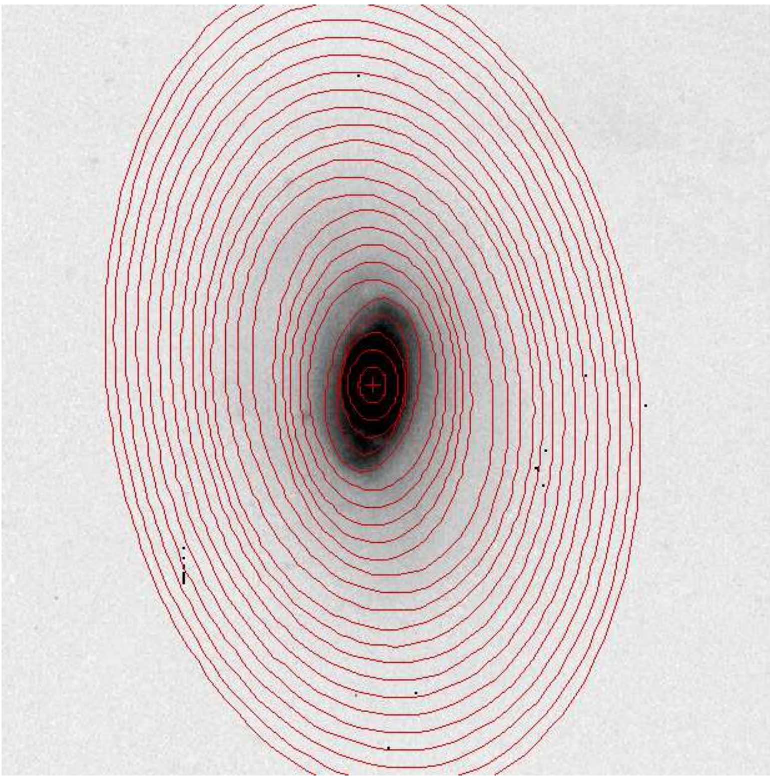

Figure 2.4: A photometric profile of a spiral galaxy, with elliptical isophotes superimposed on the image (courtesy D. Barkats). Note the change in shape of the isophotes with radius; the ellipticity is defined based on the outermost isophotes.

The photometric fits for both V and I bands must be applied to the surface brightness profiles of the relevant galaxy images. Because the flux-to-magnitude conversion function has an explicit dependence on the $V-I$ color of the object observed, it is necessary to apply an iterative process to determine the color using only the I or V magnitude (but not both). This was accomplished by examining a graph of I vs. color and choosing a reasonable first guess for the color based on that graph (see Figure 2.5). Any number close to 1 turns out to be good enough. Then, by fitting a line through the resulting I vs. color plot, a somewhat more accurate color can be predicted. Although for individual galaxies the color predicted in this fashion scattered about the fitted relation by up to 0.2 mag, the resulting changes in the calculated magnitudes were ≤ 0.01 mag, so further iterations were deemed unnecessary.

At this point, the photometric calibrations were ready for application to individual galaxies. The important properties — V and I magnitudes, surface brightness, exponential scale length, etc. — of each galaxy were tabulated (see Appendix A). This table includes data from two photometry runs at Kitt Peak and one in Chile, which represents a subset of 101 spirals out of the 240 for which spectroscopic data was reduced. These 101 galaxies are the ones to which the TF analysis of chapters 3 and 4 will refer.

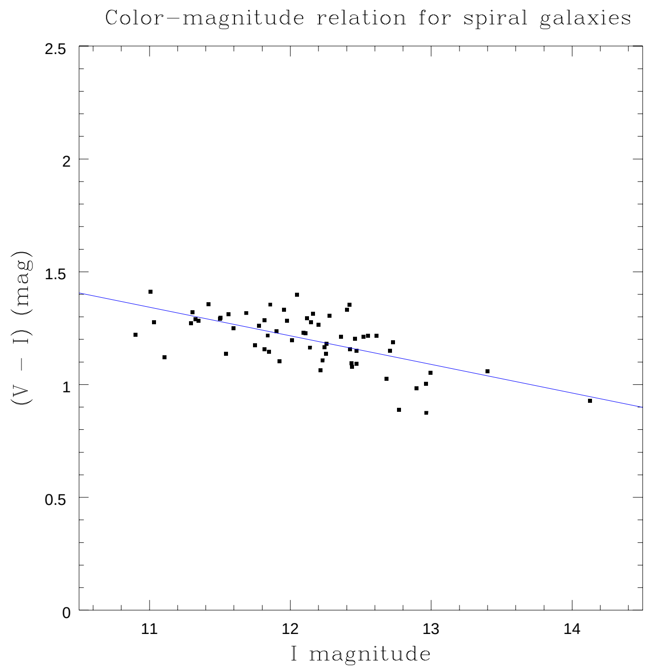

Figure 2.5: This plot shows the color-magnitude relation for a sample of 63 of our spirals. The best-fit line is also included. We find that $V - I = -0.127I + 2.74$.

Chapter 3

Tully-Fisher Results

In this chapter we discuss the findings of the research. We present the results of the photometric analysis and two parameterizations of the RC data set. We test various definitions of the velocity width for TF applications using these two parameterizations.

3.1 Photometry Results

In Section 2.2.3, the procedures for producing photometry solutions for our standard stars and photometric profiles for our galaxies were described. Now we present the photometric solutions. The galaxies analyzed in this thesis were observed on three runs: one at Kitt Peak in October 1996, one at Kitt Peak in March 1997, and one at Cerro Tololo in April 1997. One to two hundred standard star observations were made during each run. The results of the fits to Equation 2.7 are displayed below.

Photometry Solutions

observing run	C_V	f_V	g_V	σ_V	N_V	C_I	f_I	g_I	σ_I	N_I
KPNO 10/96	-4.425	-0.013	-0.119	0.021	170	-4.976	0.016	-0.083	0.017	64
KPNO 3/97	-3.687	-0.024	-0.105	0.024	165	-4.269	0.011	-0.068	0.021	214
CTIO 4/97	-4.368	0.016	-0.142	0.015	140	-5.290	0.014	-0.052	0.013	134

Note: N_V and N_I are the number of stars used in the photometry fits for V and I, respectively. Pixel scales for the photometry were 0.40 ″/pixel at CTIO and 0.68 ″/pixel at KPNO.

Table 3.1

3.2 RC and Fit Comparisons

As mentioned before, all of the spectroscopic data were reduced independently and simultaneously — starting from the original raw spectra — by Stéphane Courteau in order to check for and eliminate any systematic errors. Courteau's software was entirely separate and he used a somewhat different method to extract RCs from the spectra. He explicitly removed the galaxy continuum from each image as part of the preliminary reductions, rather than estimating the continuum level and subtracting it as necessary within the extraction program [9]. His RC tracing procedure was also unrelated to ours and did not use the sum-over-columns approach in regions of poor signal quality. Hence, if the results of his efforts and mine are the same to a high degree of precision, we can be confident that our data are meaningful and untainted by systematic problems.

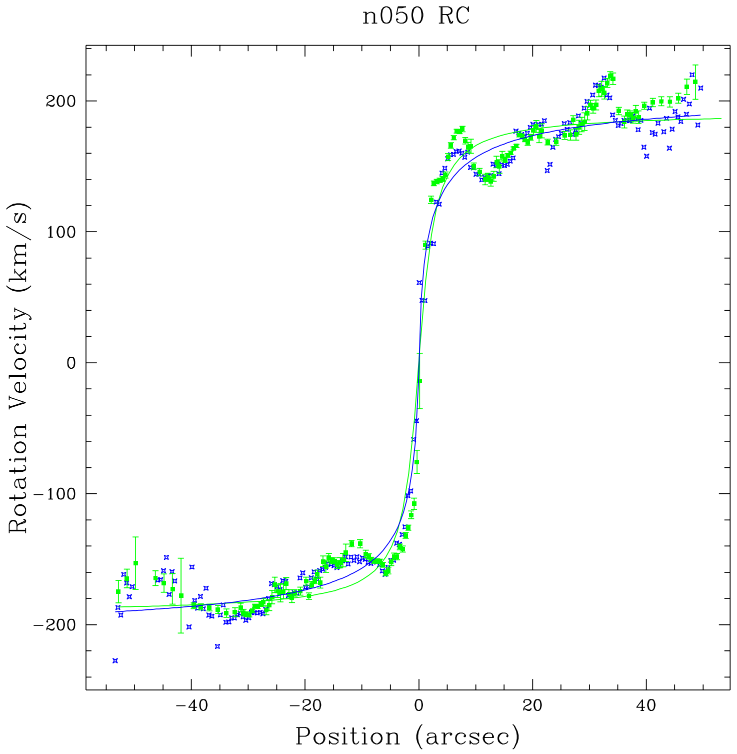

Figure 3.1: A rotation curve with a velocity peak at the turnover radius (7") - note the discrepancy of almost 20 km/s in the way the two sets of points trace the peak. This RC has $V_a = 191.4$ km/s and $R_t = 2.14$". My data points and fits are the light ones; Courteau's are dark.

The actual data points that trace the RC of each galaxy as determined by Courteau and me are virtually identical in the vast majority of cases (see Appendix C for the graphical compilation of the comparison). In 24 RCs (about 10 %) there was some appreciable difference. Many of these stem from the fact that the zero points of my position and velocity axes and Courteau's do not always line up - a difference that affects the fit parameters only minimally and thus is not very worrisome in terms of TF analysis. Also, in low signal-to-noise regions where I summed columns together ($R = 40 - 50$" in the figure above, for example) there are sometimes noticeable deviations of my data points from Courteau's as a result of smoothing. In some of the other cases, there are transition features at the turnover radius that are not reproduced in Courteau's RCs (see above). These features, however, tend not to affect the curve fitting procedure, because we do not include nearly enough parameters to model them accurately.

On the other hand, the positive results of the comparison are extensive and too numerous to recapitulate in detail. In almost every RC that has peaks, dips, a declining or rising tail or any other nonlinear feature, both Courteau's data and mine trace them indistiguishably. Furthermore, the fits to the data, using two different parameterizations of the RCs (see following sections and Appendix C) are highly similar.

Courteau fits rotation curves with the function

$$V(R) = V_c \frac{(1+\frac{R_t}{R-\delta R})^{\beta}}{[1+(\frac{R_t}{R-\delta R})^{\gamma}]^{1/\gamma}} + \delta V \tag{3.1}$$

The parameters have roughly the same meaning as they do in Equation 2.2. V_c estimates the asymptotic rotation velocity, R_t defines the point at which the RC turns over (although the numerical value of this point is different than in the case of the arctangent), γ describes the sharpness of the turnover, and β allows an exponential dropoff of the RC after it flattens out [9]. For almost all fits, β turns out to be 0, so except in the rare cases where a galaxy's rotation velocity decreases in its outer regions, the function gives a three-parameter characterization of the RC.

It is to be expected that Equation 3.1 will trace RCs somewhat more in detail than a simple arctangent function. The parameter γ does make the function follow the turnover of the RC a little more closely, although it is still unable to account for large peaks in rotation velocity at this radius. In the center of the galaxy, though, and in the flat part of the RC, Equations 2.2 and 3.1 usually give identical predictions. In fact, when printed one on top of the other, they are often barely separable. The most significant advantage of the Courteau fits is their ability to model galaxies with declining RCs.

The overall agreement between the Courteau RCs and fits and mine was quite good. This leaves little doubt that my RC reductions can be trusted as representative of the true RCs. Further analysis in the upcoming sections will examine which method of tracing and parameterizing the rotation curves leads to a more useful Tully-Fisher relation.

3.3 Tully-Fisher Fits

With a simple linear fit, it is straightforward to compile the spectroscopic and photometric data into a Tully-Fisher relation, as written in Equation 1.6. Absolute magnitudes are calculated with Equation 1.4. A galaxy's redshift can be substituted for the distance in the formula because redshift scales linearly with distance as a result of Hubble's Law,

$$cz = H_o d$$

Taking logarithms of both sides, we see that we can separate out H_o quite conveniently:

$$\log cz = \log d + \log H_o \tag{3.2}$$

The Hubble constant H_o can then be absorbed into an overall constant whose value is unimportant. This technique is particularly useful because H_o is not known to much better than 20 % accuracy.

Two corrections to these magnitudes are particularly important. First, except in the case of face-on galaxies, we cannot observe all of the light coming from a spiral. The spiral arms of galaxies contain massive amounts of dust which scatters their light out of our line of sight. Since these dust lanes are oriented in the plane of the galaxy's disk, they have the effect of making galaxies in which we can see them appear dimmer. The dimming is merely a function of the inclination of the galaxy with respect to us, which can be calculated from its apparent ellipticity. We take the internal extinction of a galaxy to be

$$X = -A_I \log(1-\epsilon) \tag{3.3}$$

where X is the extinction in magnitudes, A_I is a constant that we take to be 0.95 (for I band photometry), and ϵ is the galaxy's ellipticity. This quantity is subtracted from the absolute magnitude. A further brightening occurs when the effect of dust in our own galaxy is taken into account. We are situated in the disk of the Milky Way, so when we observe any object we look through some of its dust and see objects to be dimmer than they actually are. This correction is entirely a function of the position of the object on the sky, and is most pronounced near the galactic equator and more or less negligible towards the poles. We use the new Schlegel-Finkbeiner-Davis dust maps to find the reddening this causes, which is linearly related to the galactic extinction: $X_{gal} = 1.94E(B-V)$ [22].

The quality of TF fits is usually judged by their scatter in magnitudes, which is the sum of the root-mean-square deviations of each point from the best-fit line. Since our fits have η as the dependent variable rather than M, we must convert the scatter in η calculated by the fitting routine to a scatter in M by dividing by the slope of the relation.

$$\sigma_{TF} = \frac{\sqrt{\frac{\chi^2}{N-p}}}{\gamma} \tag{3.4}$$

where χ^2 measures the quality of the fit, N is the number of data points, p is the number of degrees of freedom (2), and γ is the slope. Unfortunately, this means that the minima of σ_{TF} and χ^2 do not occur at the same place in $M-\eta$ space. Although there is not a unique way to choose the best fit to the data, we take it to be at the minimum of σ_η, which is equal to $\sqrt{\chi^2/(N-p)}$. We then convert to σ_{TF} using Equation 3.4 in order to assess the accuracy of our TF relation as a distance indicator. The distance error is defined as $\delta d/d = 0.46\sigma_{TF}$.

Because we lack error bars on our calculation of V_a, the χ^2 discussed above does not give us the actual uncertainty in the linear fit. We can estimate this quantity after the fact by calculating a "true" χ^2, $\chi^2_{true} = (N-p)^2\sigma^2_{old}/\sigma^2_\eta$, where σ_{old} is the value defined by the particular fit in question and σ_η is the best-fit value. A change of 1 in χ^2_{true} defines the size of the 1σ error bars.

3.3.1 Velocity Widths

The remaining question is the appropriate definition of the velocity width η. Since nearly every investigator has his or her own favorite definition, the only proper way to choose one is by experiment. We test the velocity at all of the characteristic radii of the galaxies that we have information about and pick the one that results in the lowest scatter. We use a simple linear fit to Equation 1.6. The results of this analysis using various velocity widths are presented in Table 3.2.

TF Fit Results

Velocity evaluated at radius	γ	η_o	σ_η
$1.67R_e$	0.1407	-0.8726	0.0557
$2.20R_e$	0.1365	-0.8325	0.0562
$2.20R_s$	0.1440	-0.8882	0.0598
$3.25R_s$	0.1372	-0.8296	0.0589
R_{24}	0.1346	-0.8208	0.0553
R_{50}	0.1319	-0.7928	0.0569
R_{83}	0.1284	-0.7580	0.0593
∞	0.1237	-0.7126	0.0625

R_e is an effective exponential scale length, R_s is the actual exponential scale length of the disk as derived from the photometric profile, R_{24} is the radius enclosing 24 % of the total light (similarly for R_{50} and R_{83}), and $V(\infty)$ is the asymptotic velocity V_a. 1σ limits are at approximately $+0.0006$ in σ_η and therefore ± 0.4 in the coefficient of R_e.

Table 3.2

We find that the TF relation with the lowest σ_η evaluates the rotation velocity at R_{24} (see Figure 3.3.1). An almost equally good fit is provided by using $1.67R_e$. R_e is a photometrically defined quantity that corresponds to an effective exponential scale length of the galaxy based on moments of the intensity distribution. If we calculate the forward Tully-Fisher scatter, $\sigma_{TF} = \sigma_\eta/\gamma$, for these definitions of η, we get $\sigma_{TF} = 0.411$ for R_{24} and $\sigma_{TF} = 0.396$ using $1.67R_e$. Although σ_η is essentially identical for the two fits, $1.67R_e$ yields a lower TF scatter because of its higher slope. Given these otherwise indistinguishable results, we choose $1.67R_e$ as the best radius for the TF relation. Both of these numbers conflict with previous claims of the best velocity width, such as those of Courteau, who chooses $2.2R_s$ [9], and Schlegel, who uses the 83 % light radius for his TF relation [16].

It is interesting to note that the most obvious choice of η, the actual asymptotic velocity of the RC as estimated by V_a, performs poorly in relation to the other definitions. The scatter for η_{V_a} is 0.0628, 13 % higher than that for η_{R_e}. Thus, the best place to evaluate the rotation velocity of a galaxy is *not* at the edge of the galaxy where the RC is completely flat, but closer to the center where the velocity is still increasing with radius. That is, the shape of the RC is an essential part of the velocity width definition. By fitting a two-parameter functional form to our RCs, we have obtained much more information about the galaxies and how they obey the TF relation than we would have if we had merely found the velocity difference between the two ends of the RC.

The overall TF scatter of ~ 0.4 mag is relatively low for an inverse TF relation. It corresponds to an 18 % uncertainty in distance. Most investigators who use the TF relation

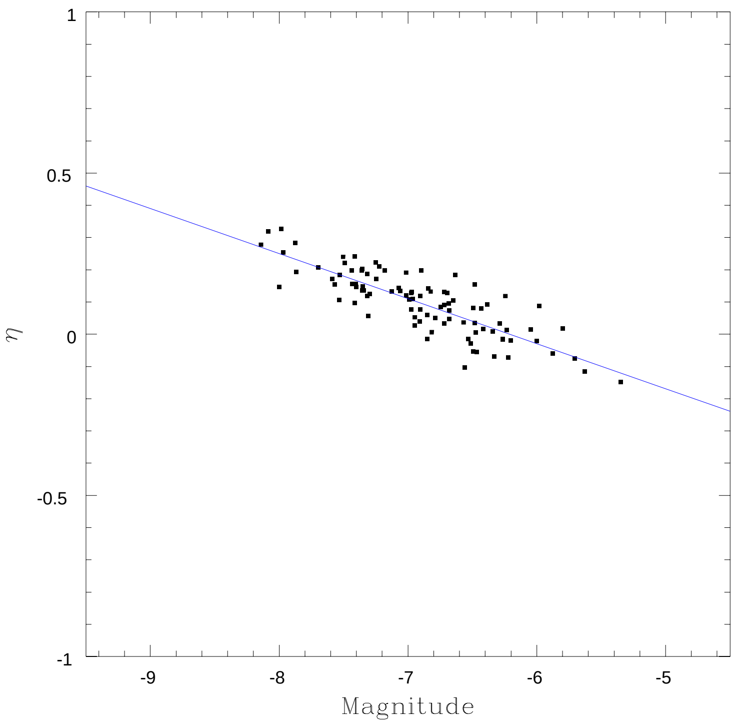

Figure 3.2: The Tully-Fisher relation using $1.67R_e$ as the fiducial radius.

find scatters between 0.25 and 0.5 mag, but the lower values are often artificially improved by sample selection [11, 14, 23, 24]. It is now believed that high-luminosity galaxies may have a lower intrinsic TF scatter [25]. A substantial fraction of the scatter in our data comes from the five points distributed well above the best-fit line between $M = -6$ and $M = -7$. These galaxies all have large rotation velocities and small turnover radii. This hints at the possibility of using an additional parameter to tighten the relation (see Section 4.1.1).

The difference from Courteau's earlier analysis of the exponential radii is surprising, although from Figure 3.3 it does not seem to be highly significant. It may be caused by the fact that virtually all of the RCs in this sample are of the "classic" variety; that is, they reach their turnover radius relatively quickly, well inside the end of the observed RC. There are no RCs that appear completely linear and only a fraction that have asymptotic velocities substantially higher than the velocity at the last observed point. A related property of our galaxy sample (see Figure 4.3) is that it consists largely of high luminosity galaxies. In these galaxies, as in ones with small turnover radii, we expect their bulges and inner disks to be dominated by luminous matter. In fainter galaxies with larger turnover radii, the portion of the galaxy described by the observed RC is much more affected by dark matter. This difference is not well understood, though, and the most we can say is that it surely has some effect on the best TF radius that we identify.

The more unexpected result is that the radius containing 24 % of the total light yields the lowest TF scatter of any of the fractional light radii. We can compare the fractional light

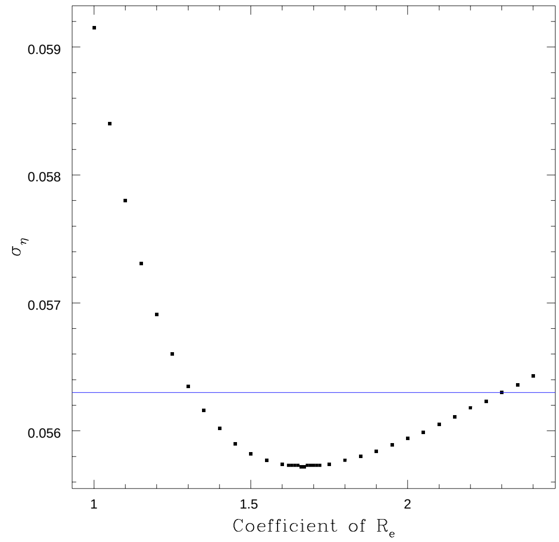

Figure 3.3: Varying the coefficient of R_e does not put a very tight constraint on the scatter. The line shows the 1σ limits.

radii to R_e by assuming it is a purely exponentially defined quantity:

$$f = \frac{\int_0^{kR_e} e^{-r/R_e} r\,dr}{\int_0^{\infty} e^{-r/R_e} r\,dr} \tag{3.5}$$

Thus, R_{24} should correspond to $0.93R_e$, R_{50} to $1.67R_e$, and R_{83} to $3.2R_e$. So we would expect, given our result for R_e, that R_{50} would be the best fractional light radius. This turns out not to be the case. Our analysis also suggests that R_{83} provides a worse TF fit than R_{24} and R_e at the 5σ level. Schlegel claims that the 83 % light radius is the natural choice, both because it minimizes the scatter and because it corresponds closely to the optical radius [16]. We can offer no such physical basis for our result, but its robustness is borne out by the comparison in Section 3.4.

3.3.2 Analysis of Residuals

Six of the 101 galaxies intended to be included in the TF analysis were discarded as outliers (see Figure 3.4). The initial determination of which points to eliminate was made using the residuals of the TF fits. For most of them, a simple examination of their RCs reveals the reason for their unsuitability. N589 has a very strangely-shaped RC that obviously cannot be approximated by an arctangent. The feature at about 12" is interpreted by the fitting function as the turnover radius, while in actuality the turnover radius may not be reached in this RC because the RC still seems to be rising at the last observed point. S295 has a declining RC with an exponential tail. It is the best example of an RC that can be fit accurately by Equation 3.1 but is dealt with poorly by the arctangent. This galaxy still marginally fit in with the derived TF relation, but had the largest (negative) residual of any remaining data point. Given the clear inability of the arctangent to model its behavior, it was eliminated from the fits.

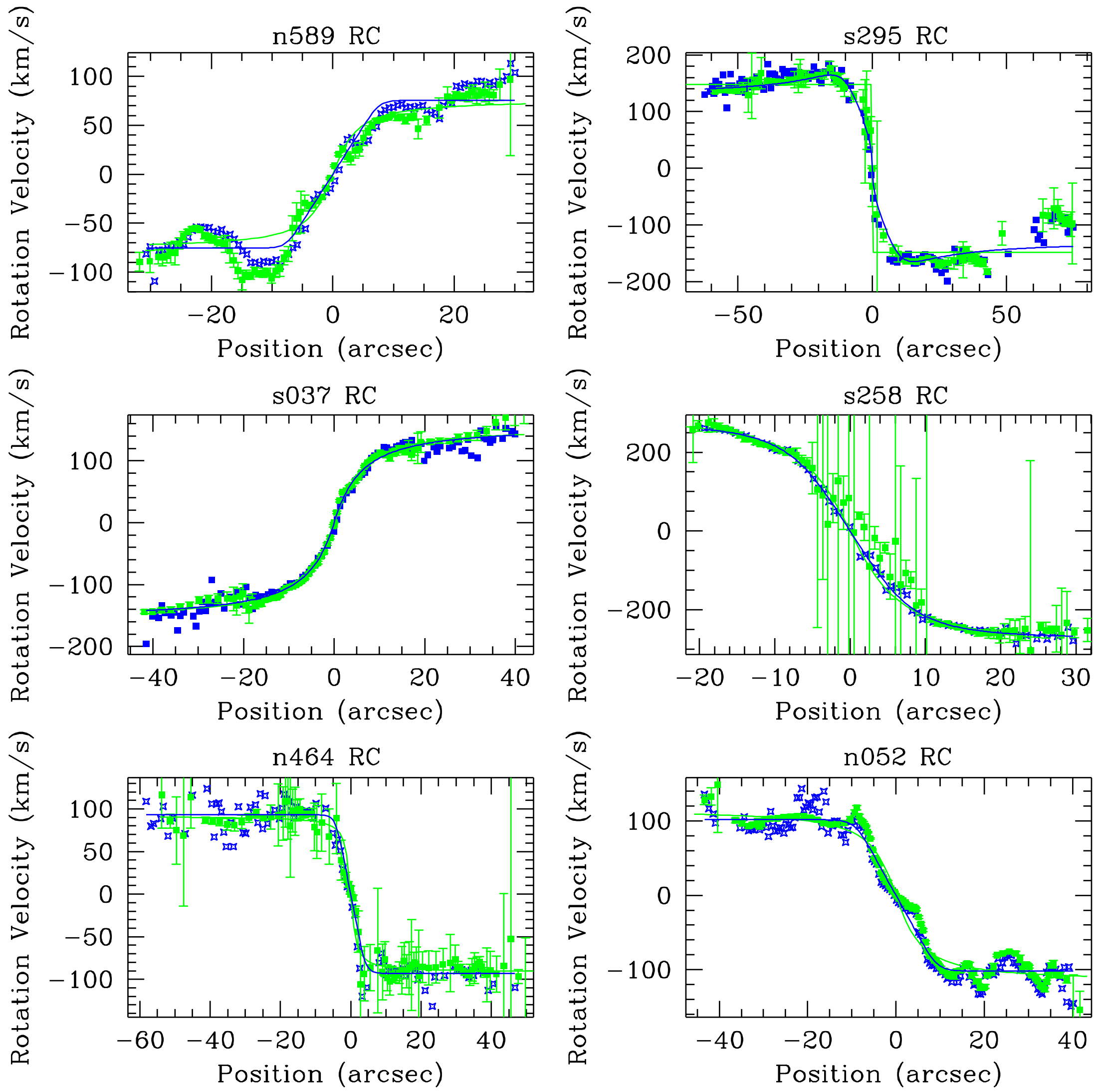

Figure 3.4: RCs of the six galaxies discarded from TF fits. My data points and fits are the light ones; Courteau's are dark.

Two of the other galaxies, s037 and s258, have rising rotation curves that are traced perfectly by Equation 2.2. We would expect that the use of the arctangent would compensate for the fact that they flatten out only at large radii, but in these cases it did not. Therefore, our decision to exclude them is based purely on their abnormally large residuals. Of the remaining two galaxies, both have anomalously slow rotation velocities — they are two of the slowest rotaters in the sample. In addition, n052 shows a number of velocity oscillations past the turnover radius (including one which is present in Courteau's data but not in mine). These oscillations could be caused by the projection of the galaxy's spiral arms in such a way that we are measuring the velocity of parts of multiple arms. It is also possible that this galaxy and n464 were simply misidentified during the observations and that the photometric observations are of brighter galaxies with higher rotation velocities. Additional errors could have been made in assuming that images of the galaxies were photometric when in fact they were not, or in using an incorrect position angle during the spectroscopic observations. The slit of the spectrograph must be lined up with the long axis of the galaxy as viewed by the observer, and if the slit is misaligned the measured velocity width will be too small.

As well as revealing which galaxies are modeled poorly by the TF fits, the residuals can give us more valuable information. Any trends of the TF residuals with galactic properties (magnitude, scale radius, inclination) indicate either that there are errors in the processing or that the variable in question may be a third parameter for the TF relation. A correlation between the residuals and galactic longitude and latitude would be a signal of possible bulk flows (see Chapter 4).

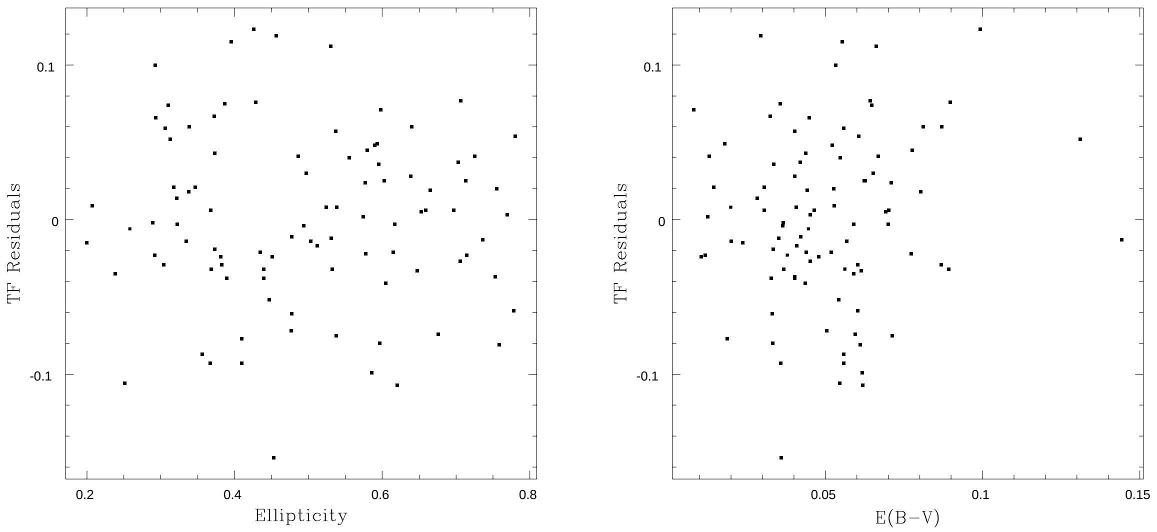

Figure 3.5: These plots demonstrate that our inclination and extinction corrections are not flawed.

Because any of these findings would be interesting, we subjected our residuals to a close examination. This did allow us to note and correct several mistakes, but did not reveal any obvious trends with photometric or RC shape characteristics of the galaxies (see Figures 3.5 and 3.6). We found suggestive small trends with the galactic coordinates that we will discuss in relation to the bulk flow analysis in Chapter 4. We also now have confidence that all of our crucial parameters are being calculated properly.

3.4 TF comparisons

I performed the same procedures using Courteau's data and functional form for RCs. The results are very similar, but with slightly higher scatter for choices of velocity width not involving the exponential scale radii (see Table 3.3). The distinction between the best fit using a multiple of R_e and the best fractional light radius to use was more obvious in this case, with $1.39R_e$ as the clear winner (see Figure 3.7). The TF relation evaluated at this

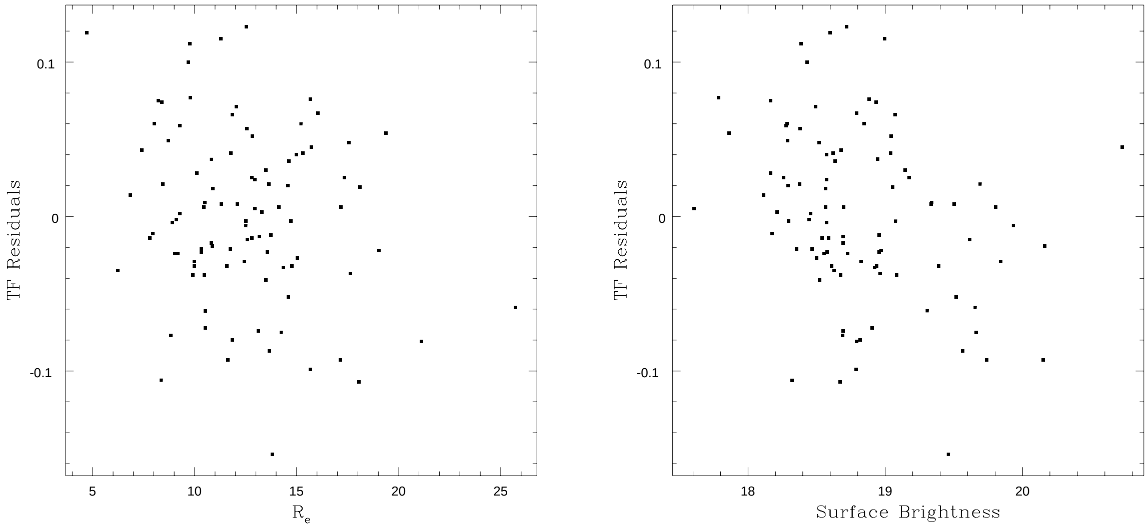

Figure 3.6: No correlation with the exponential scale radius is evident; however, surface brightness does seem related to the residuals. This may be a result of the fact the surface brightness correlates with rotation velocity, as do the residuals because η is our dependent variable. It could also be evidence that surface brightness should be included in the TF relation, as it is in the Fundamental Plane.

radius had a scatter of 0.387, corresponding to a 18 % distance error, the same as the 18 % error using my RC fits. Since σ_η is slightly larger than it was in my fits, the lower TF scatter results from the higher TF slope fit by Courteau's data. Although the best coefficient of R_e and the best fractional light radius are somewhat different than I found with the arctangent fits, the changes in scatter between them are small, and the results are probably consistent given the broad range of values that yield similar results (again, see the small slope on either side of the minimum in Figure 3.3). These data strengthen the result of my TF fits in that the velocity widths are best defined at smaller radii than have been chosen by other astronomers.

It should also be noted that of the six discarded galaxies of Section 3.3.2, none fared any better using Courteau's description of them. Even s295, the galaxy with the exponentially declining RC, still wound up with an anomalously large residual and was discarded. This suggests that the poor fit to this galaxy may be a result of the photometry rather than the declining RC (as discussed in the preceding section).

TF Fit Results From Courteau's Data

Velocity evaluated at radius	γ	η_o	σ_η
$1.39R_e$	0.1459	-0.9172	0.0565
$2.20R_e$	0.1369	-0.8377	0.0567
$2.20R_s$	0.1439	-0.8906	0.0587
$3.16R_s$	0.1369	-0.8318	0.0573
R_{31}	0.1349	-0.8231	0.0571
R_{83}	0.1297	-0.7724	0.0593
$99R_t$	0.1222	-0.7151	0.0633
∞	0.1298	-0.7591	0.0726

Note: The fit evaluating the velocity at R_t actually continues to improve in scatter as the coefficient increases, but has nearly reached its asymptotic value when the coefficient is 99.

Table 3.3

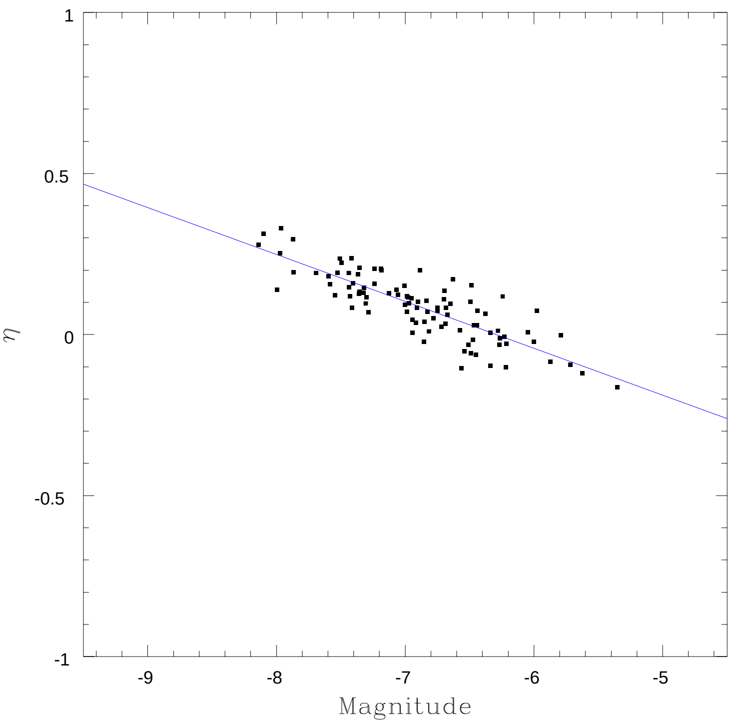

Figure 3.7: The Tully-Fisher relation using Courteau's data with $1.39R_e$ as the fiducial radius.

Chapter 4

Bulk Flows and Conclusions

In this chapter we present the results of a multi-parameter TF fit that yields bulk flow data. We also investigate a potential third parameter of the TF relation. Finally, we review the important conclusions that have been reached.

4.1 Bulk Flows

A multi-parameter fitting program using the Powell routine [19] was used to provide up to four additional degrees of freedom to the TF fits. Using the linear fits with R_e as the fiducial radius, we performed fits with TF slope, TF y-intercept, TF scatter in η, coefficient of R_e, bulk flow velocity, and bulk flow direction in galactic coordinates as the free parameters. This fit does not treat redshift as a straight Hubble Law as in the previous chapter (Section 3.3), but rather

$$cz = H_o d + \vec{v}_p \cdot \hat{n} \tag{4.1}$$

where $\vec{v}_p$ is the peculiar velocity vector of a galaxy. We can only detect the radial portion of peculiar velocities, of course, which is why we project them along the line-of-sight vector $\hat{n}$. Then, the TF relation we use becomes

$$\eta = \eta_o - \gamma m + 5\gamma \log\left(cz - \vec{v}_p \cdot \hat{n}\right) \tag{4.2}$$

We discovered that little was gained by allowing the direction of the bulk flow to vary. The best direction was approximately $l = 245^o$ and $b = 60^o$, but with very large and unquantifiable uncertainties. Since this is close to the orientation we expect — that of the CMB dipole — we fix the direction at the CMB coordinates of $l = 276^o$ and $b = 30^o$ [26]. We also fix the small-scale velocity dispersion at 200 km/s. Allowing the remaining five parameters to vary, we used a maximum likelihood method [27] and found that the best fit occurred with the following values:

Bulk Flow Fit Results

Parameter	Best Value
γ	0.142
η_o	-0.938
σ_η	0.0531
coeff of R_e	1.66
V_{bulk} (km/s)	186

Table 4.1

The best value of σ_η in this fit is noticeably lower than in the previous chapter. The slope and σ_η combine to yield the more interesting quantity of σ_{TF}, which is 0.373 mag, an improvement of 6 % on the linear fit. The coefficient of R_e in this fit is exactly the same as the one from the linear fit of the previous chapter. The slope and zero-point of the TF relation are also very similar, which encourages us that the improvement is purely a result of fitting to the detected bulk flow.

By holding one parameter at a time fixed, we were able to find one and two sigma limits on the bulk flow velocity and the coefficient of R_e. The 1σ limits are as follows:

$$\text{Coefficient of } R_e = 1.66 \,{}^{+0.39}_{-0.27}$$
$$V_{bulk} = 186 \pm 138 \text{ km/s}$$

2σ limits are $R_e = 1.66^{+1.05}_{-0.46}$ and $V_{bulk} = 186 \pm 280$ km/s. Thus, our bulk flow measurement is significant at the 80 % level.

Detection of a bulk flow is very sensitive to the sky coverage of the galaxy sample involved. If there are large regions of the sky that do not contain any of our galaxies, the signature of a bulk flow in that direction would be weak. The sky coverage of our 95 galaxies is shown below in Figure 4.1.

The correlation of residuals with galactic longitude and latitude (in Figure 4.2) offers some confirmation of the detected bulk flow. If a bulk flow is indeed present, then we expect that the direction on the sky that the peculiar velocities are biased towards would show the largest deviation from a linear TF relation. We see in the graphs that galaxies at high longitude ($l \approx 300^o$) have the highest residuals, which is consistent with our finding of a velocity in the direction of the CMB dipole. The latitude plot also seems to reveal a quadratic signature in the residuals peaked near $b = 25^o$, again consistent with our finding. Linear fits to the residuals as a function of each of these coordinates confirmed nonzero slopes of order 10^{-4}, even though the trends may be difficult to discern by eye. The significance of these trends is increased by the fact that they were discovered after the decision to fix the bulk flow direction towards the CMB dipole was made. Thus, they lend additional support to the claim of a bulk flow detection in that direction.

There are two other possible explanations for the nonuniformity of residuals with galactic longitude and latitude: our galactic extinction correction could be incorrect, or we might be seeing sensitivity to the sky coverage of the galaxy sample. The second possibility cannot

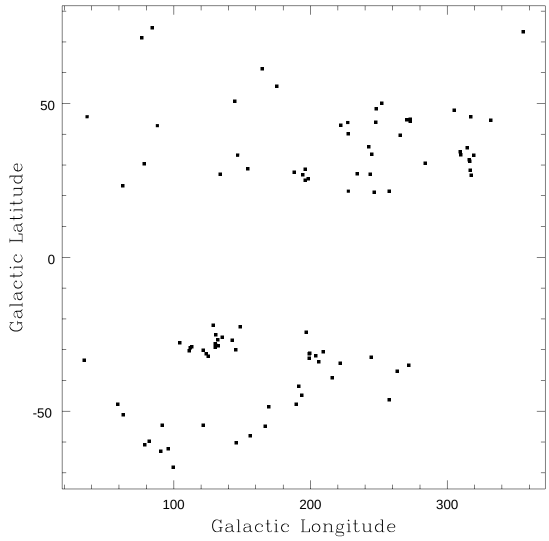

Figure 4.1: Distribution of the galaxy sample in galactic longitude (l) and galactic latitude (b). The blank region at $|b| < 15^o$ is the so-called zone of exclusion through the plane of the Milky Way.

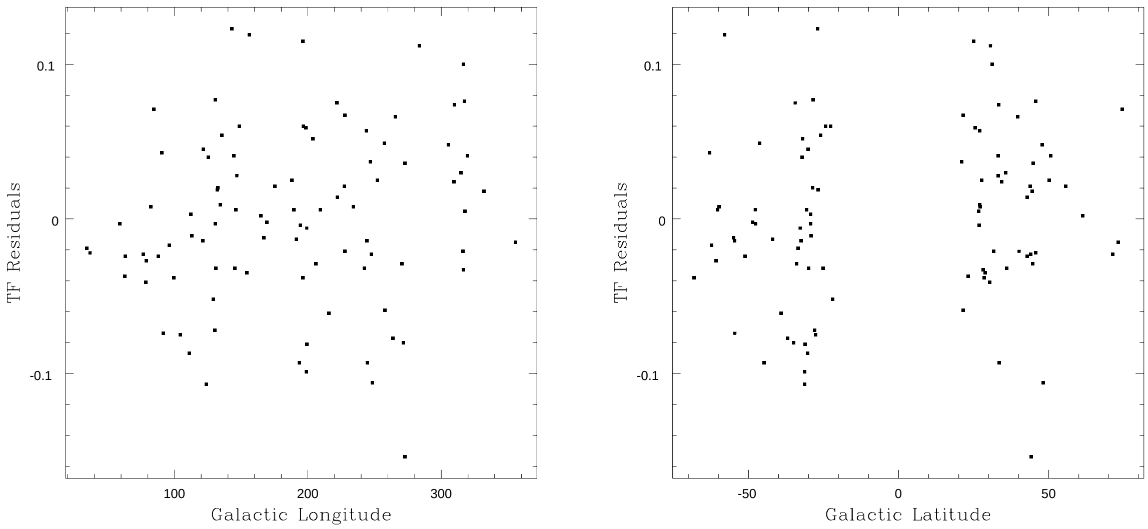

Figure 4.2: Small trends of TF residuals as a function of galactic longitude and latitude are visible. Note the slight skew of the left-hand graph towards higher residuals at high longitudes and the presence of the highest residuals at $b \approx 25$ in the right-hand plot.

be ruled out at this point, but the first is unlikely because the SFD dust maps should be quite accurate, and most of our observations are confined to regions where extinction is low anyway.

We can offer a comparison between our bulk flow result and other recent findings. The direction of our flow, considering likely angular uncertainties, is consistent with the Great

Attractor observations of Dressler et al., although the flow amplitude we find is much smaller [28]. More recent results on a similar scale (up to 6000 km/s) also show rough agreement, again with higher velocities. We can comment with more confidence on the controvesial Lauer-Postman (LP) claim of 700 km/s bulk flows on scales greater than 10,000 km/s [29]. Fixing our bulk flow direction along the vector they define (l = 343, b = 52), we find a best-fit velocity of about 160 km/s (with a somewhat lower likelihood), which excludes a large velocity on the 4σ level. Since this velocity is lower than our actual best-fit to V_{bulk}, we see that our preferred direction is also not consistent with LP. While the LP sample incorporates a much larger volume, it is difficult to understand how coherent bulk motions would increase in magnitude between 5000 and 10000 km/s.

4.1.1 A Three-Parameter TF Relation

In addition to the linear fit described in Section 3.3.1, we used the Powell routine to allow variation in a third TF parameter. We attempted a TF relation of the form

$$\eta = \eta_o - \gamma M + C X_t \tag{4.3}$$

where $X_t = R_t/R_e$. Since $\eta = \log(2V_a) - 2.5$ here, this fit uses R_t as a third parameter in the TF relation rather than as part of the definition of the velocity width. This additional freedom turns out to add only slight value to the fits. The likelihood is maximized for C = .182, with σ_{TF} = 0.372 mag and σ_η = 0.0531, virtually identical to the bulk flow fit result (this fit fixed the bulk flow parameters at 0; it was not possible to completely remove them from the fit). Interestingly, if X_t is defined as R_e/R_t, the coefficient C is 0 and the fit becomes equivalent to the worst of the those displayed in Table 3.2, with $\eta = V_a$.

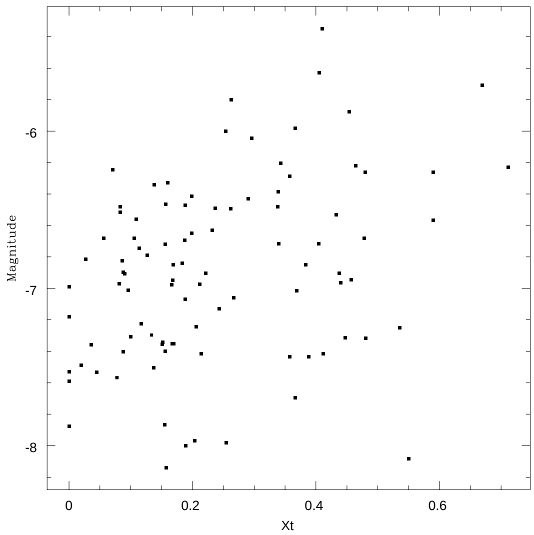

Figure 4.3: The relationship between magnitude and X_t demonstrates a correlation between luminosity and RC shape.

The relationship between X_t and magnitude in Figure 4.3 is further evidence that RC shape is important in the TF relation. However, the fact that the relationship is weak (with a scatter of at least 1 mag) indicates that the claim of Persic and Salucci that RC shape can be predicted solely on the basis of luminosity is incorrect [30].

4.2 Conclusions

Chapters 2 and 3 of this thesis have provided detailed and useful information about how to extract optical rotation curves from longslit spectra and how to obtain a Tully-Fisher relation from them. We have investigated various choices of the Tully-Fisher velocity width and concluded that the best one to use in order to minimize the scatter of the TF relation is the fitted velocity evaluated at a multiple of the scale radius R_e. There remains some question about which multiple of this radius is the appropriate one to use, due to the discrepancy between my findings and those of Courteau. I conclude that the most useful value is $1.67R_e$, as determined by both my linear and multi-parameter fits. We find that this sample of 95 spirals produces a TF relation with a scatter of 0.373 mag when a bulk flow is included in the fit. Including all 300 galaxies that are part of the Shellflow survey will likely provide further information about the velocity widths, although it may not appreciably reduce the TF scatter.

We have found that the two-parameter arctangent function defined by Equation 1.3 is at least as good as, and perhaps slightly better than, a three-parameter RC fit for Tully-Fisher work. We also reach the preliminary conclusion that the local universe has a peculiar velocity of 186 ± 138 km/s in the direction of the CMB dipole. This bulk flow detection is marginally statistically significant, and will certainly be improved by the addition of the remaining 200 Shellflow galaxies to the sample.

4.2.1 Possible Sources of Systematic Errors

There are a few remaining corrections to the data other than the ones described in Section 3.3 that we have not used. The redshifts used in our analysis were treated as heliocentric, but they actually represent geocentric redshifts, and therefore need to be corrected for the motion of the Earth around the Sun. This correction should be no more than 20 km/s, and could be much less in many cases, so it should have a minimal impact on our results. The k-correction was also not applied to any of our photometric data, but should have a similarly small effect.

Finally, the problem of Section 2.2.2 in properly calculating the errors in our arctangent fits could have impeded our efforts to define the TF scatter. Since we did not have accurate error bars on the fit parameters V_a and R_t, we were forced to set the standard deviations of each point as provided to the fitting routine to one. This eliminates our ability to weight the points in the fit toward those we have the most confidence in. Because we removed the worst points from the fit anyway, we would expect this change to yield at most a slight improvement. Also, because we were unable to calculate the covariance between V_a and R_t, we cannot state categorically that they are completely independent variables. Nevertheless, it is obvious that very few of our RCs were at all linear and so we are not concerned about the risk of covariance.

4.2.2 Future Work

I look forward to the upcoming completion of Shellflow for confirmation of my findings. I do not expect the results of the TF fits to change significantly, although there is room for improvement in my bulk flow analysis. Shellflow was designed to detect a 350 km/s bulk flow at the 5σ level, and my preliminary results offer no reason to challenge that assumption. The results of Shellflow will be particularly interesting because it will be the first peculiar velocity survey to offer uniform calibration and full-sky coverage on the 6000 km/s scale. As such, of course, it probably will not provide the final word on the bulk flows in the nearby universe, but it is an important step toward that goal. Further peculiar velocity surveys will still be needed, both at these low redshifts, and especially at the higher redshifts probed by Lauer and Postman. The methods developed in my thesis have been demonstrated to be appropriate for these purposes.

Bibliography

[1] Pasachoff, J. M. 1998, *ASTRONOMY: from the Earth to the Universe* (New York: Harcourt Brace & Company).

[2] Binney, J. & Tremaine, S. 1987, *Galactic Dynamics* (Princeton: Princeton Univ. Press).

[3] Rubin, V. C. & Ford, W. K. 1970, ApJ, 159, 379.

[4] Freeman, K. C. 1970, ApJ, 160, 811.

[5] Milgrom, M. 1983, ApJ, 270, 365.

[6] Alcock, C. et al. 1997, ApJ, 486, 697.

[7] Totsuka, Y. et al. 1998, Physical Review Letters (submitted).

[8] Tully, R. B. & Fisher, J. R. 1977, A & A, 54, 661.

[9] Courteau, S. 1997, AJ, 114, 2402.

[10] Willick, J. A. 1997, to appear in *Formation of Structure in the Universe*, A. Dekel and J. Ostriker, Eds.

[11] Strauss, M. A. & Willick, J. A. 1995, Physics Reports, 261, 271.

[12] Dressler, A., Faber, S. M., Burstein, D., Davies, R. L., Lynden-Bell, D., Terlevich, R., & Wegner, G. 1987, ApJ, 313, L37.

[13] Djorgovski, S. & Davis, M. 1987, ApJ, 313, 59.

[14] Willick, J. 1991, Ph.D. thesis, University of California, Berkeley.

[15] Han, M. S. 1991, Ph.D. thesis, California Institute of Technology.

[16] Schlegel, D. J. 1996, Ph.D. thesis, University of California, Berkeley.

[17] Santiago, B. X., Strauss, M. A., Lahav, O., Davis, M., Dressler, A., & Huchra, J. P. 1995, ApJ, 446, 457.

[18] Mathewson, D. S., Ford, V. L., & Buchorn, M. 1992, ApJ, 389, L5.

[19] Press, W. H., Teukolsky, S. A., Vetterling, W. T., & Flannery, B. P. 1992, *Numerical Recipes in C* (Cambridge: Cambridge Univ. Press).

[20] Kasen, D. 1997, Senior Honors Thesis, Stanford University.

[21] Landolt, A. 1992, AJ, 104, 340.

[22] Schlegel, D. J., Finkbeiner, D. P. & Davis, M. 1998, ApJ (accepted).

[23] Willick, J. 1990, ApJ, 351, L5.

[24] Schommer, R. A., Bothun, G. D., Williams, T. B., & Mould, J. R. 1993, AJ, 105, 97.

[25] Federspiel, M., Sandage, A., & Tammann, G. A. 1994, ApJ, 430, 29.

[26] Kogut, A. et al. 1993, ApJ, 419, 1.

[27] Willick, J. A., Strauss, M. A., Dekel, A., & Kolatt, T. 1997, ApJ, 486, 629.

[28] Dressler, A. 1987, ApJ, 317, 1.

[29] Lauer, T. R. & Postman, M. 1994, ApJ, 425, 418.

[30] Persic, M., Salucci, P., & Stel, F. 1996, MNRAS, 281, 27.

Appendix A

Data Table

This table lists the useful properties of the 101 galaxies for which I had both photometric and spectroscopic data. Please note that all pages in the appendices are double-sided.

Galaxies

name	RA	Dec	cz	V	I	SB	ellip	conc	V_a	R_t	R_e	R_s	f_2	f_1	f_0
g021	1:31:46.00	33:27:33.00	4363.00	13.196	11.977	18.293	0.7553	2.1160	-250.80	6.380	14.581	13.605	0.35	0.38	1.28
g023	1:32:22.00	35:20:31.00	4528.38	13.077	11.841	19.056	0.6653	3.2390	-224.20	3.020	18.109	11.276	-0.27	1.18	1.10
g079	3:40:33.00	-6:25:32.00	5272.85	13.626	12.470	20.149	0.4098	2.4320	128.06	2.690	17.143	19.250	-1.39	2.80	0.56
g080	3:46:55.00	-3:28:40.00	3987.62	13.582	12.420	18.693	0.7364	2.1980	-178.60	2.610	13.165	11.780	0.60	-0.09	1.43
g087	4:31:13.99	-3:55:57.00	4773.83	13.999	12.897	19.933	0.2580	2.1930	128.10	8.370	12.509	10.433	0.71	-0.25	1.48
g090	4:37:17.00	-3:13:30.00	4762.14	12.833	11.561	18.793	0.7588	2.1710	-207.90	0.950	21.101	19.916	1.18	-0.81	1.82
g092	4:41:34.00	-7:06:10.00	4549.15	13.092	11.858	19.043	0.3127	2.3540	-185.10	2.350	12.834	13.579	0.71	-0.18	1.47
g103	4:54:56.00	-10:41:43.0	4546.99	13.132	11.904	18.566	0.6968	2.7390	-215.90	1.360	14.126	16.037	0.64	0.09	1.33
g104	4:55:59.00	2:09:02.00	4548.68	12.943	11.688	18.845	0.6400	2.3330	-244.30	0.000	15.214	15.050	0.58	0.17	1.29
g242	16:05:43.00	21:29:36.00	4409.32	12.628	11.326	18.969	0.5777	2.2640	225.46	2.960	19.034	18.368	0.73	-0.17	1.58
n003	0:04:14.00	31:27:12.00	4954.59	13.597	12.436	19.565	0.3561	2.7820	-118.30	2.190	13.673	14.120	0.84	-0.34	1.55
n005	0:07:09.00	32:35:24.00	5081.56	13.299	12.095	18.214	0.7692	2.3990	240.03	3.240	13.305	12.826	0.87	-0.40	1.51
n012	0:17:20.00	-6:50:36.00	7308.05	13.496	12.321	18.674	0.4392	2.3360	-222.30	4.680	10.463	10.163	0.53	0.05	1.31
n050	0:47:51.00	8:16:43.99	5289.07	12.818	11.544	18.540	0.3347	2.5860	191.44	2.140	12.803	10.415	0.66	-0.14	1.43
n052	0:49:59.00	-5:12:41.00	5497.43	13.378	12.186	18.704	0.3283	2.2320	-116.40	4.510	9.760	14.849	0.40	0.13	1.31
n067	1:00:25.00	30:39:03.00	4777.05	12.646	11.347	18.574	0.5555	3.0320	251.19	0.300	14.978	30.567	1.72	-0.99	1.57
n104	1:22:28.00	34:25:13.99	4850.45	13.460	12.279	18.904	0.4768	2.9760	-138.90	0.870	10.518	17.182	0.99	-0.14	1.23
n105	1:22:44.00	33:09:26.00	5471.63	12.784	11.505	18.296	0.6168	2.4190	287.75	5.400	14.726	13.507	0.58	-0.04	1.47
n106	1:23:50.00	33:52:27.00	4858.35	13.259	12.049	17.784	0.7062	2.2870	285.02	3.610	9.797	11.739	0.90	-0.39	1.37
n131	1:35:50.00	0:38:46.00	5182.04	13.338	12.140	18.698	0.3677	3.4320	-159.70	0.590	10.441	13.250	0.58	0.14	1.24
n148	1:47:04.00	35:32:48.99	4672.32	12.349	11.006	17.861	0.7800	1.9240	-419.50	10.670	19.378	19.653	0.43	0.29	1.44
n223	2:46:14.00	3:35:24.00	6808.30	13.083	11.848	18.447	0.2894	3.1080	-186.00	0.000	9.111	14.969	0.89	0.02	1.11
n226	2:48:04.00	34:24:21.99	5266.49	13.437	12.253	18.284	0.3382	2.6630	185.34	1.500	8.017	10.802	0.37	0.57	0.95
n297	6:58:31.00	80:00:29.00	4946.19	13.599	12.438	19.337	0.2069	1.8870	-146.80	7.470	10.502	9.805	0.70	-0.22	1.40
n301	7:34:32.00	62:33:09.00	4778.79	14.084	12.994	18.626	0.2385	2.2850	-101.20	2.530	6.248	6.051	0.11	0.65	0.87
n699	20:55:13.00	-13:27:19.0	7403.35	14.439	13.401	20.162	0.3729	2.2130	146.63	3.730	10.866	9.455	0.56	0.00	1.31
n720	22:22:26.00	-4:08:14.00	4952.39	13.023	11.779	19.075	0.3222	2.7030	-161.20	0.000	12.514	16.727	-2.07	3.83	0.08
n729	22:39:26.00	-4:14:43.00	7455.68	13.531	12.360	18.556	0.4508	2.7440	-206.70	1.370	9.024	9.937	-0.06	1.05	0.84
n748	23:31:43.00	-5:01:29.00	5193.22	13.055	11.816	18.501	0.7058	2.3720	-229.50	2.270	15.040	16.213	0.67	-0.02	1.42
s001	0:02:55.00	-1:55:52.00	7292.35	13.439	12.256	18.693	0.5122	1.9370	-247.60	4.200	10.824	8.090	0.53	-0.04	1.35
s007	0:10:31.00	32:57:54.00	4823.35	13.585	12.423	18.174	0.4771	2.0210	-154.50	1.100	7.957	7.931	0.42	0.30	1.06
s017	0:46:08.00	32:39:21.99	4877.64	13.326	12.126	20.727	0.5800	2.3580	-212.50	1.360	15.726	11.370	-0.11	1.03	1.07
s021	0:54:57.00	31:31:26.00	5482.03	12.532	11.216	18.670	0.6203	2.5370	232.96	3.420	18.049	20.329	0.51	0.23	1.38
s032	1:21:09.00	40:28:15.00	5863.42	13.429	12.243	19.517	0.4466	2.1830	169.94	2.450	14.599	15.028	1.05	-0.63	1.65
s037	1:23:00.00	33:30:46.00	6024.67	12.964	11.711	19.135	0.3618	3.8740	154.10	5.000	12.938	37.471	-2.27	4.80	-0.42
s040	1:27:29.00	37:09:57.00	5176.17	13.340	12.142	18.608	0.5321	2.0600	-198.40	4.440	11.584	10.953	0.77	-0.31	1.47
s057	1:58:31.00	0:30:49.00	7025.59	14.578	13.560	18.597	0.4563	3.2030	-202.40	1.730	4.727	4.171	0.02	1.14	0.39
s069	2:16:00.00	32:37:43.00	4808.83	13.391	12.200	18.718	0.4256	1.9890	-231.60	2.910	12.530	5.474	0.56	-0.20	1.42
s071	2:19:41.00	29:01:17.00	4973.64	13.309	12.107	19.388	0.4398	2.2080	-165.20	1.870	14.756	16.801	0.73	-0.09	1.46
s073	2:25:39.00	-0:21:19.00	6416.12	13.228	12.013	18.957	0.5310	1.9760	220.82	1.210	13.744	13.164	1.07	-0.67	1.62
s095	3:24:52.00	-5:45:24.00	5678.59	12.638	11.338	19.804	0.6588	2.3780	-304.80	3.490	17.167	13.671	0.34	0.32	1.38
s105	4:35:56.00	-3:05:02.00	4923.45	12.899	11.637	18.788	0.5857	2.3500	-180.10	1.560	15.663	12.947	0.40	0.22	1.40
s106	4:37:46.00	-9:31:30.00	4990.01	12.790	11.512	18.824	0.3043	2.7430	172.90	1.660	12.429	17.766	-0.11	1.17	0.96
s239	17:48:33.00	51:09:31.00	6756.73	12.998	11.750	18.522	0.6047	2.2800	255.70	2.090	13.501	13.695	0.93	-0.40	1.50
s241	18:11:09.00	36:00:24.00	6482.64	13.344	12.146	18.963	0.7533	2.2960	-236.50	1.370	17.642	17.878	0.47	0.30	1.35
s258	20:52:24.00	-5:43:23.00	6041.31	14.022	12.923	20.807	0.1378	2.5180	-311.40	5.170	9.089	9.919	0.44	0.31	1.10
s290	23:33:31.00	32:21:55.00	4999.92	13.853	12.729	19.663	0.5378	1.9860	-152.00	6.610	14.247	13.571	1.38	-1.21	1.86
s291	23:34:29.00	-3:06:15.00	5195.95	14.059	12.965	19.504	0.5245	2.2740	-155.90	2.870	11.312	11.788	0.71	-0.11	1.35
s292	23:41:09.00	3:59:58.00	6293.55	13.356	12.161	18.693	0.6758	2.1330	232.85	5.400	13.112	13.561	0.41	0.25	1.31
s295	23:46:54.00	29:27:55.00	5199.51	12.257	10.902	18.956	0.3935	2.3820	-148.20	0.000	20.866	14.314	0.31	0.45	1.40
s299	23:55:03.00	-3:45:53.00	6541.08	13.834	12.708	18.679	0.3734	3.2160	-183.60	1.470	7.403	8.439	0.49	0.30	0.99

Galaxies (cont.)

name	RA	Dec	cz	V	I	SB	ellip	conc	V_a	R_t	R_e	R_s	f_2	f_1	f_0
s126	07:59:02.00	32:55:21.00	5230.35	13.202	11.984	18.261	0.7129	2.0380	-255.70	2.640	12.798	14.004	1.34	-1.19	1.82
s127	08:02:25.00	27:26:42.00	5248.52	13.627	12.470	18.573	0.4935	2.0170	180.46	3.010	8.898	8.633	0.86	-0.37	1.33
s128	08:20:19.00	68:36:34.00	4694.76	13.367	12.173	18.164	0.6383	2.2290	-201.40	1.070	10.110	9.769	0.54	0.05	1.26
s134	09:05:55.00	-04:21:19.9	6454.44	13.795	12.664	19.336	0.5387	2.5620	-189.50	1.380	12.088	12.691	0.61	0.11	1.26
s139	09:38:50.00	06:58:10.00	5000.52	13.139	11.912	18.354	0.4349	2.5560	-181.90	2.290	10.324	7.737	0.23	0.41	1.20
s146	09:48:46.00	-08:02:20.0	6597.91	13.970	12.864	19.739	0.3667	1.9960	128.76	2.760	11.635	9.110	0.49	0.02	1.37
s167	10:55:04.00	61:18:14.00	5203.81	13.555	12.389	19.040	0.4865	2.6650	-193.70	3.080	11.778	16.635	0.19	1.08	0.77
s170	11:02:01.00	45:54:15.00	6566.78	13.653	12.500	18.455	0.5745	2.0210	234.05	4.090	9.287	8.211	0.68	-0.23	1.37
s221	13:40:34.00	38:41:48.00	5948.25	13.084	11.849	18.492	0.5977	2.4900	-290.60	2.580	12.056	18.833	1.01	-0.57	1.51
s235	16:19:03.00	57:42:11.00	5102.41	13.648	12.494	18.725	0.3814	1.9930	-164.30	5.410	9.177	13.436	0.65	-0.22	1.38
g121	07:57:46.00	25:10:07.00	4669.73	13.373	12.180	18.997	0.3954	3.8620	198.71	0.940	11.300	13.575	0.19	0.56	1.15
g123	08:02:57.00	23:23:55.00	4714.72	13.137	11.909	18.277	0.3057	2.6090	-196.30	3.750	9.268	8.166	-0.13	1.20	0.76
g129	08:34:24.00	-02:32:17.0	4241.74	12.490	11.168	18.793	0.3721	2.7510	-224.50	1.880	16.052	19.266	0.81	-0.27	1.55
n321	08:12:18.00	26:22:10.00	6308.22	13.696	12.550	19.085	0.3892	2.0830	-167.30	3.370	9.925	9.828	0.29	0.43	1.12
n354	09:40:32.00	11:54:29.00	6690.95	13.462	12.282	18.113	0.3213	2.1690	-191.60	1.830	6.852	6.758	0.51	0.09	1.11
n363	09:50:57.00	09:01:17.00	5237.67	13.691	12.544	19.691	0.3468	2.0300	161.08	4.870	13.633	8.253	0.51	0.02	1.43
n365	09:51:35.00	-05:01:31.0	6335.57	13.475	12.296	18.938	0.3683	2.5830	-171.90	2.110	9.978	14.659	0.60	0.08	1.20
n379	10:20:21.00	43:08:45.00	6712.94	13.435	12.250	18.377	0.3174	2.6030	-188.20	1.590	8.453	7.802	0.11	0.68	0.99
n382	10:26:26.00	-02:49:45.0	5856.21	14.234	13.167	18.955	0.7146	1.8330	187.04	4.960	10.337	3.180	0.55	-0.17	1.42
n550	13:33:04.00	-16:06:26.0	6120.41	12.655	11.357	18.882	0.4285	3.1580	-327.00	3.990	15.674	22.837	0.17	0.62	1.26
n560	13:46:44.00	16:17:11.99	5757.14	13.540	12.371	19.617	0.2000	2.1440	145.50	7.420	12.577	6.803	0.06	0.60	1.23
n575	14:00:13.00	38:55:40.00	5383.51	12.545	11.231	18.576	0.2920	2.8750	180.44	0.000	13.558	22.209	0.65	-0.01	1.39
n589	14:12:07.00	15:51:17.00	5223.87	13.454	12.273	18.756	0.1900	2.1570	76.60	3.010	8.964	16.495	-0.20	1.04	0.94
g112	05:27:28.80	-39:27:36.5	4622.84	13.893	12.775	18.589	0.5033	1.7710	152.70	3.540	7.808	6.503	0.52	0.06	1.41
g149	09:44:55.80	-24:36:23.0	4295.90	13.212	11.995	19.655	0.7779	2.2700	181.75	2.320	25.719	22.562	0.62	-0.01	1.86
g164	11:35:45.90	-29:27:06.3	4128.89	13.456	12.275	18.386	0.5301	2.3880	199.12	0.690	9.768	10.564	1.20	-0.73	1.69
g188	13:16:10.00	-28:16:08.6	4467.25	13.017	11.771	18.572	0.5766	2.2910	211.36	1.060	12.949	13.488	0.41	0.38	1.40
g190	13:18:04.50	-29:13:09.6	4280.99	13.772	12.637	18.935	0.3103	2.3750	142.88	2.200	8.380	10.792	0.69	0.17	1.25
g204	13:43:15.50	-29:47:20.7	4648.81	13.346	12.149	18.466	0.6149	1.9940	-208.20	5.620	11.742	9.182	0.50	0.02	1.60
g206	13:45:19.80	-30:12:12.2	4824.97	13.012	11.766	18.431	0.2924	3.1010	-197.90	0.850	9.689	9.526	0.74	-0.12	1.50
g208	13:49:22.50	-33:03:16.2	4227.40	13.396	12.206	18.922	0.6472	1.8920	169.03	2.700	14.349	9.836	1.23	-0.94	2.02
g226	14:15:05.40	-13:38:34.0	4623.80	13.156	11.931	18.564	0.3378	2.0230	-167.50	1.700	10.887	7.751	0.60	-0.05	1.57
n261	04:08:34.90	-49:35:26.6	5116.57	13.670	12.520	18.288	0.5931	2.0090	-206.40	2.530	8.705	11.168	1.36	-0.91	1.68
n283	04:56:38.60	-21:38:36.6	6766.05	13.367	12.173	18.163	0.3866	3.2900	280.45	4.410	8.237	12.715	0.05	1.17	0.89
n288	05:04:31.30	-55:31:42.7	6624.14	13.578	12.415	18.691	0.4099	2.7810	-176.40	4.040	8.836	10.980	0.85	-0.18	1.46
n290	05:14:01.80	-62:17:00.2	5091.55	13.354	12.158	18.816	0.5965	3.4960	156.59	0.320	11.852	16.021	1.16	-0.58	1.67
n340	09:14:10.90	-17:23:15.1	5022.92	14.126	13.042	18.945	0.7032	2.1830	-184.50	3.210	10.828	12.228	0.74	-0.08	1.53
n345	09:26:15.40	-11:32:33.3	5394.82	12.825	11.552	18.379	0.5368	3.1830	272.98	1.720	12.560	10.578	0.57	0.16	1.47
n390	10:39:44.10	-00:06:56.0	5558.50	13.303	12.100	18.321	0.2513	2.4970	118.51	1.410	8.364	10.063	2.15	-2.12	2.13
n400	10:51:56.80	-00:32:39.1	5564.14	13.035	11.792	19.175	0.6024	2.7750	280.05	6.200	17.341	20.745	0.36	0.65	1.38
n406	10:56:26.30	-14:41:36.2	4544.46	13.332	12.133	19.071	0.2931	1.8960	171.67	4.010	11.841	10.670	0.46	0.04	1.62
n424	11:19:22.70	-12:15:57.0	4836.00	14.429	13.389	19.843	0.3824	1.9150	111.97	4.100	9.997	7.106	0.34	0.25	1.47
n431	11:25:39.80	-12:55:11.7	4948.26	12.825	11.551	18.636	0.5949	3.0650	-244.40	0.520	14.618	17.346	0.43	0.55	1.36
n464	11:46:31.60	-09:27:06.3	5731.72	13.066	11.828	19.190	0.4826	2.1600	-91.53	1.120	16.970	12.388	0.51	0.03	1.73
n517	12:57:47.80	-15:00:51.9	4912.94	12.387	11.051	18.518	0.5896	3.1040	-292.50	0.000	17.570	22.429	0.50	0.51	1.42
n567	13:53:47.20	-27:36:23.7	5484.68	13.221	12.005	18.622	0.7250	2.3070	271.84	2.600	15.296	10.703	0.35	0.25	1.61
n572	13:55:28.90	-34:16:31.4	5026.27	12.287	10.936	17.607	0.6528	2.6950	314.37	2.040	12.948	15.782	-0.31	1.21	1.26
s104	04:31:09.80	-18:46:54.4	6282.16	13.905	12.790	19.306	0.4774	2.0930	166.42	4.560	10.527	8.402	0.34	0.33	1.40
s174	11:24:43.60	-13:33:21.9	5382.23	13.576	12.413	19.460	0.4527	2.4530	-116.30	1.500	13.811	12.803	0.91	-0.51	1.84
s218	13:33:47.90	-26:17:53.6	6696.24	13.410	12.222	19.144	0.4968	2.2340	-273.80	6.490	13.501	14.789	1.31	-1.05	2.00

Notes: RA and dec are in current epoch.
Redshifts are geocentric.
Magnitudes are apparent and uncorrected for extinction.
V_a is not corrected for inclination or for redshift broadening.
The parameters f_2, f_1, and f_0 are defined such that $10^{f_2 x^2 + f_1 x + f_0}$ is the radius containing 100x % of the galaxy's light.

Appendix B

Programs

This is the Fortran program used for RC extraction. The Numerical Recipes routines it uses have not been included, for the sake of brevity.

```
program rotcurve

c Determine the rotation curve from a calibrated 2-D spectral image.
c Inputs: "pieces" of the rotation curve with more or less continuous
c signal, as well as the spectroscopic calibration.
c Ouput: lambda(peak) versus x-x_cont, where x_cont is the
c x-position of the continuum.
c JW, begun 6/3/97
C JS, continued 6/3 - ?

        parameter (maxfit=11, maxparm=3, nparm=3, maxpiece=35)
real rn2,gain
real pixels(750,1050),temp(1050)
real lstart,dl,slope,top,bottom
real intens, cent, centroid,center
real errora, errorb, error1, error2, errorc
        character*15 image,outfile,datafile
integer axlen(7),dtype,naxis
integer lwidth,rwidth,fwidth,leftedge,riteedge
        integer max_x,max_y
integer piece (maxpiece, 2, 2)
integer l,r
integer icol(200),count,ixs,ixe,iys,iye,numcol
        dimension xfit(50),yfit(50),sig(50)
dimension y1(100)
        dimension a(maxparm)
        dimension u(maxfit,maxparm+1)
        dimension vv(maxfit,maxparm+1)
        dimension w(maxfit,maxparm+1)
dimension cvm(3,3)
logical sumcol(maxpiece)
dimension sumline1(500),sumline2(500)
dimension fluxval(19)

common /image_data/ pixels, ier, max_x,max_y


C  Beginning of program
c ***   read input parameters
        call clargc(1,image,ier) !image name
if (ier.ne.0) goto 91
call clargr(2,lstart,ier)
call clargr(3,dl,ier)
call clargi(4,l,ier)
```

```
call clargi(5,lwidth,ier)
call clargi(6,r,ier)
        call clargi(7,rwidth,ier)
        call clargi(8,fwidth,ier)
call clargr(9,rn2,ier)
call clargr(10,gain,ier)

if (fwidth .gt. maxfit) then
   print *, 'Maximum fit width allowed is ',maxfit
   print *, 'try again.'
   stop
end if

c ***   open the output file for the velocity data:
lim=numchar(image)
outfile=image((lim-3):lim)//'.sdat'
open (2, file=outfile, status='unknown')
datafile=image((lim-3):lim)//'.rc'
open (3, file=datafile, status='unknown')
write(3,*),' COL     CENTER         ERROR        CENTROID       CHI^2'
write(3,*),' '
c ***   open and read image
C print *, 'Opening image and getting size ...'

        call imopen(image,1,im1,ier)
        if (ier.ne.0) goto 91
        call imgsiz(im1,axlen,naxis,dtype,ier)

        max_x=axlen(1)
        max_y=axlen(2)

C        print *, 'Have opened image, it has size max_x,max_y = '
C        print *, max_x,max_y
C        print *, 'Now loading image data into array pixels...'


do j = 1,axlen(2)
   call imgl2r(im1,temp,j,ier)
   do i = 1,axlen(1)
      if (temp(i) .eq. 0.) temp(i)=-999.
      pixels(i,j) = temp(i)
           end do
end do
C print *, 'done.'

        do i = 1, maxpiece
   sumcol(i) = .false.
end do
c  Call the spectrum "piece" routine to obtain the piecewise continuous
c  portions of the images:
call pspect(image,piece,npiece,sumcol)
number = 1
count = 1
numcol = axlen(1) + 1

c  Loop through the individual pieces
do i=1,npiece-1
   if (sumcol(i)) then
      call lowsn(piece,maxpiece,i,pixels,axlen,icol,count,
     +           ixs,ixe,iys,iye,numcol)
      ix0 = ixs
   else
      ixs=piece(i,1,1)
      ix0=ixs
      iys=piece(i,1,2)
      ixe=piece(i,2,1)
      iye=piece(i,2,2)
           endif
```

```
   top = iye - iys
   bottom = ixe-ix0
   if (bottom .eq. 0) then
      slope = 0
   else
      slope=(iye - iys)/bottom
   endif
   if (ixs .eq. piece(i-1,2,1)) ixs=ixs+1

c  Loop through columns in each piece
C    print *, 'working on piece ',i,' for which I have ixs,ixe = '
C    print *, ixs,ixe
   do j=ixs,ixe
      ycent=iys+slope*(j-ix0)
      iyc=nint(ycent)
c  First find the centroid:
      centr = 0
      intens = 0
c  Loop through pixels in each column
C       print *, 'computing the centroid in row ',j
      do k=iyc-4,iyc+4
 centr = float(k)*pixels(j,k)+centr
 intens = pixels(j,k) + intens
      end do
      centroid = centr/intens
C       print *, 'done: result = ',centroid

c  Now get the integer closest to the centroid:
      lcent=nint(centroid)

C  Now find and subtract the median of the continuum:
C print *, 'now finding and subtracting continuum near line...'
      n = 0
      leftedge=lcent-l
      do k = (leftedge - lwidth+1), leftedge
 y1(n) = pixels(j,k)
 n = n + 1
      end do
      riteedge=lcent+r
      do k = riteedge, (riteedge + rwidth-1)
 y1(n) = pixels(j,k)
 n = n + 1
      end do
      ndata = n
        call mdian2(y1,ndata,ymed)

C print *, 'now setting up array for parabolic fit...'

      m = 0
      do k = lcent-fwidth/2,lcent+fwidth/2
 pix = pixels(j,k) - ymed
 if (pix .gt. 0.) then
    m=m+1
    yfit(m)=alog(pix)
    xfit(m)=float(k-lcent)
    deltay=sqrt(rn2+pixels(j,k)/gain)
    sig(m)=deltay/pix
 end if
      end do

      n = 0
      do k = lcent-fwidth/2,lcent+fwidth/2
 pix2 = pixels(j,k) - ymed
 if (pix2 .gt. 0) then
    n = n + 1
    fluxval(n) = pix2
 else
    n = n + 1
```

```
    fluxval(n) = 1
 endif
              end do

C  Now fit a parabola to the log of the continuum-subtracted pixel
C  values near the center:

      nfit=m
      if (nfit .ge. nparm) then
C                print *, 'calling svdfit with nfit = ',nfit
                 call svdfit(xfit, yfit, sig, nfit, a, 3,
     +              u, vv, w, maxfit, maxparm+1, chisqr, fpoly)
C                print *, 'back from svdfit.'
C          print*,'ln(pixels) = ',a(3),'y^2 + ',a(2),'y + ',a(1)
 cent = -0.5*a(2)/a(3)
 center = cent + lcent
 center = lstart + dl*(center - 1)
 centroid = lstart + dl*(centroid - 1)
C  Now calculate error in position of center
                 if (nfit .gt. nparm) then
    call svdvar(vv, 3, maxparm+1, w, cvm, 3)
    errora = cvm(3,3)
    errorb = cvm(2,2)
    errorab = cvm(2,3)
    error1 = -0.5/a(3)
    error2 = 0.5*a(2)/a(3)**2
    error3 = -0.25*a(2)/a(3)**3
    errorc = dl*sqrt(errorb*error1**2 + errora*error2**2 +
     +               2*errorab*error3)
         else
    center = centroid
    errors=0
    denom = 0
    n = 1
    do k=iyc-4,iyc+4
       errors = fluxval(n)*(centr/intens - k)**2/gain + errors
       denom = fluxval(n) + denom
       n = n + 1
    end do
    errorc = dl*sqrt(errors)/denom
    errord=errorc
 endif

C  Decide which points to keep and output them to a file
         if (errorc .le. 1000) then
    if (j .le. axlen(1)) then
       write(3,93) j,center,errorc,centroid,chisqr
    else
       write(3,93) icol(number),center,errorc,centroid,chisqr
    endif

 endif

      else
 if (nfit .eq. 1) then
C            print*,nfit,' point left - cannot perform a fit'
C            print*,' '
 else
C            print*,nfit,' points left - cannot perform a fit'
C            print*,' '
 endif
      endif
      if (j .gt. axlen(1)) number = number + 1


   end do
end do
```

```
C  determine x-position of the galaxy continuum
jupper = piece (npiece,1,1)
kupper = piece (npiece,1,2)
C do m = 1,axlen(1)
do m = jupper - 50, jupper + 50
   do n = (kupper-10),(kupper+10)
      sumline1(m) = pixels (m,n) + sumline1(m)
   end do
end do
xmax1 = 0
xmaxpos1 = 0
do m = 1,axlen(1)
   if (sumline1(m) .gt. xmax1) then
      xmax1 = sumline1(m)
      xmaxpos1 = m
   end if
end do
        cen = 0
flux = 0
do k = xmaxpos1 - 4, xmaxpos1 + 4
   cen = k*sumline1(k)+cen
   flux = sumline1(k) + flux
end do
upcent = cen/flux

jlower = piece (npiece,2,1)
klower = piece (npiece,2,2)
C do m = 1,axlen(1)
do m = jlower - 50, jlower + 50
          do n = (klower-10),(klower+10)
      sumline2(m) = pixels (m,n) + sumline2(m)
   end do
end do
xmax2 = 0
xmaxpos2 = 0
do m = 1,axlen(1)
   if (sumline2(m) .gt. xmax2) then
      xmax2 = sumline2(m)
      xmaxpos2 = m
   end if
end do
cen = 0
flux = 0
do k = xmaxpos2 - 4, xmaxpos2 + 4
   cen = k*sumline2(k)+cen
   flux = sumline2(k) + flux
end do
downcent = cen/flux
        contcent = (upcent + downcent)/2

write(2,94),image,lstart,dl,l,lwidth,r,rwidth,fwidth,rn2,gain
write(2,95),contcent


        close(2)
close(3)

 93 format(i4,5x,f9.4,5x,f8.4,7x,f9.4,3x,f9.4)
 94 format('rc',1x,a10,1x,f11.6,2x,f9.7,1x,i2,1x,i2,1x,i2,1x,
     +     i2,1x,i2,2x,f5.2,2x,f4.2)
 95 format('The center of the continuum is at column',1x,f9.5)

stop
91 print *, 'usage: rc image ls dl left lwidth right rwidth
     +   fitwidth rn2 gain'
stop
end
```

```
subroutine lowsn(piece,maxpiece,i,pixels,axlen,icol,count,
     +     ixs,ixe,iys,iye,numcol)

integer xstart,ystart,xend,yend,numcol,num,count
integer ixs,ixe,iys,iye
integer piece(maxpiece,2,2)
integer icol(200)
integer axlen(7)
real sum(41)
real pixels(750,1050)
integer i

C  Sum over columns that have low signal-to-noise
do jay = 1,41
   sum(jay) = 0
end do

xstart = piece(i,1,1)
ystart = piece(i,1,2)
xend = piece(i,2,1)
yend = piece(i,2,2)
ixs = numcol
 10 if ((xend-xstart) .ge. 2) then  !4
C  Add up pixel values in each row
   index = 1
   do k = (ystart - 15), (ystart + 15)
      do l = xstart, xstart + 2 !4
 sum(index) = pixels(l,k) + sum(index)
      end do
      index = index + 1
   end do
   icol(count) = xstart + 1 !2
   num = 1
C  Put the summed and averaged pixel values for each column at the
C   end of pixels(i,j)
   do j = (ystart - 15), (ystart + 15)
C       pixels(numcol,j) = sum(num)/3 !5
      pixels(numcol,j) = sum(num)
      num = num + 1
   end do
   xstart = xstart + 3 !5
   numcol = numcol + 1
   count = count + 1
   if (xstart .le. xend) goto 10
else
C  Same procedure for the last couple columns in case there aren't
C   as many of them
   index = 1
   do k = (ystart - 15), (ystart + 15)
      do l = xstart, xend
 sum(index) = pixels(l,k) + sum(index)
      end do
      index = index + 1
   end do
   g = xstart + (xend-xstart)/2
   icol(count) = nint(g)
   num = 1
   do j = (ystart - 15), (ystart + 15)
C       pixels(numcol,j) = sum(num)/(xend - xstart + 1)
      pixels(numcol,j) = sum(num)
      num = num + 1
   end do
   numcol = numcol + 1
   count = count + 1
endif
C  Rename the columns in the piece so that they're the correct ones
```

```
ixe = numcol - 1
iys = ystart
iye = yend
return
end



subroutine pspect(image,piece,npiece,sumcol)

parameter (maxpiece = 35)
character*12 image,newfile
real xs, ys, xe, ye
integer piece (maxpiece, 2, 2), npiece
logical sumcol (maxpiece)

C beginning of program

length=numchar(image)
newfile = image(1:length)//'.xy'
open(1, file = newfile, status = 'old')
npiece = 1
goto 19
 18 sumcol(npiece) = .true.
read (1,*, end = 500, err = 18) xs, ys
read (1,*) xe, ye
goto 20
 19 read (1, *, end = 500, err = 18) xs, ys
read (1, *) xe, ye
 20 piece (npiece, 1, 1) = nint(xs)
piece (npiece, 1, 2) = nint(ys)
piece (npiece, 2, 1) = nint(xe)
piece (npiece, 2, 2) = nint(ye)
npiece = npiece + 1
goto 19
500 npiece=npiece+1
close (1)
npiece = npiece - 2
i = 1

return
end
```

This is the IRAF script used to perform the preliminary reductions and run rc.f.

```
##########################################################################
# getrc.cl
# ===================================
# Josh Simon -- July 9, 1997
# -----------------------------------
# Runs FORTRAN program rc.f on spectra to extract rotation curves
#
# Uses scripts sect.cl, yesorno.cl, and getparams.cl
# Uses IRAF tasks display, imexam, imgets, and cosmicrays
##########################################################################

procedure getrc (filename)

string    filename  {prompt = 'Name of file containing image list'}

begin

# Define variables
char name, pieces
real lstart, dl, rn, g, rn2
real l, r, lwidth, rwidth, fitwidth
char tempname
string answer, section
bool crzap

list = filename

# Go to proper package so IRAF task cosmicrays doesn't get lost
imred
ccdred

# Loop through images in list
while(fscan(list,name) != EOF) {

# Creates a file named "image.xy" in which the spectrum is broken up
# into continuous, linear pieces
tempname = list
print ('Now working on ',tempname)
display (image = tempname, frame = 1)
pieces = tempname//'.xy'

# Query for cosmic ray removal
print ('Type y or n at the prompt')
yesorno
answer = yesorno.root
if (answer == 'y')
   crzap = yes
else
   crzap = no

# Interactive cosmic ray removal until user is satisfied
while (crzap) {
   print ('Enter the bounds of the section to zap at the prompt.')
   sect
   section = sect.root
   cosmicrays(input = tempname//section, output = tempname//section,
thresho = 2., fluxrat = 25., npasses = 25, window = 5, interac = yes,
train = no,)
   display (image = tempname, frame = 1)
   print ('Cosmic rays removed in that section.  Repeat?')
   yesorno
   answer = yesorno.root
   if (answer == 'y') {
      crzap = yes}
   else {
```

```
      crzap = no}
}

# Open the image and use IRAF task imexamine to write to file "image.xy"
print ('Use the x key to delineate pieces of the spectrum')
imexam (input = tempname, frame = 1, image = tempname,
keeplog = no, defkey = "x", >> pieces)

# Read values needed by rc.f out of the image header file
imgets (image = tempname, param = "CRVAL2")
lstart = real(imgets.value)
imgets (image = tempname, param = "CDELT2")
dl = real(imgets.value)
imgets (image = tempname, param = "RDNOISE")
rn = real(imgets.value)
imgets (image = tempname, param = "GAIN")
g = real(imgets.value)
rn2 = rn**2

# Call another task, getparams, to have the user define more values
# needed by rc.f
print ('Enter the value of the parameter l at the prompt.')
getparams
l = real(getparams.root)
print ('Enter the value of the parameter lwidth at the prompt.')
getparams
lwidth = real(getparams.root)
print ('Enter the value of the parameter r at the prompt.')
getparams
r = real(getparams.root)
print ('Enter the value of the parameter rwidth at the prompt.')
getparams
rwidth = real(getparams.root)
print ('Enter the value of the parameter fitwidth at the prompt.')
getparams
fitwidth = real(getparams.root)

# Use getparams again in case the read noise and gain were not present
# in the image header
if (rn2 == 0) {
   print ('Enter the value of the parameter rn^2 at the prompt.')
   getparams
   rn2 = real(getparams.root)
}
if (g == 0) {
   print ('Enter the value of the parameter g at the prompt.')
   getparams
   g = real(getparams.root)
}


# Print out the call to rc.f
print ('rc ',tempname,' ',lstart,' ',dl,' ',l,' ',lwidth,' ',r,
' ',rwidth,' ',fitwidth,' ',rn2,' ',g)

# Run program rc.f using the information obtained with getrc
rc (tempname,lstart,dl,l,lwidth,r,rwidth,fitwidth,rn2,g)

print ('Got RC for image ',tempname)
print (' ')
}

end
```

This is the C program used for RC fitting. Again, Numerical Recipes routines have been left out.

```
/**********************************************************/
/*                     ARCTANFIT.C
 * Daniel Kasen, 1996
 * modified by Josh Simon, 10/97
 *
 * This program reads in an RC data from a Persic and Salucci
 * formatted file.  The RC is fit with an arctan and the
 * covariance matrix of the fit is calculated.  The fit and
 * galaxy parameters are written to the chart file; a fit
 * file, which can be used to plot the fit, is also created.
 **********************************************************/

# include <stdio.h>
# include <stdlib.h>
# include <math.h>
# include <string.h>
# include <malloc.h>
# define N 1000
# define TABLE_FILE "MAT_table"
# define DATA_TAILER ".info"
# define CHART_FILE "chart"
# define SIGMA_ERROR 1
# define PI 3.14159
# define MAX_STRING_LENGTH 1000


typedef struct {
  float mag, Ropt, gl, gb, Deso, eta;
  int redshift, ID;
  char name[MAX_STRING_LENGTH];
} galaxyData;

typedef struct {
  float Va, Vr, Vmax, Rt, Rmax, RCoef, VarVa, VarRt, chisq, errorbar,voff,
roff,vuncert,runcert;
} fitData;

typedef struct {
  float position[N];
  float velocity[N];
  float dr[N],dv[N];
  int ndata;
} curveData;

  /* global variable */

curveData Curve;
float vstart,vnaught,rnaught,rtmax,vamax;
int sign,count,nlines;

  /* functions */

void ReadData(char*);
void ReadTable(galaxyData*);
void FitCurve(fitData*, galaxyData);
void FitCovarianceMatrix(fitData*);
void WriteFitFile(fitData, galaxyData);
void WriteDataToChart(galaxyData, fitData);
float ArctanFunct(float*, float);
float TwoDArctan(float*, float);
float DimensionlessArctan(float*,float);
void MakeIdentityMatrix(float**, int);
void SetMatrix(float**, float, float);
void SetVector(float*, float, float, float, float*);
```

```
int GetNumberOfLines(FILE*);
FILE* OpenFile(char*, char*);

/* NR functions  */

float GetChiSquared();
float TwoDChiSquared();
float DimlessChiSquared();
void powell();
int *ivector();
float **matrix();
double **dmatrix();
float *vector();
double *dvector();
void ludcmp();
void lubksb();

void main(int argc, char *argv[])
{
  galaxyData galaxy;
  fitData fits;

  if (argc !=2) {
    printf ("you must type: FIT2 <input file>\n");
    exit(0); }
  sprintf(galaxy.name, "%s", argv[1]);
  /*ReadTable(&galaxy);*/
  ReadData(galaxy.name);
  nlines = Curve.ndata;
  fits.Rmax = fabs(Curve.position[Curve.ndata-3]);
  if (fabs(Curve.position[1]) > fits.Rmax) {
    fits.Rmax = fabs(Curve.position[1]);
  }
  printf("%f  %f\n",fits.Rmax,Curve.position[Curve.ndata-3]);
  fits.Vmax = fabs(Curve.velocity[Curve.ndata-3]);
  if (fabs(Curve.velocity[1]) > fits.Vmax) {
    fits.Vmax = fabs(Curve.velocity[1]);
  }
  if (fits.Vmax == Curve.velocity[Curve.ndata-3]) {
    sign = 1; }
  else {
    sign = -1;}
  vstart = fits.Vmax;
  printf("fits.Rmax is %f,  fits.Vmax is %f\n",fits.Rmax,fits.Vmax);
  FitCurve(&fits, galaxy);
  fits.errorbar = sqrt(fits.chisq/(Curve.ndata-4));
  vnaught = fits.Va;
  rnaught = fits.Rt;
  FitCovarianceMatrix(&fits);
  WriteDataToChart(galaxy, fits);
  WriteFitFile(fits, galaxy);
}


/**************************************************************************/
/* Function: ReadData
 * Reads in the curve data for the galaxy -- First the number of data
 * points, then the position and velocity of each point.
 * All information is put into the global data structure Curve.
 **************************************************************************/
void ReadData(char *name)
{
  char line[MAX_STRING_LENGTH], filename[MAX_STRING_LENGTH];
  FILE *datafile;
  int i, j;
  float position, velocity, deltav, deltar;

  sprintf(filename, "%s%s", name, DATA_TAILER);
```

```
  datafile = OpenFile(filename, "r");
  Curve.ndata = GetNumberOfLines(datafile);
  fgets(line, MAX_STRING_LENGTH, datafile);
  fgets(line, MAX_STRING_LENGTH, datafile);
  fgets(line, MAX_STRING_LENGTH, datafile);
  j = 1;
  for (i=3;i<Curve.ndata;i++)
  {
    fgets(line, MAX_STRING_LENGTH, datafile);
    sscanf (line, "%f %f %f %f\n", &position, &deltar, &velocity, &deltav);

    Curve.position[j] = position;
    Curve.velocity[j] = velocity;
    Curve.dv[j] = deltav;
    Curve.dr[j] = deltar;
    j= j +1;
  }
  fclose(datafile);
}

/***************************************************************************/
/* Function: ReadTable
 * Reads in galaxy data for the named galaxy from TABLE_FILE
 * The table should be formatted with each line as:
 * ==> name, ID#, Ropt, magnitude, redshift, eta, gl, gb, Deso
 * If a table entry for the galaxy cannot be found, exits.
 **************************************************************************/
void ReadTable(galaxyData *galaxy)
{
  FILE *tablefile;
  int entry, numEntries;
  char line[MAX_STRING_LENGTH], s1[MAX_STRING_LENGTH];
  float f3, f4, f6, f7, f8, f9, f10;
  int d2, d5;

  tablefile = OpenFile(TABLE_FILE, "r");
  numEntries = GetNumberOfLines(tablefile);
  for (entry=1; entry<numEntries; entry++) {
    if (fgets(line, MAX_STRING_LENGTH, tablefile)==NULL) break;
    sscanf (line, "%s %d %f %f %d %f %f %f %f %f\n", &s1, &d2, &f3, &f4,
    &d5, &f6, &f7, &f8, &f9, &f10);
    if (!strncmp(galaxy->name, s1, 8)) {
      galaxy->mag = f4;
      galaxy->redshift = d5;
      galaxy->ID = d2;
      galaxy->gl = f7;
      galaxy->gb = f8;
      galaxy->eta = f6;
      galaxy->Deso = f9;
      galaxy->Ropt = f3;
      fclose(tablefile);
      return;
    }
  }
  printf (" %s -- couldn't find entry in table", galaxy->name);
  exit(0);
}

/***************************************************************************/
/* Function: FitCurve
 * This function uses the NR routine powell to fit a curve to
 * the data in Curve.  xi is the direction matrix, and p is the
 * array of two parameters.  These quantities are initialized and
 * then powell is called to minimize the function GetChiSquared.
 **************************************************************************/
void FitCurve(fitData *fit, galaxyData galaxy)
{
  float p[5], fret, ftol = 1e-4,pNew[5],newp[5];
```

```
  int iter, i, q;
  float **xi;

  xi = matrix(1,5,1,5);
  p[1] = sign*vstart;
  p[2] = 0;
  q = 1;
   if (sign > 0) {
    while (Curve.velocity[q] < vstart/2)  {
      p[2] = fabs(Curve.position[q]);
      q++;
    }
  }
  else {
    while (-Curve.velocity[q] < vstart/2)  {
      /*printf ("%f  %f\n",-Curve.velocity[q],vstart/2);*/
      p[2] = fabs(Curve.position[q]);
      q++;
    }
  }
  p[3] = 0;
  p[4] = 0;
  p[5] = 0;
  MakeIdentityMatrix(xi, 5);

  /*for (i = 1; i<5; i++) {
    printf("%f %i\n",p[i],i);}*/
  powell (p, xi, 5, ftol, &iter, &fret, GetChiSquared);
  fit->Va = p[1];
  fit->Rt = p[2];
  fit->voff = p[3];
  fit->roff = p[4];
  newp[1] = p[1];
  newp[2] = p[2];
  newp[3] = 0;
  newp[4] = 0;
  fit->Vr = ArctanFunct(newp, fit->Rt);
  fit->chisq = fret;
  rtmax = fabs(p[2]);
  vamax = fabs(p[1]) ;
  /* pNew[2] = p[2];
  pNew[3] = p[3];
  pNew[4] = p[4];
  for (i = 0;i<11;i++) {
    pNew[1] = p[1] + .02*(i-5)*p[1];
    printf("%f  %f\n",pNew[1],GetChiSquared(pNew));
  }*/



}


/*************************************************************************/
/* Function: FitCovarianceMatrix
 * This function uses LU decomposition to minimize the chisquared
 * of the covariance fit.  First a data set of the arctan chisquared
 * is created by computing it at several values of Va and Rt.
 * This information is put into the matrix A.
 *************************************************************************/
void FitCovarianceMatrix(fitData *fit)
{
  float pNew[5];
  int *indx, i, j,s;
  float dx,dv,varV,varR,Cov,d,check,n;
  float **A, *b;

  A = matrix(1,3,1,3);
```

```
  b = vector(1,3);
  indx = ivector(1,3);
  n = .9;

  pNew[3] = fit->voff;
  pNew[4] = fit->roff;
blah:      pNew[1] = n*fit->Va + ((1-n)/5)*fit->Va;
  pNew[2] = fit->Rt;
      if ((GetChiSquared(pNew)-fit->chisq) > fit->chisq/1000)
{/* printf("%f\n", GetChiSquared(pNew) - fit->chisq);*/
  n = n + .00005;
  goto blah;}
      n = n - .000016;
      /*printf("n is %f\n",n);*/

  for (i=0;i<=10; i++){
    for (j=0;j<=10; j++) {
      pNew[3] = fit->voff;
      pNew[4] = fit->roff;
      pNew[1] = n*fit->Va + ((1-n)/5)*fit->Va*i;
      pNew[2] = .98*fit->Rt + .004*fit->Rt*j;

      dv = pNew[1]/vamax - 1;
      dx = pNew[2]/rtmax - 1;

      pNew[1] = dv;
      pNew[2] = dx;

      /*dv = pNew[1] - fit->Va;
      dx = pNew[2] - fit->Rt;*/

      /* printf("%f  %f  %f  %f",pNew[1],pNew[2],pNew[3],pNew[4]);
      printf("  %f\n",GetChiSquared(pNew));*/
      SetVector(b, dx, dv, fit->chisq, pNew);
      SetMatrix(A, dx, dv);
    }

  }
  printf("\n");
  /* A[1][3]=A[2][3]=A[3][1]=A[3][2]=0;
  printf("%f  %f  %f\n",A[1][1],A[1][2],A[1][3]);
  printf("%f  %f  %f\n",A[2][1],A[2][2],A[2][3]);
  printf("%f  %f  %f\n",A[3][1],A[3][2],A[3][3]);*/
printf("(b1,b2,b3) = (%f, %f, %f)\n",b[1],b[2],b[3]);

  ludcmp(A, 3, indx, &d);
  lubksb(A, 3, indx, b);
  printf("(C11,C22,C12) (dimensionless) = (%f, %f, %f)\n",b[1],b[2],b[3]);

  b[1] = b[1]/(vamax*vamax);
  b[2] = b[2]/(rtmax*rtmax);
  b[3] = b[3]/(vamax*rtmax);

printf("(C11,C22,C12) = (%f, %f, %f)\n",b[1],b[2],b[3]);
  varV = b[2]/(b[1]*b[2] - 1*b[3]*b[3]);
  varR = b[1]/(b[1]*b[2] - 1*b[3]*b[3]);
  Cov = -1*b[3]/(b[1]*b[2] - 1*b[3]*b[3]);
  fit->RCoef = Cov/sqrt(varV*varR);
  /*printf("%f  %f\n",vamax,rtmax);*/

  fit->vuncert = sqrt(varV)*fit->errorbar;
  fit->runcert = sqrt(varR)*fit->errorbar;
  printf("Va error is +/- %f, Rt error is +/- %f, Cov is %f\n",fit->vuncert,
fit->runcert,Cov);

 printf("\n");
  for (i=0;i<=10; i++){
    /*printf("dv = %f, dx = %f -> %f\n",(-1+n + (1-n)*i/5), -.02, .02);*/
```

```
    for (j=0;j<=10; j++) {
      pNew[3] = fit->voff;
      pNew[4] = fit->roff;
      pNew[1] = n*fit->Va + ((1-n)/5)*fit->Va*i;
      pNew[2] = .98*fit->Rt + .004*fit->Rt*j;
      dv = pNew[1]/vamax - 1;
      dx = pNew[2]/rtmax - 1;
      pNew[1] = dv;
      pNew[2] = dx;
      check = fit->chisq + b[1]*dv*dv*vamax*vamax + b[2]*dx*dx*rtmax*rtmax +
2*b[3]*dv*dx*vamax*rtmax;
      /*printf("%.6.4f ",DimlessChiSquared(pNew) - fit->chisq);*/
  }
    /*printf("\n");*/
  }
}

/****************************************************************/
/* Function: SetMatrix
 * This function is used to initialize the matrix used to solve
 * the covariance fit.  It simply adds on the increments
 * of x and v appropriately
 ****************************************************************/

void SetMatrix(float **A, float dx, float dv)
{
  A[1][1] += dv*dv*dv*dv;
  A[1][2] += dv*dv*dx*dx;
  A[1][3] += 2*dv*dv*dv*dx;
  A[2][1] += dv*dv*dx*dx;
  A[2][2] += dx*dx*dx*dx;
  A[2][3] += 2*dv*dx*dx*dx;
  A[3][1] += dv*dv*dv*dx;
  A[3][2] += dv*dx*dx*dx;
  A[3][3] += 2*dv*dv*dx*dx;
}

/*****************************************************************/
/* Function: SetVector
 * This function is used to initialize the vector b for the
 * covariance fit
 ****************************************************************/

void SetVector(float *b, float dx, float dv, float chi, float pNew[5])
{
  int i;
  /* for (i=1;i<5;i++) {
    printf("%f  ",pNew[i]);
  }
  printf(" %f %f %f\n",dv,dx, DimlessChiSquared(pNew)); */
  b[1] += (-chi + DimlessChiSquared(pNew))*dv*dv;
  b[2] += (-chi + DimlessChiSquared(pNew))*dx*dx;
  b[3] += (-chi + DimlessChiSquared(pNew))*dx*dv;
}
/*************************************************************************/
/* Function: OpenFile
 * Opens the file with filename passed for the process passed
 * checks to see no error occurred during opening; if an error does
 * occur, prints an error message and exits.
  ************************************************************************/
FILE* OpenFile(char *filename, char *process)
{
  FILE *file;

  file = fopen(filename, process);
  if (file==NULL) {
    printf("Cannot open file -- %s\n", filename);
    exit(0);
```

```
  }
  return file;
}

/*************************************************************************/
/* Function: WriteDataToChart
 * appends the interesting galaxy and fit parameter to the
 * CHART_FILE
*************************************************************************/
void WriteDataToChart(galaxyData data, fitData fit)
{
  FILE *out;

  out = OpenFile(CHART_FILE, "a+");

  fprintf(out,"Galaxy %s\n",data.name);
  fprintf(out,"   Va = %5.2f +/- %6.3f\n",fit.Va,fit.vuncert);
  fprintf(out,"   Rt = %5.3f +/- %6.4f\n",fit.Rt,fit.runcert);
  fprintf(out,"   V(Rt) = %5.2f\n",fit.Vr);
  fprintf(out,"   V offset = %5.3f\n",fit.voff);
  fprintf(out,"   R offset = %5.3f\n",fit.roff);
  fprintf(out,"   max V = %5.2f\n",fit.Vmax);
  fprintf(out,"   max R = %5.2f\n",fit.Rmax);
  fprintf(out,"   R coef = %6.4f\n",fit.RCoef);
  fprintf(out,"   Chi squared = %7.3f\n",fit.chisq);
  fprintf(out,"   Sqrt(chisq/N) = %5.3f\n",fit.errorbar);
  fprintf(out,"\n");


printf("            Va    V(Rt)    Rt    dv      dr
chisq\n");
printf ("%7s   %6.2f %6.2f %6.2f %6.2f %6.2f %6.4f  %5.3f  %6.2f  %6.2f
%6.2f\n",data.name, fit.Va, fit.Vr, fit.Rt, fit.voff, fit.roff,
         fit.RCoef, fit.Rmax, fit.Vmax, fit.chisq, fit.errorbar);
}

/*******************************************************************/
/* Function: WriteFitFile
 * Creates a file that is formatted as -- FitX, FitY, X, Y
 * This can then be read by a plotting program (like SM2) so that
 * one can plot the RC (X,Y) and the overlaying fit (FitX, FitY)
 ******************************************************************/
void WriteFitFile(fitData fit, galaxyData galaxy)
{

  FILE *fitout;
  float fitvalue;
  float q, p[4];
  int i= 1,s;
  char fitfile[MAX_STRING_LENGTH];

  sprintf(fitfile, "%s.fit", galaxy.name);
  fitout = OpenFile(fitfile, "w");
  p[1] = -fit.Va;
  p[2] = fit.Rt;
  p[3] = fit.voff;
  p[4] = fit.roff;
  fprintf(fitout,"  Rt      rnaught         Vc        vnaught\n");
  fprintf(fitout,"%5.2f      %5.2f       %6.2f       %5.2f\n",p[2],p[4],p[1],p[3]);
  fprintf(fitout,"\n\n");
  fprintf(fitout,"obs pos  obs vel  vel err  fit pos  fit vel\n");
  fprintf(fitout,"\n");

  for (q =-1*fit.Rmax;q<=fit.Rmax;q++)
    {
      fitvalue = ArctanFunct(p, q);
      if (i <= nlines-3) {
fprintf (fitout, "%6.2f   %7.2f  %6.2f   %6.2f   %7.2f\n",
```

```
-1*Curve.position[i]+fit.roff, Curve.velocity[i]-fit.voff, Curve.dv[i],
-1*q+fit.roff, fitvalue-fit.voff); }
      else {
fprintf (fitout, "%6.2f   %7.2f  %6.2f   %6.2f   %7.2f\n",
-1*Curve.position[i], Curve.velocity[i], Curve.dv[i], -1*q+fit.roff, fitvalue-fit.voff); }

      i++;
    } /* of for */

  if (i - 1 <= Curve.ndata)
    {
      for (s = 1;s<nlines - i-1;s++) {
fprintf (fitout, "%6.2f   %7.2f  %6.2f\n",-1*Curve.position[s+i-1]+
fit.roff,Curve.velocity[s+i-1]-fit.voff,Curve.dv[s+i-1]);
      }
    }

}

/*******************************************************************/
void MakeIdentityMatrix(float **A, int n)
{
  int i, j;
  for (i=1;i<=n;i++)
    for (j=1;j<n;j++) {
      A[i][j] = 0;
      if (i==j) A[i][j] = 1;
    }
}
/******************************************************************/

float ArctanFunct(float p[], float x)
{
return ((2*p[1]/PI)*atan((x-p[4])/p[2]) + p[3]);
}

/******************************************************************/

float TwoDArctan(float pNew[], float x)
{
return ((2*vnaught/PI)*atan((x - pNew[2])/rnaught) + pNew[1]);
}

/******************************************************************/
float DimensionlessArctan(float ptwo[], float x)
{
return ((2*(1 + ptwo[1])/PI)*atan((x - ptwo[4])/((1 + ptwo[2])*rtmax)) + ptwo[3]/vamax);
}

/******************************************************************/
/* Function: GetChiSquared
 * returns the chisquared of the arctan fit.   This function is
 * passed to powell so that it can be minimized with respect to the
 * parameters in p
 *******************************************************************/

float GetChiSquared(float p[])
{
float x, delta, obsvalue, fitvalue, rerr;
float RMS, chisq;
int i,s;
chisq = 0;
for (i=1; i<Curve.ndata-2; i++) {
  /*printf("%i\n",i);*/
  x = Curve.position[i];
  obsvalue = Curve.velocity[i];
  delta = Curve.dv[i];
  rerr = Curve.dr[i];
```

```
  fitvalue = ArctanFunct(p, x);
  RMS = (fitvalue - obsvalue)*(fitvalue - obsvalue)*fabs(x) / (delta*delta);
  chisq = chisq + RMS; }
count++;
/*printf("Chisq is %f, loop # %i\n",chisq,count);
for (s = 1;s<5;s++) {
  printf("p[i] is %f  ",p[s]);
}
printf("\n");*/
return chisq;
}


float DimlessChiSquared(float p[])
{
float x, delta, obsvalue, fitvalue, rerr;
float RMS, chisq;
int i,s;
chisq = 0;
for (i=1; i<Curve.ndata-2; i++) {
  /*printf("%i\n",i);*/
  x = Curve.position[i];
  obsvalue = Curve.velocity[i]/vamax;
  delta = Curve.dv[i]/vamax;
  rerr = Curve.dr[i];
  fitvalue = DimensionlessArctan(p, x);
  RMS = (fitvalue - obsvalue)*(fitvalue - obsvalue)*fabs(x) / (delta*delta);
  chisq = chisq + RMS; }
count++;
/*printf("Chisq is %f, loop # %i\n",chisq,count);
for (s = 1;s<5;s++) {
  printf("p[i] is %f  .",p[s]);
}
printf("\n");*/
return chisq;
}

/****************************************************************/
/* Function: TwoDChiSquared
****************************************************************/

float TwoDChiSquared(float ptwo[])
{
float x, delta, obsvalue, fitvalue, rerr;
float RMS, TwoDchisq;
int i,s;
TwoDchisq = 0;
for (i=1; i<Curve.ndata-2; i++) {
  x = Curve.position[i];
  obsvalue = Curve.velocity[i];
  delta = Curve.dv[i];
  rerr = Curve.dr[i];
  fitvalue = TwoDArctan(ptwo,x);
  /*if (i == 50) {
    printf("Vnaught %f, rnaught %f, dv %f, dr %f\n",vnaught,rnaught,ptwo[1],ptwo[2]); }*/
  RMS = (fitvalue - obsvalue)*(fitvalue - obsvalue) / (delta*delta);
  TwoDchisq = TwoDchisq + RMS; }
/*printf("Chisq is %f\n",TwoDchisq);
for (s = 1;s<3;s++) {
  printf("ptwo[i] is %f  ",ptwo[s]);
}
printf("\n");*/
return TwoDchisq;
}
```

```
/*************************************************************/
/* Function: GetNumberOfLines
 * returns the number of lines in a file.  Used to get the
 * number of data points in the RC.
 ***********************************************************/
int GetNumberOfLines(FILE *in)
{
char ch;
int n = 0;

rewind(in);
ch = getc(in);
while (ch!=EOF) {
  while (ch!='\n') {
    ch=getc(in);}
  n++;
  ch = getc(in); }
rewind(in);
return n;
}
```

Appendix C

Rotation Curves

Here is the compilation of my comparisons to Stéphane Courteau's RC reductions and fits. All 240 galaxies are represented. Courteau's data are the dark points and curves, and mine are the light ones.

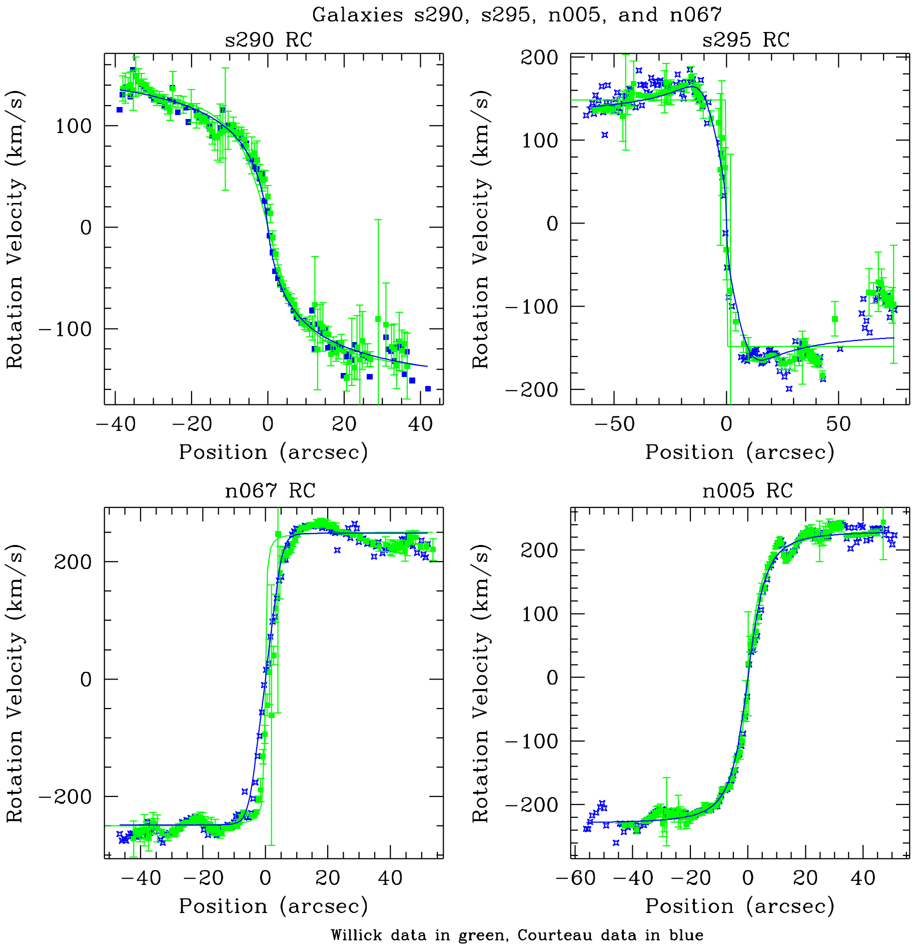

Figure C.1: Rotation curves from Oct 96 Kitt Peak run - 10/14

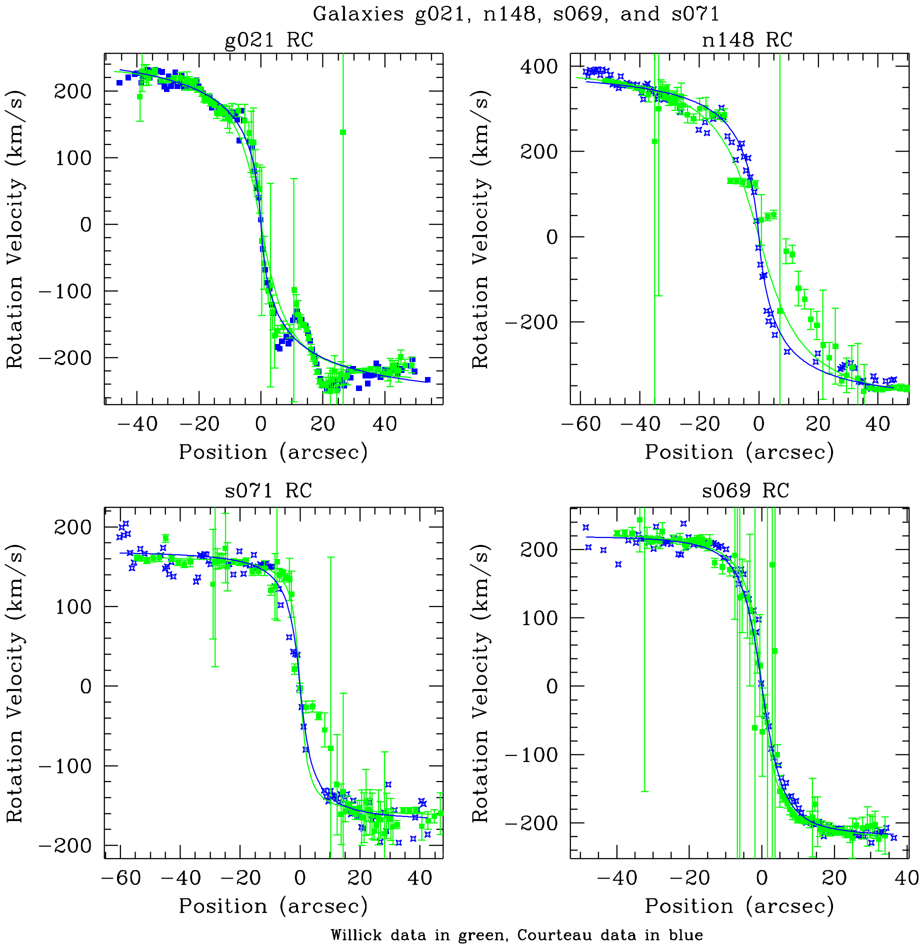

Figure C.2: Rotation curves from Oct 96 Kitt Peak run - 10/14

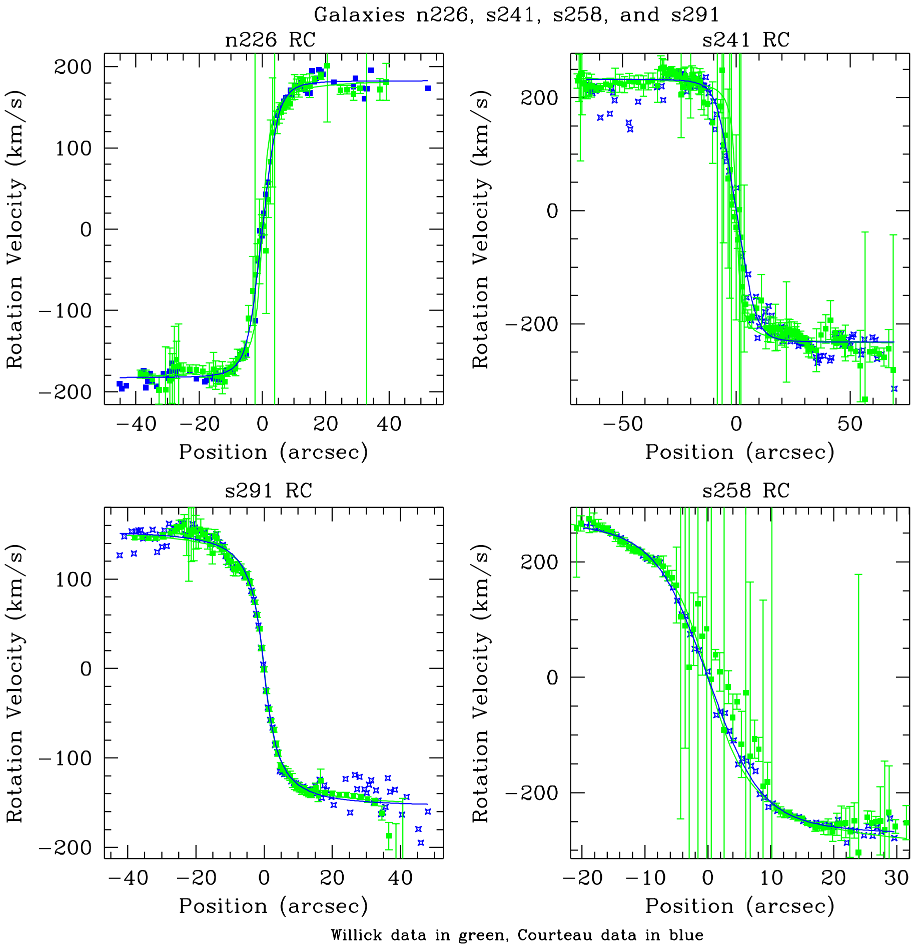

Figure C.3: Rotation curves from Oct 96 Kitt Peak run - 10/14-15

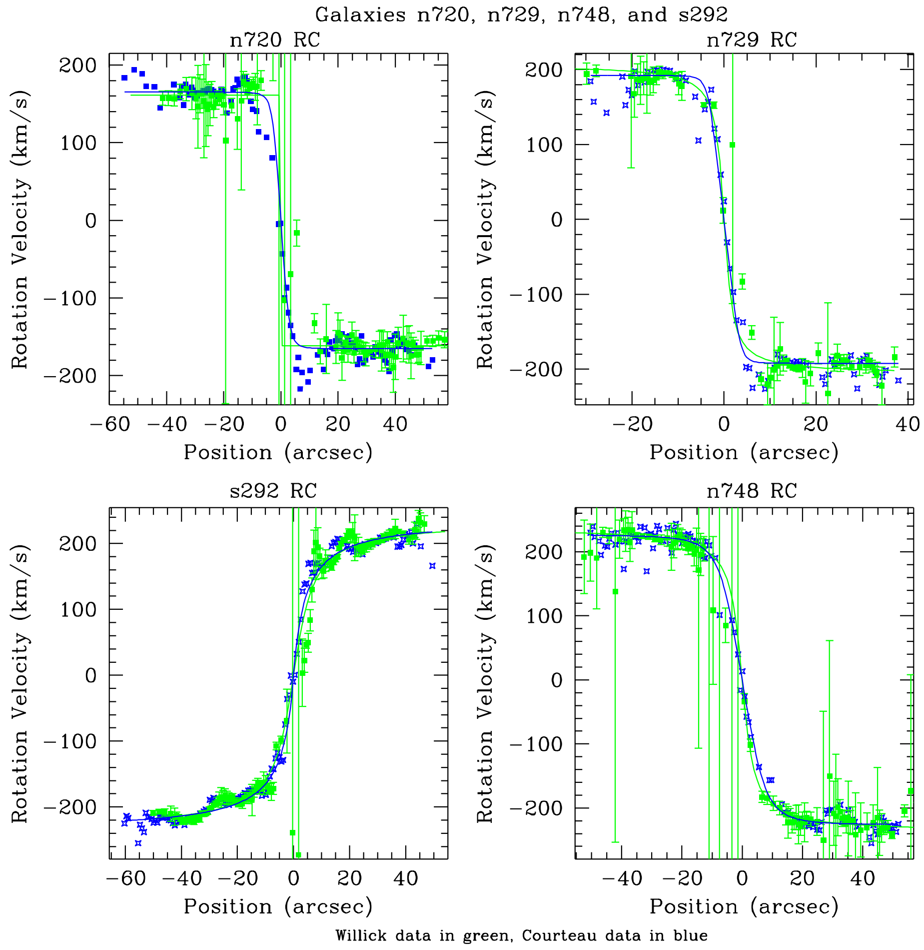

Figure C.4: Rotation curves from Oct 96 Kitt Peak run - 10/15

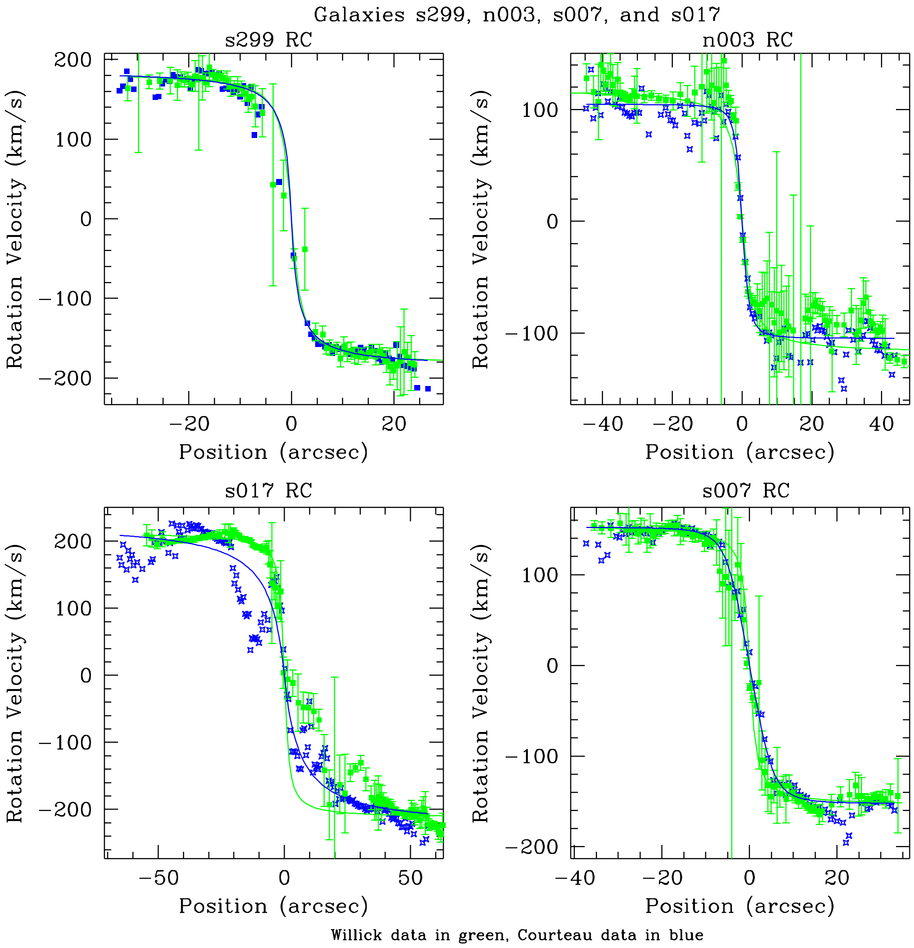

Figure C.5: Rotation curves from Oct 96 Kitt Peak run - 10/15

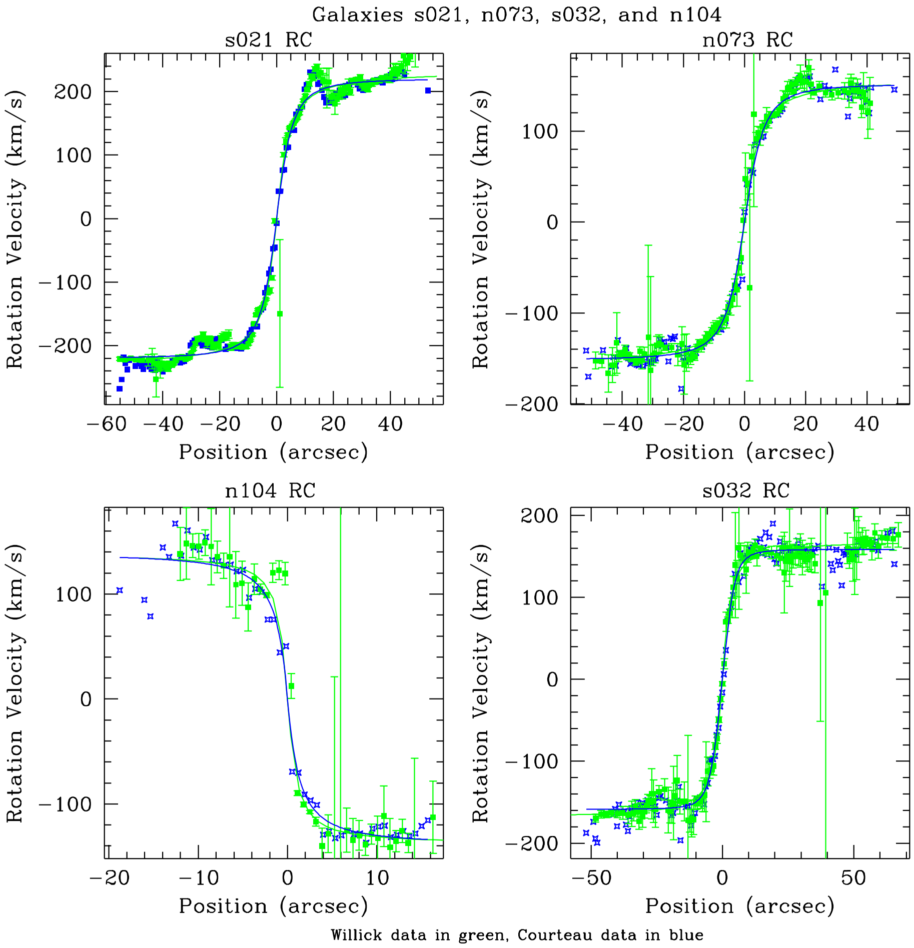

Figure C.6: Rotation curves from Oct 96 Kitt Peak run - 10/15

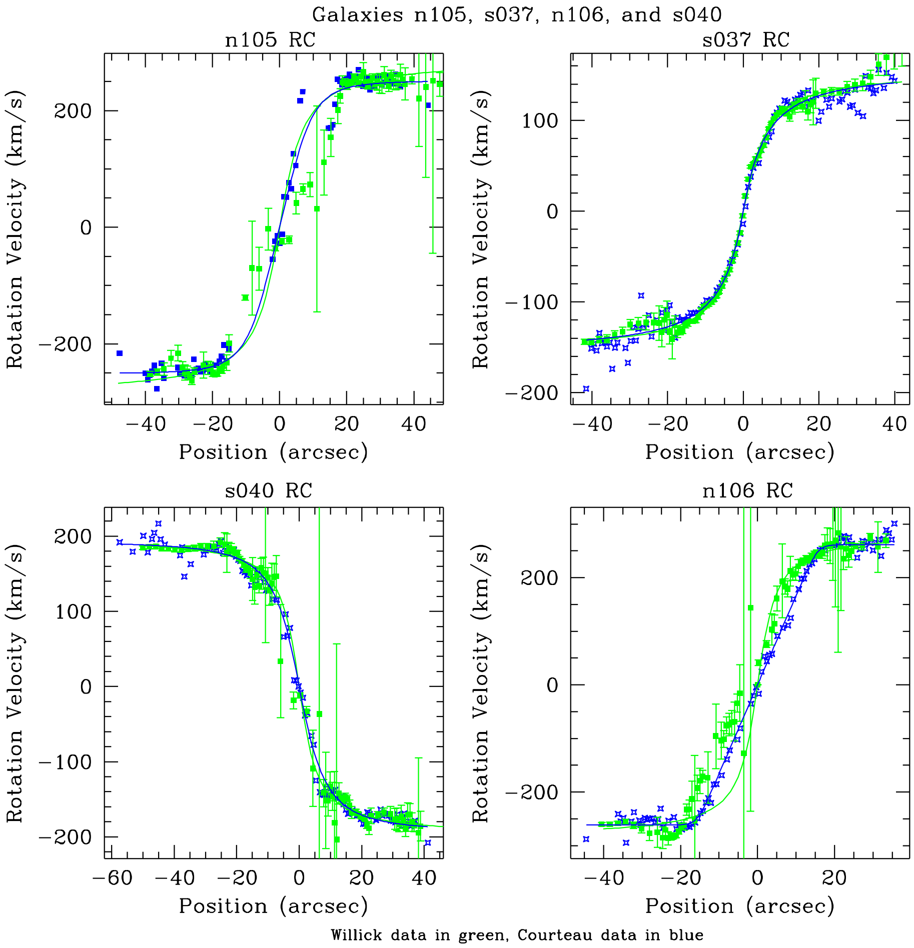

Figure C.7: Rotation curves from Oct 96 Kitt Peak run - 10/15

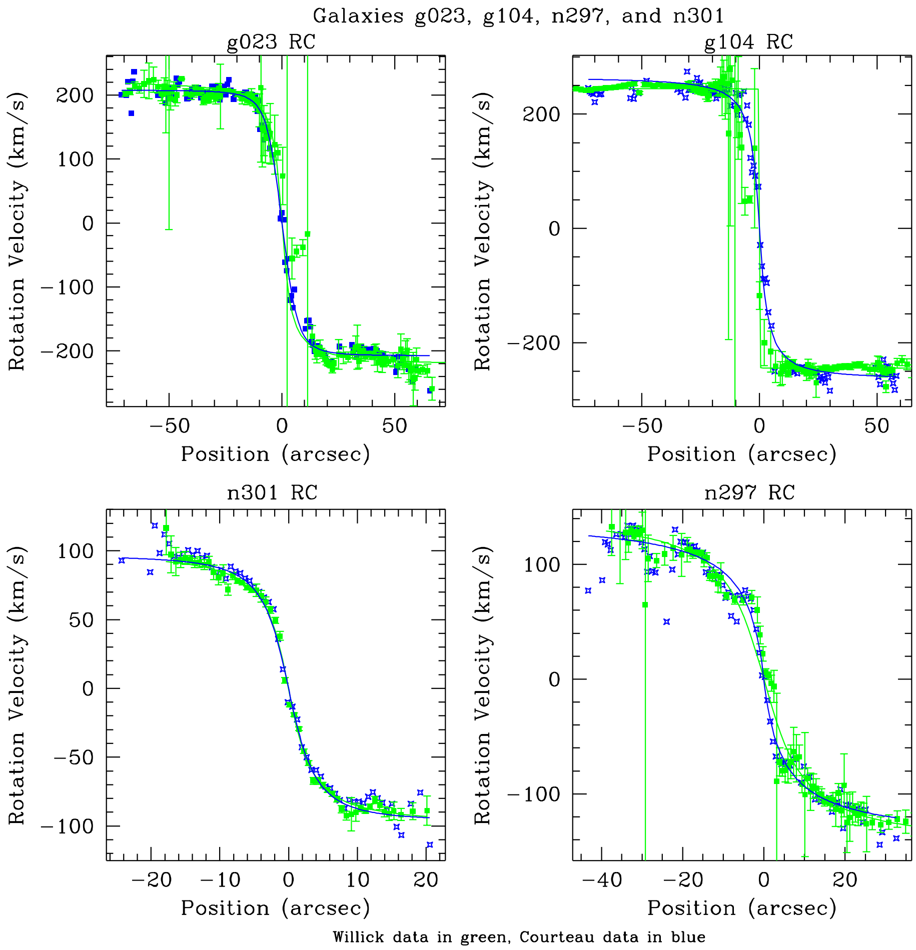

Figure C.8: Rotation curves from Oct 96 Kitt Peak run - 10/15

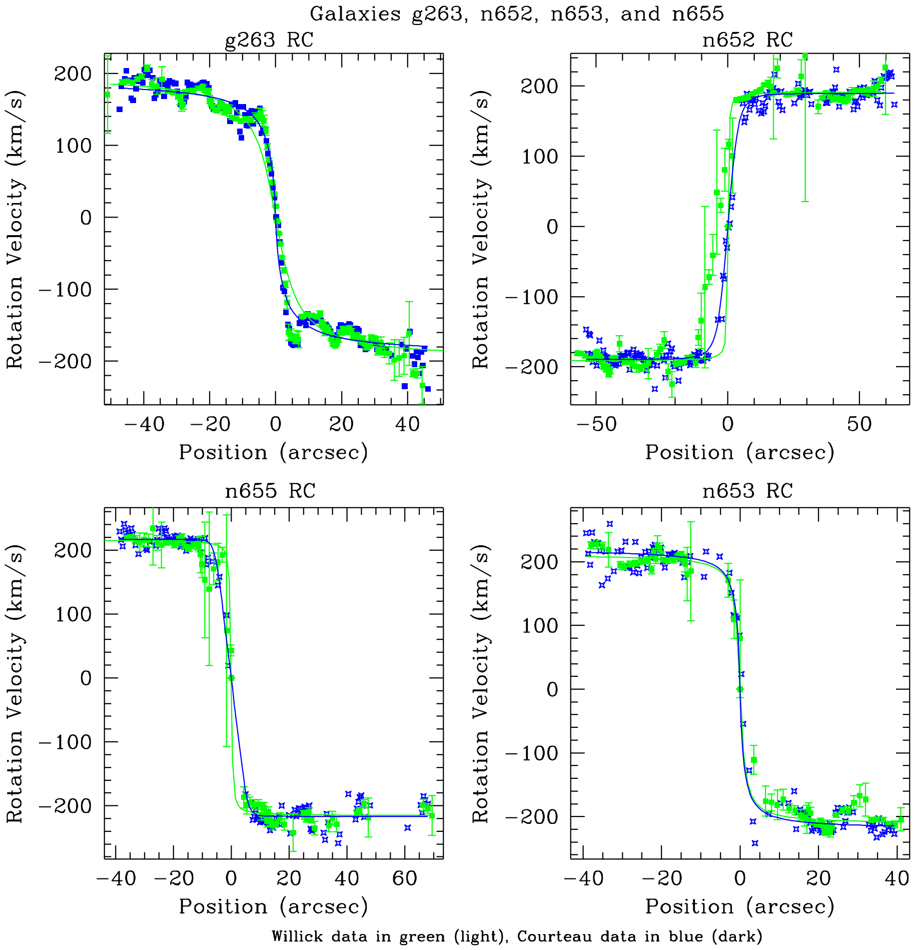

Figure C.9: Rotation curves from Oct 96 CTIO run - 10/16

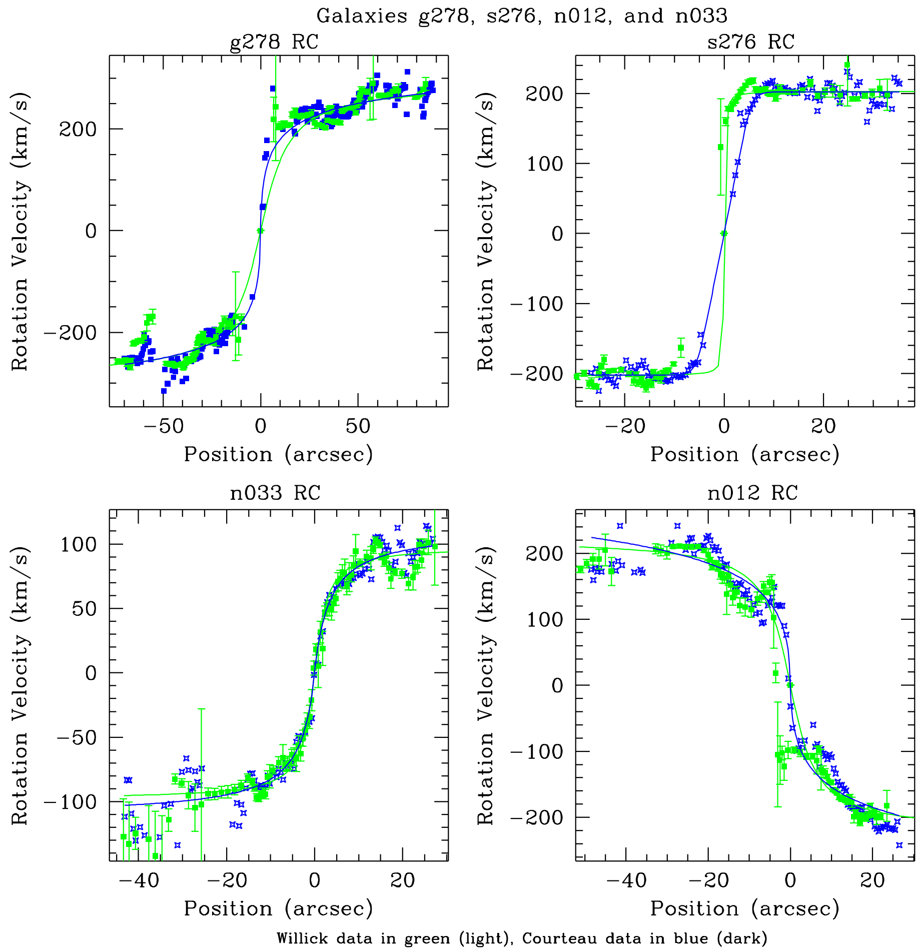

Figure C.10: Rotation curves from Oct 96 CTIO run - 10/16

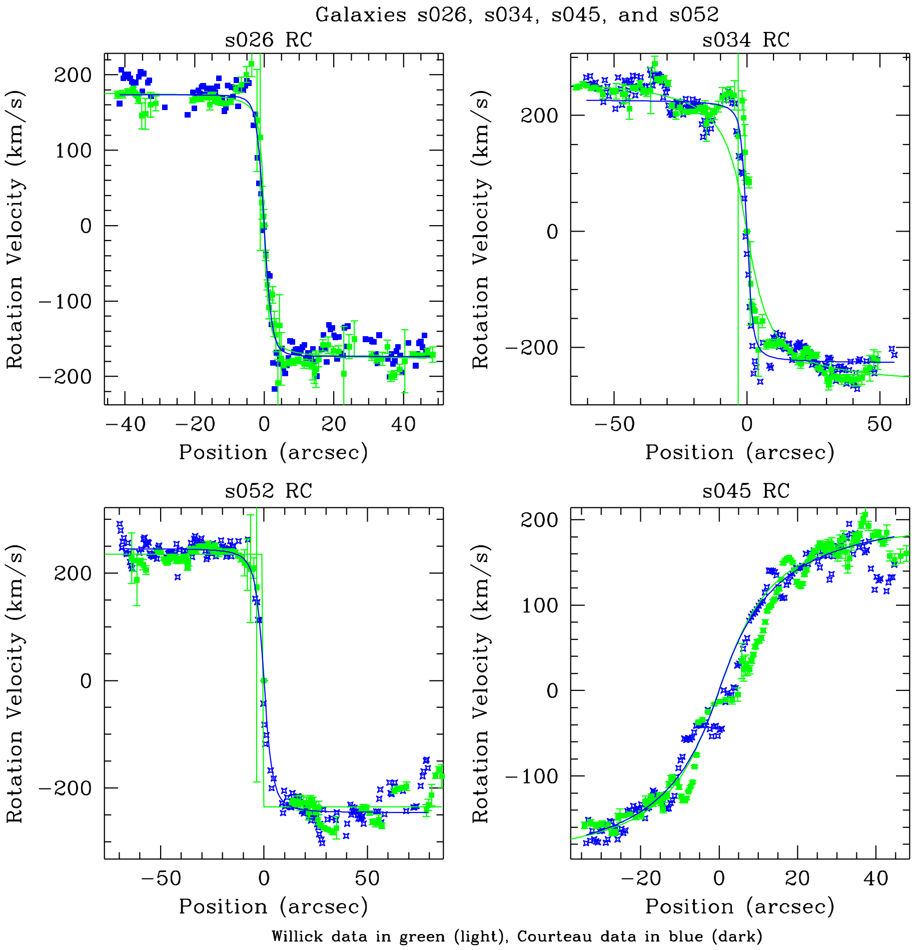

Figure C.11: Rotation curves from Oct 96 CTIO run - 10/16

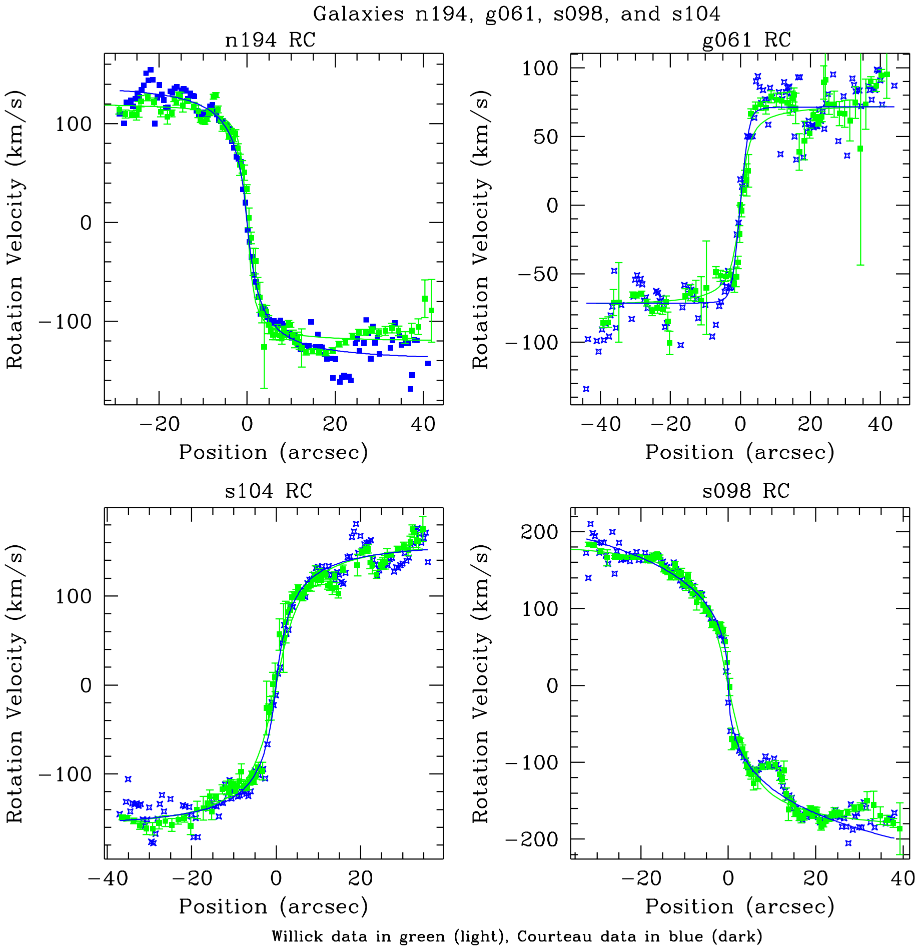

Figure C.12: Rotation curves from Oct 96 CTIO run - 10/16

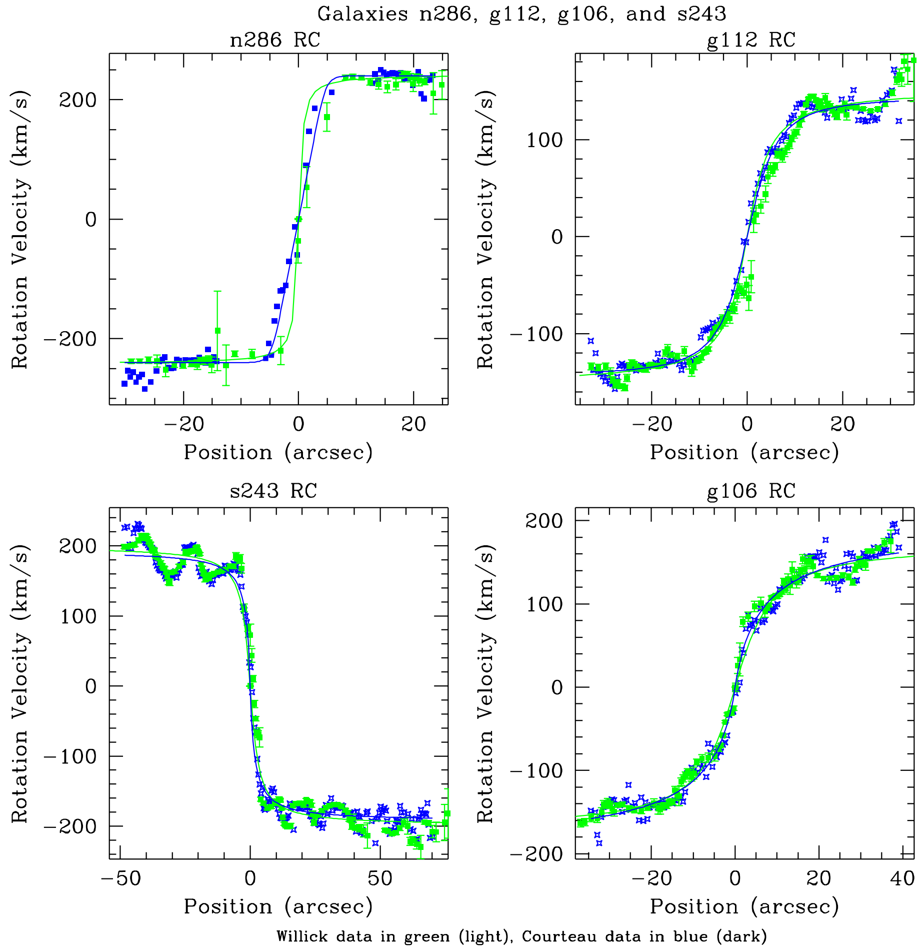

Figure C.13: Rotation curves from Oct 96 CTIO run - 10/16-17

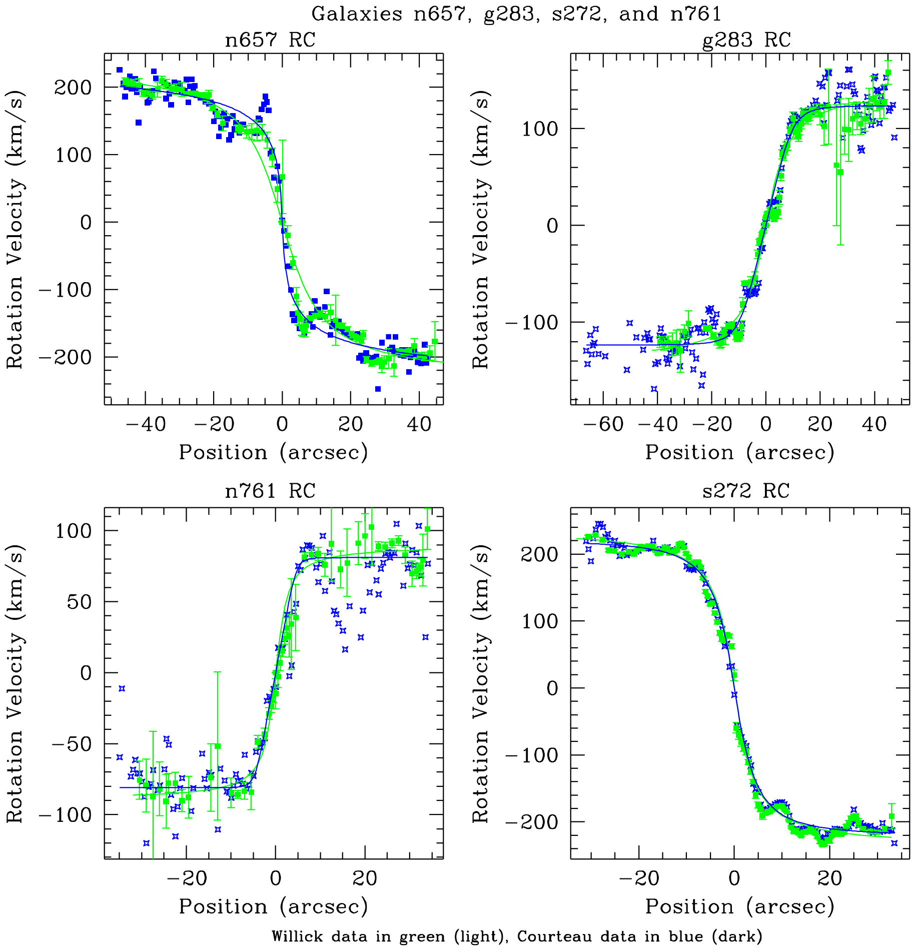

Figure C.14: Rotation curves from Oct 96 CTIO run - 10/17

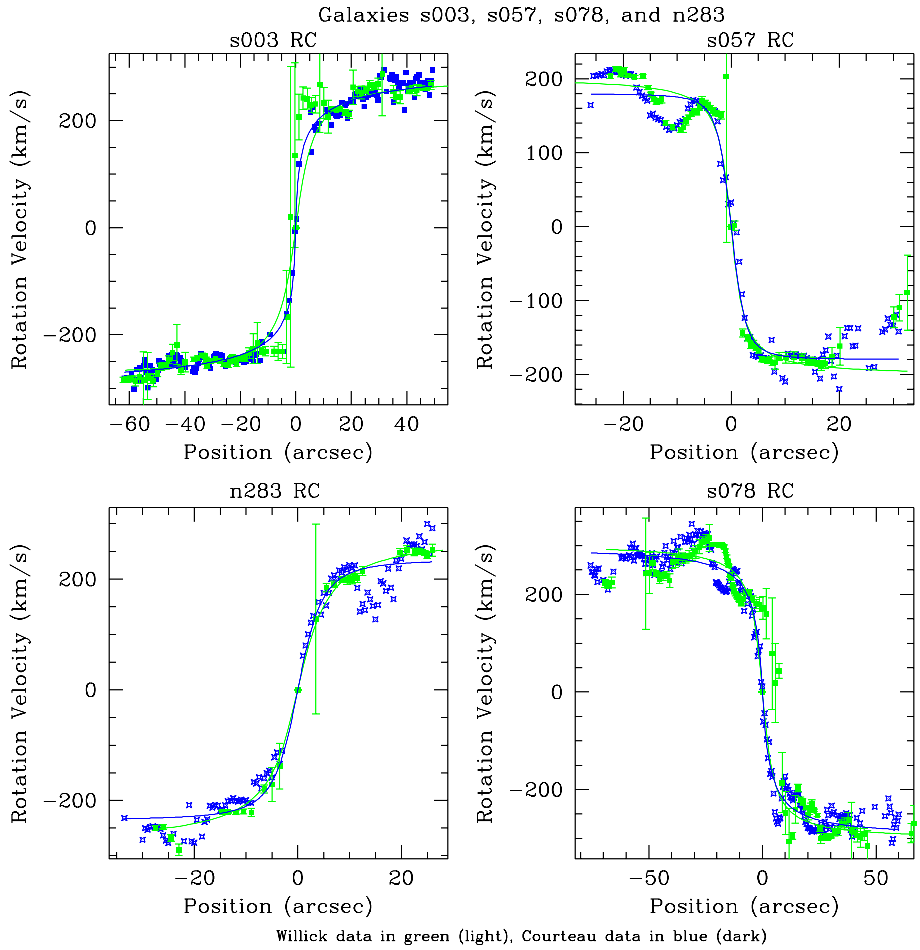

Figure C.15: Rotation curves from Oct 96 CTIO run - 10/17

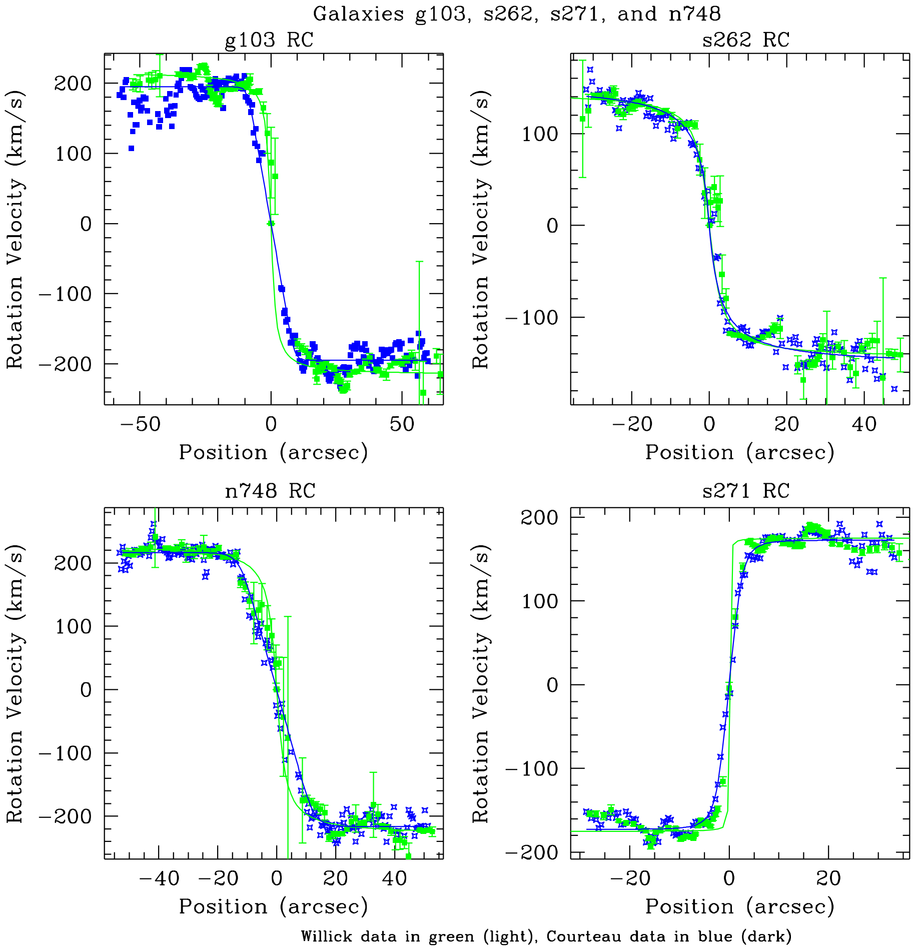

Figure C.16: Rotation curves from Oct 96 CTIO run - 10/17-18

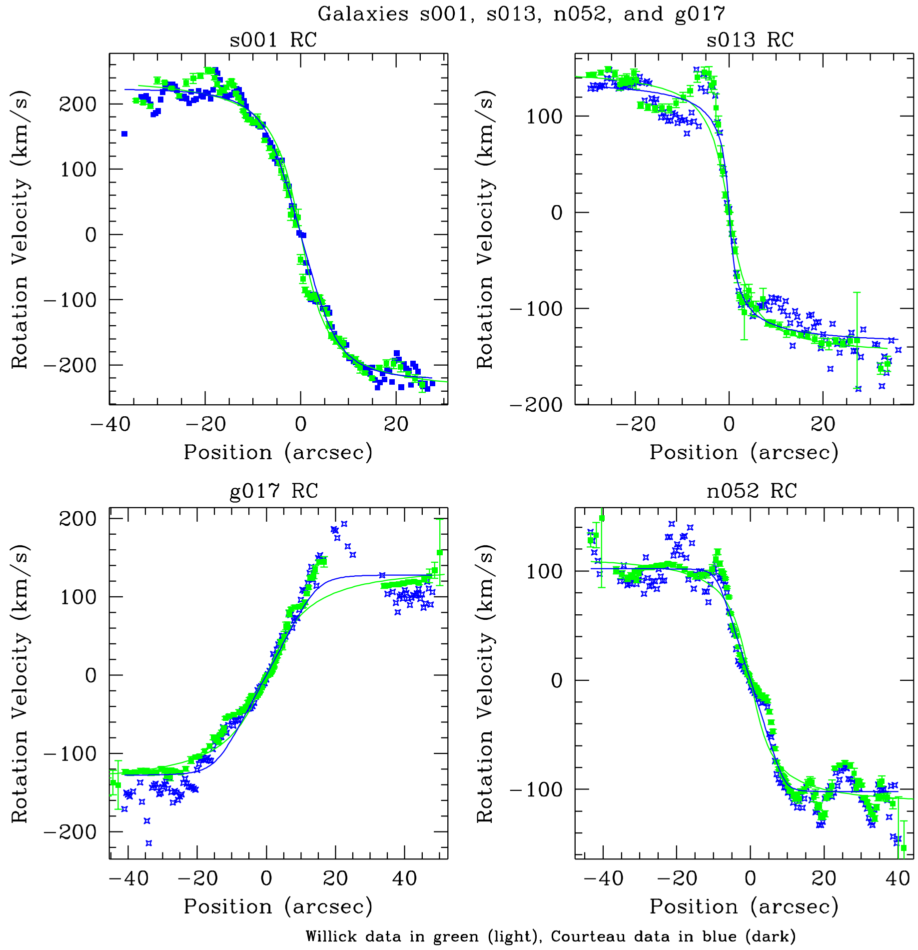

Figure C.17: Rotation curves from Oct 96 CTIO run - 10/18

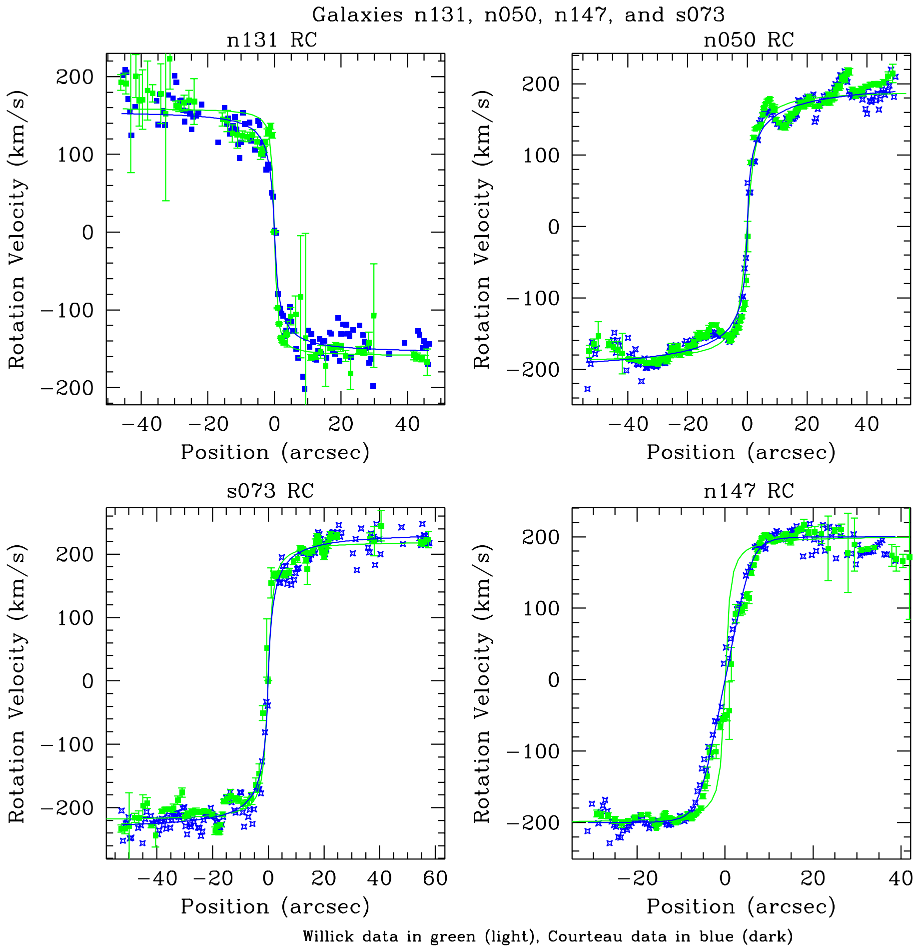

Figure C.18: Rotation curves from Oct 96 CTIO run - 10/18

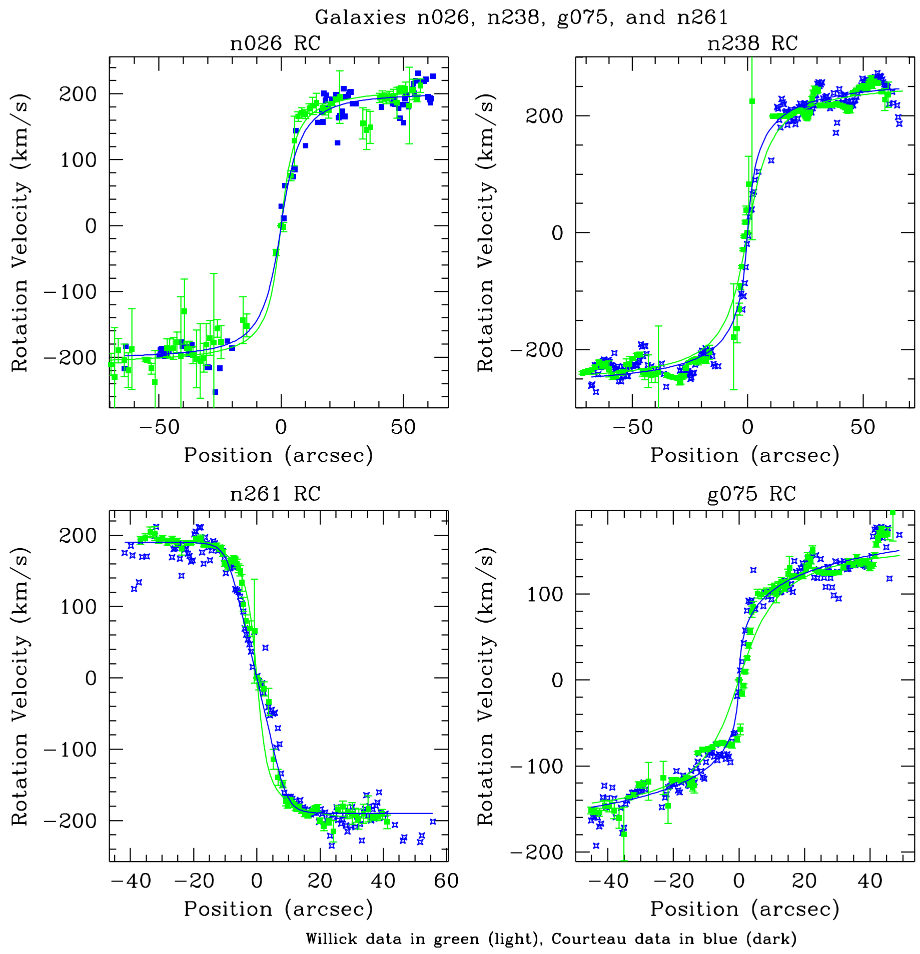

Figure C.19: Rotation curves from Oct 96 CTIO run - 10/18

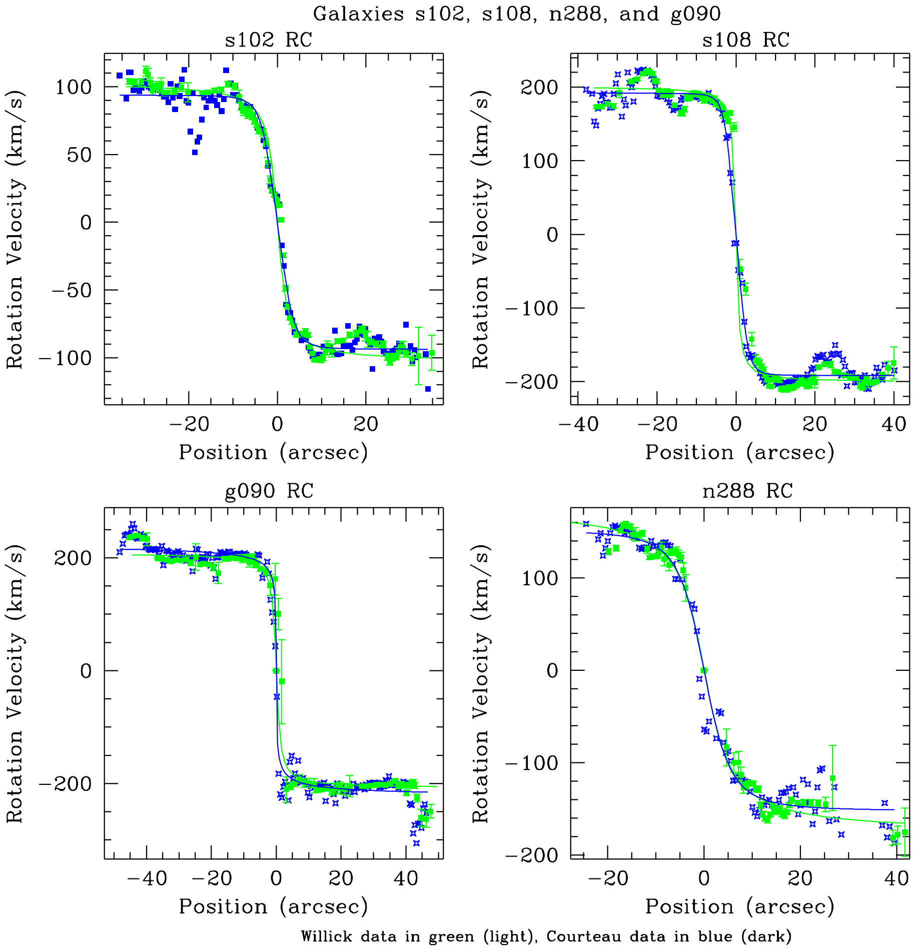

Figure C.20: Rotation curves from Oct 96 CTIO run - 10/18

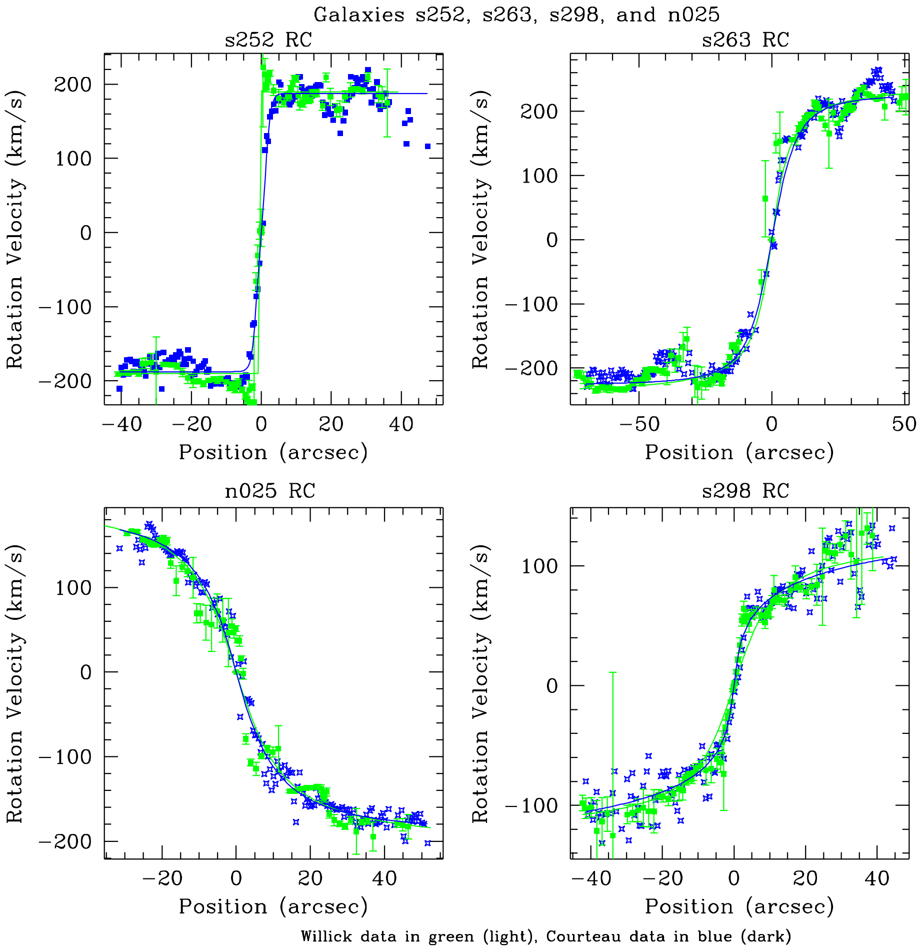

Figure C.21: Rotation curves from Oct 96 CTIO run - 10/19

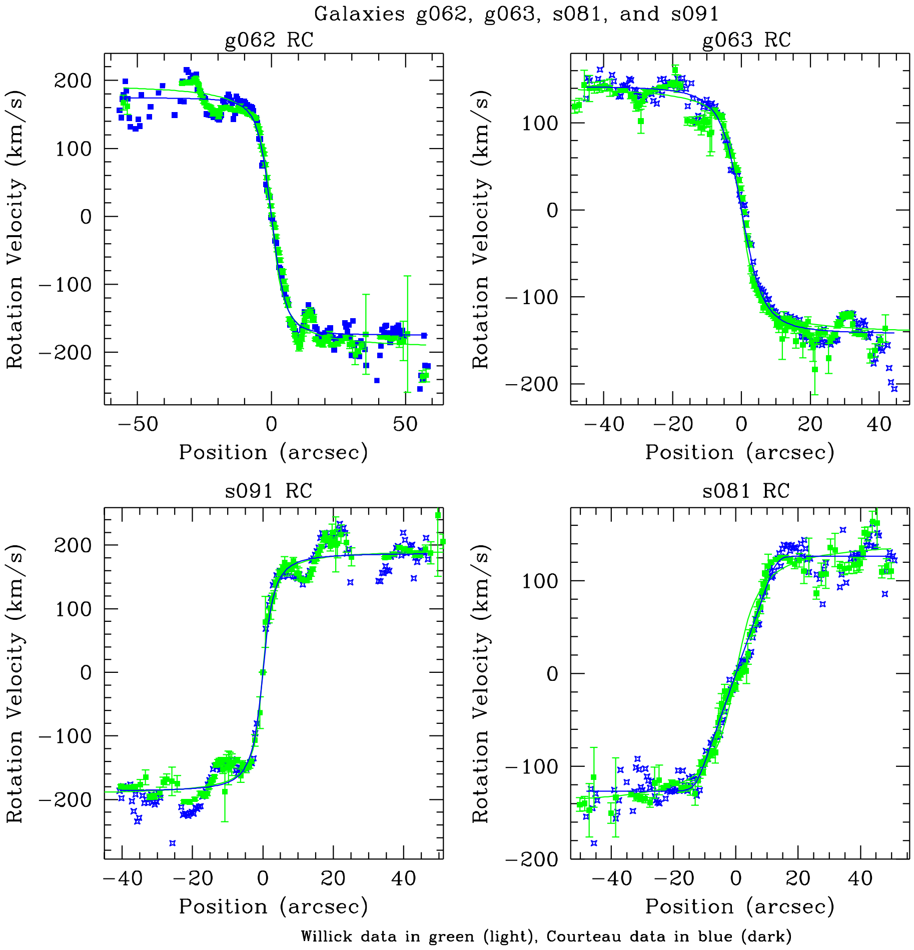

Figure C.22: Rotation curves from Oct 96 CTIO run - 10/19

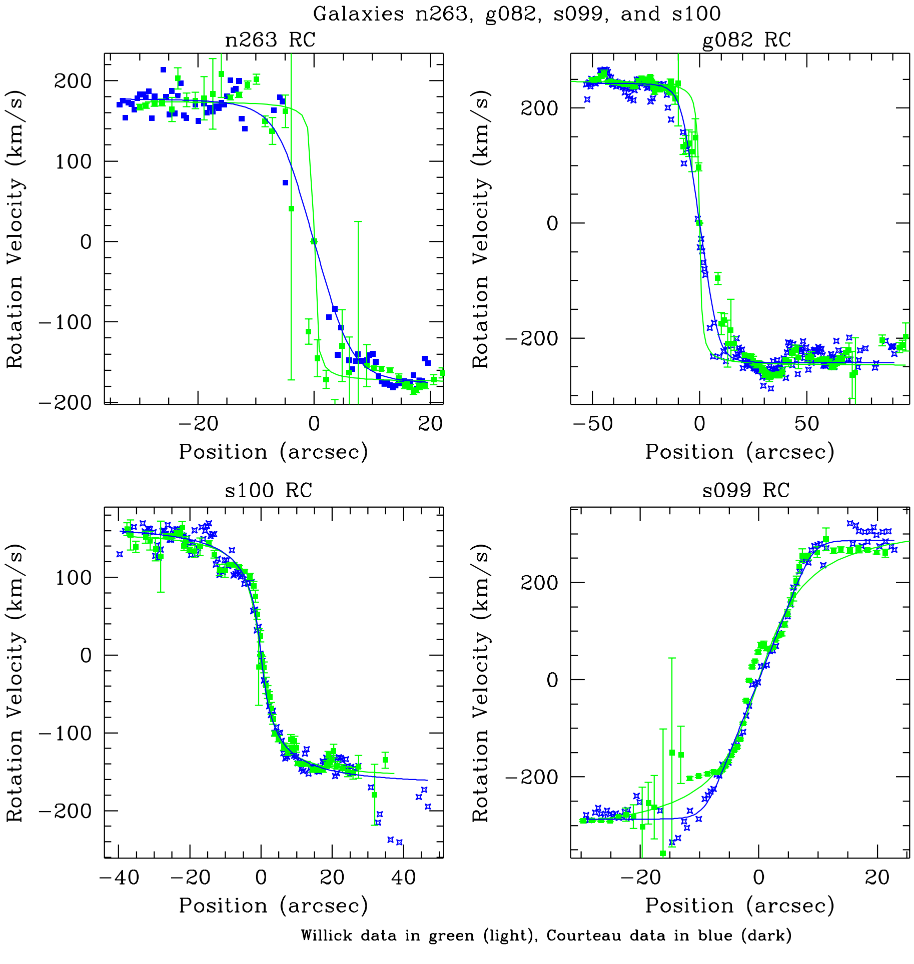

Figure C.23: Rotation curves from Oct 96 CTIO run - 10/19

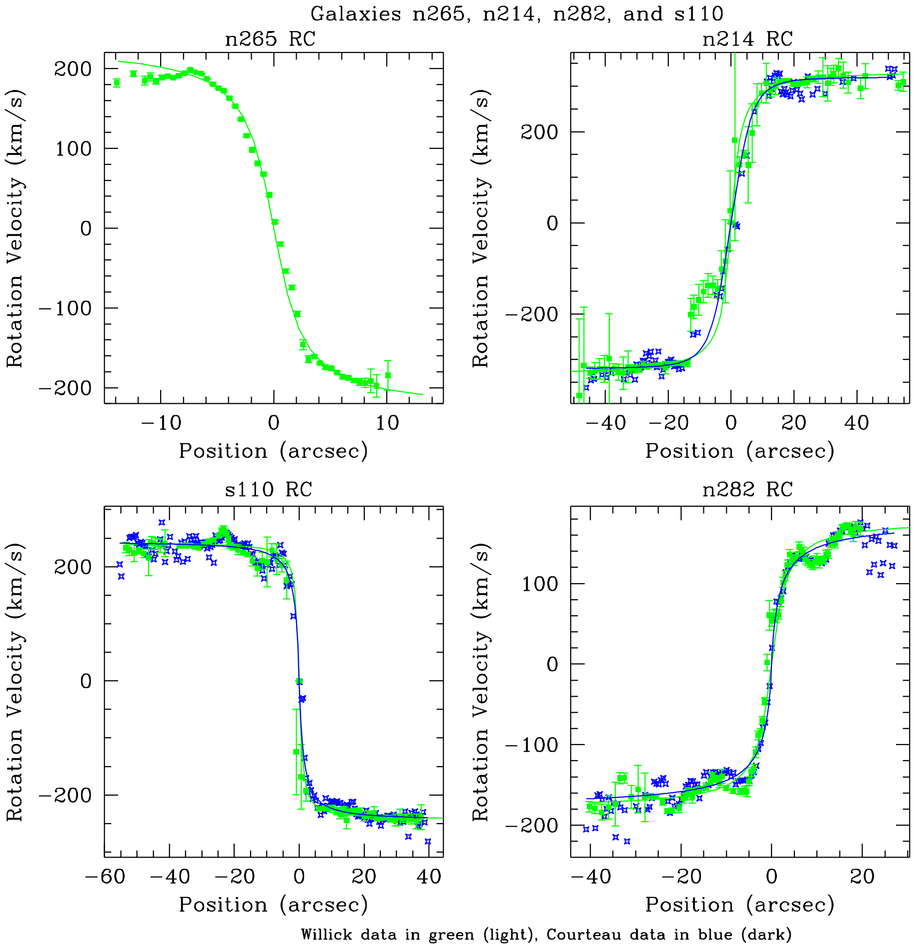

Figure C.24: Rotation curves from Oct 96 CTIO run - 10/19 Note: I don't have Courteau data for n265

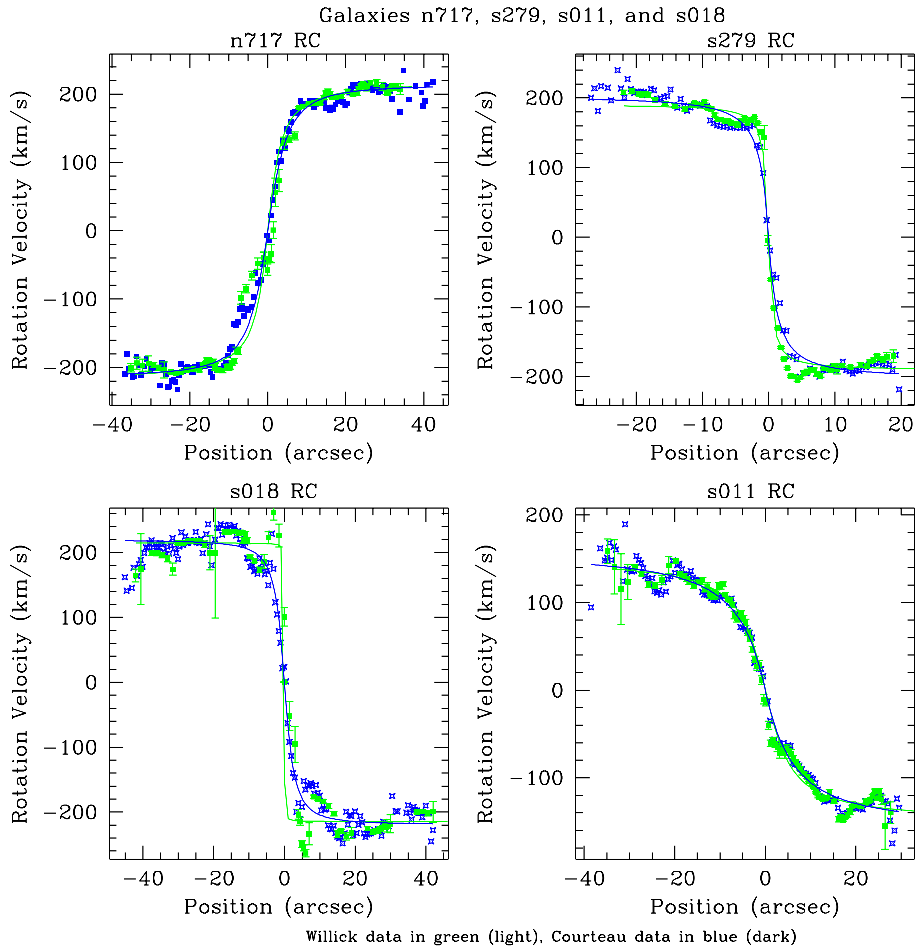

Figure C.25: Rotation curves from Oct 96 CTIO run - 10/20 Note: I think the galaxy labeled n717 is actually n171 - there was a mistake in the observing log

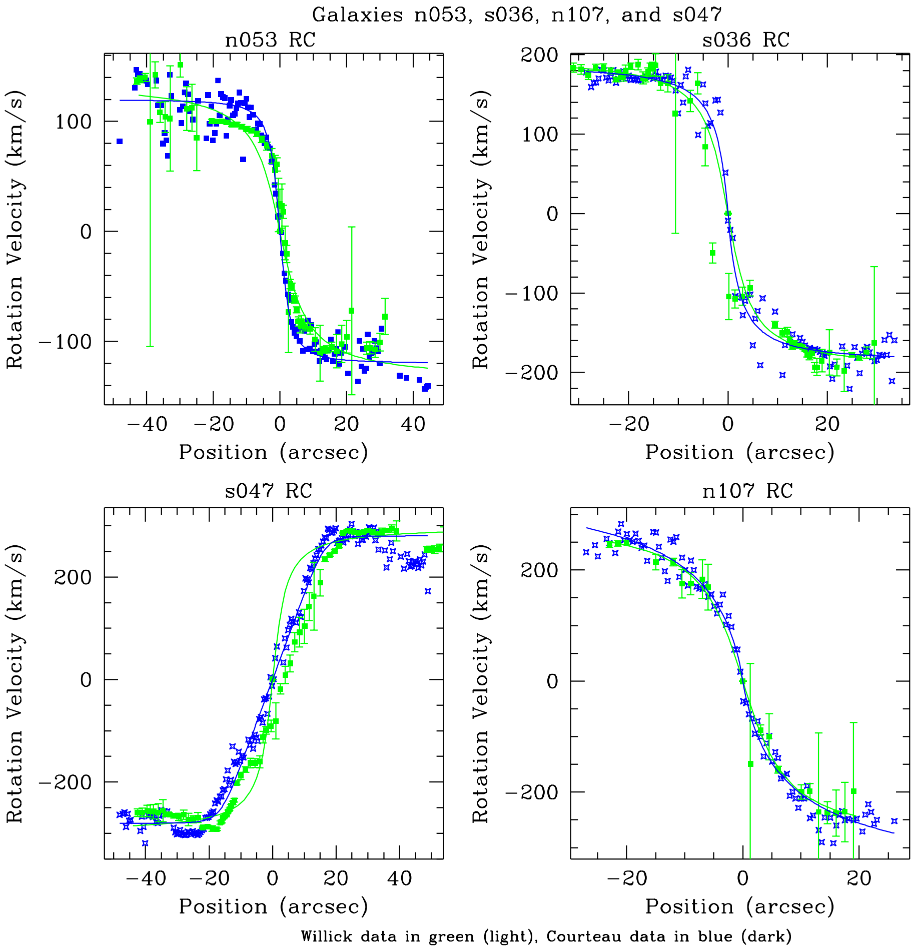

Figure C.26: Rotation curves from Oct 96 CTIO run - 10/20

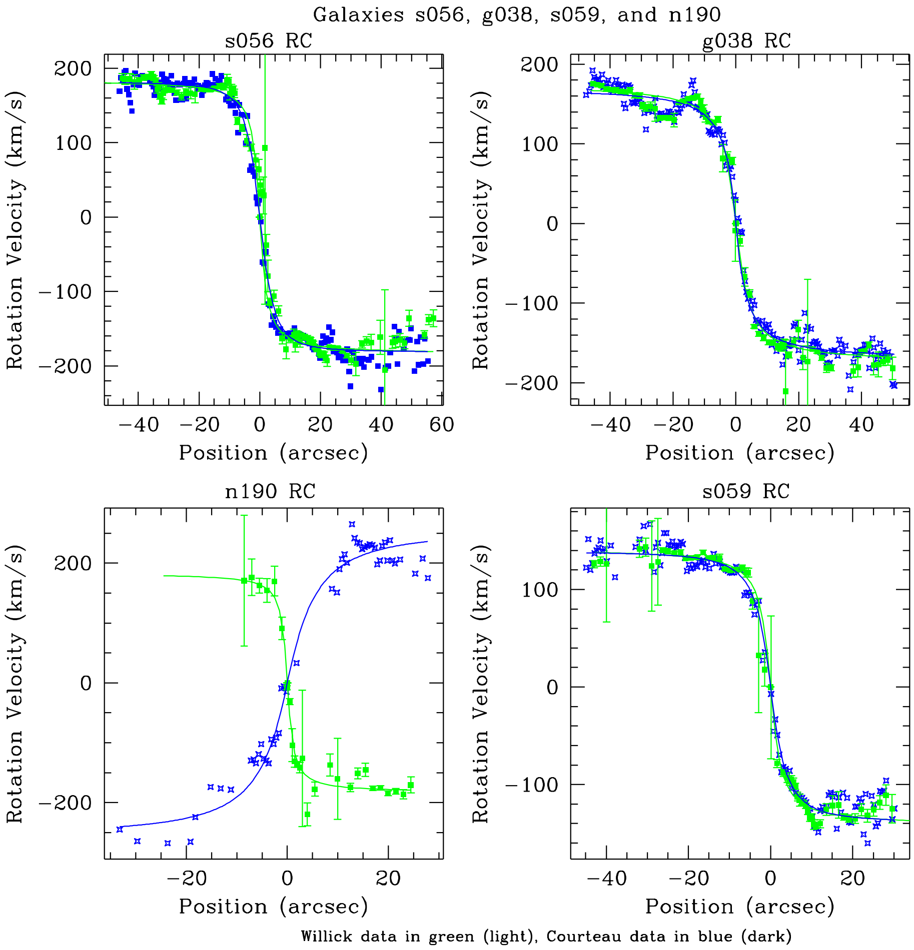

Figure C.27: Rotation curves from Oct 96 CTIO run - 10/20 Note: Willick's n190 and Courteau's n190 don't match, I'm not sure why

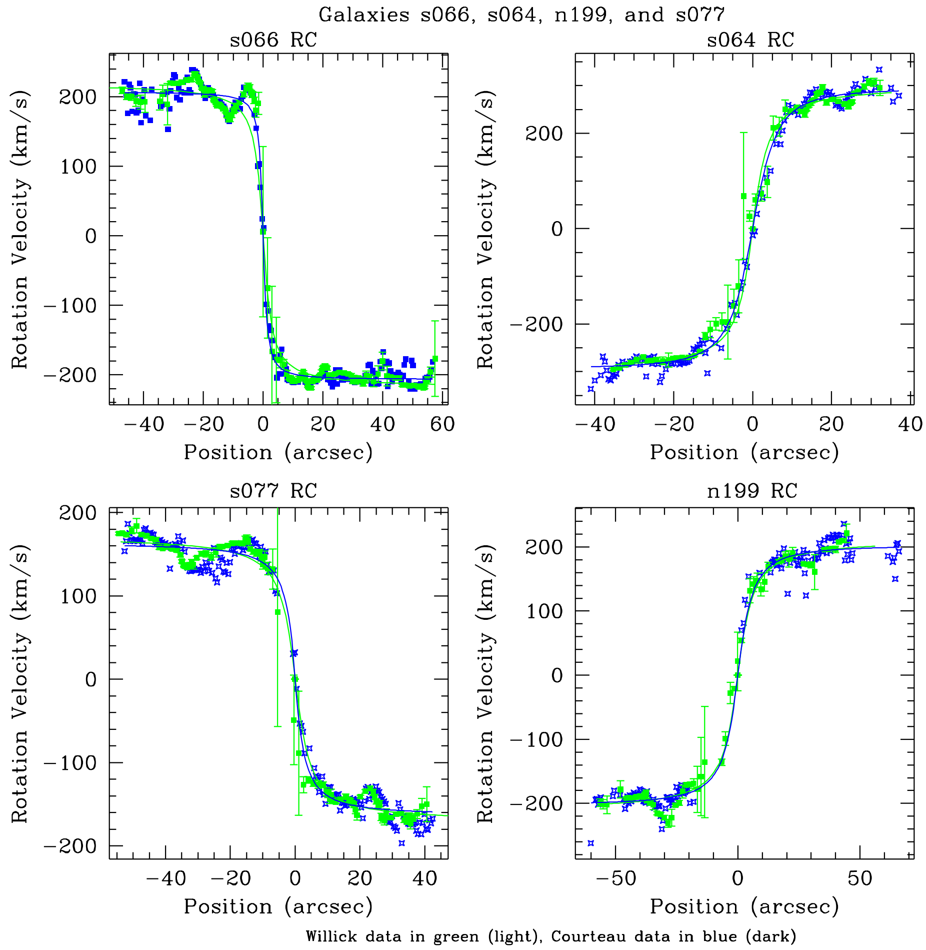

Figure C.28: Rotation curves from Oct 96 CTIO run - 10/20

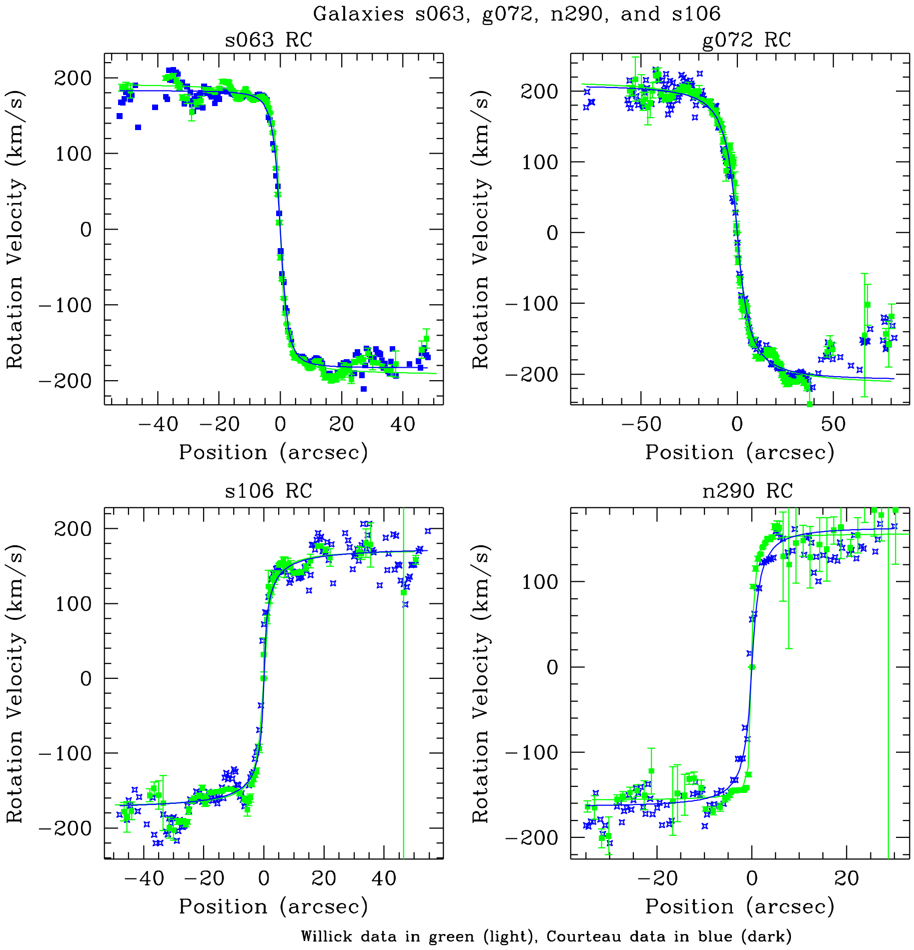

Figure C.29: Rotation curves from Oct 96 CTIO run - 10/20

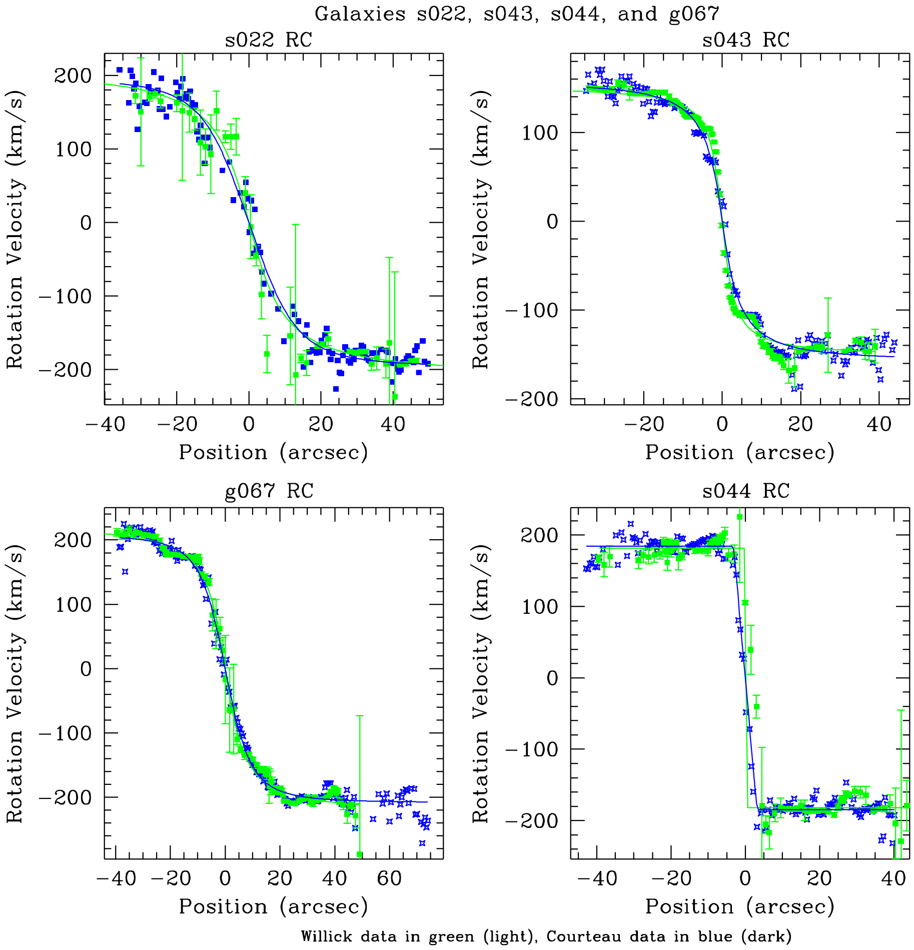

Figure C.30: Rotation curves from Oct 96 CTIO run - 10/21

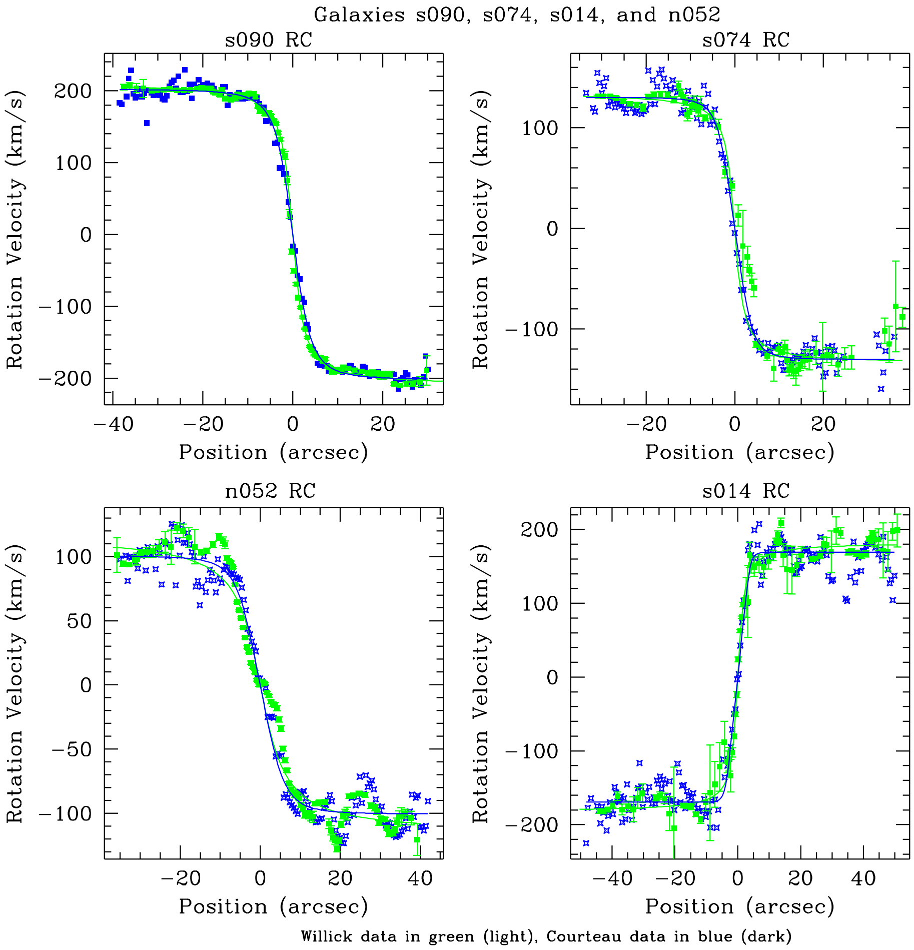

Figure C.31: Rotation curves from Oct 96 CTIO run - 10/21

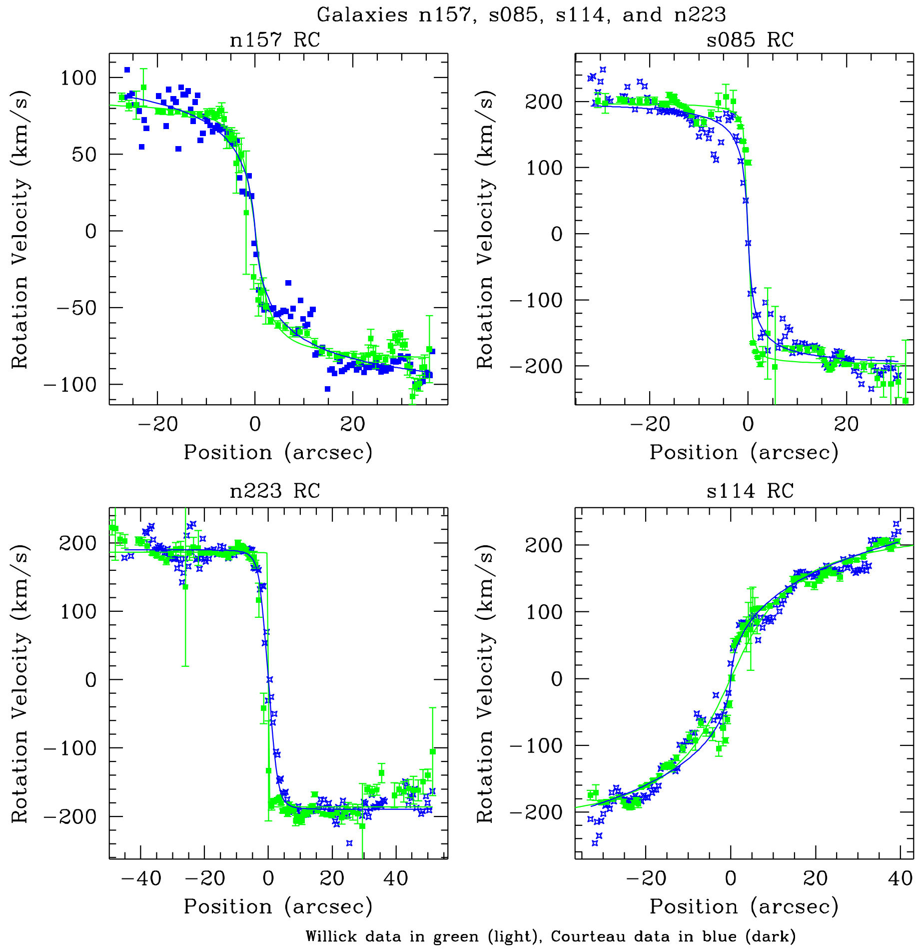

Figure C.32: Rotation curves from Oct 96 CTIO run - 10/21

Galaxy s095

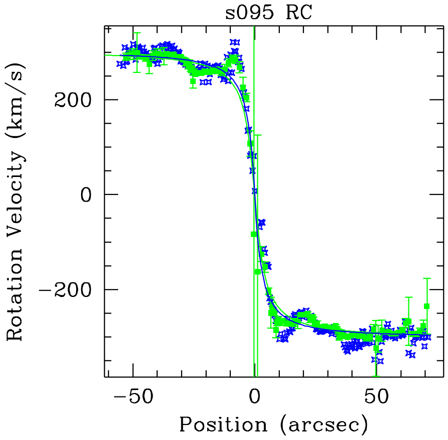

Willick data in green, Courteau data in blue

Figure C.33: Rotation curves from Oct 96 CTIO run - 10/21

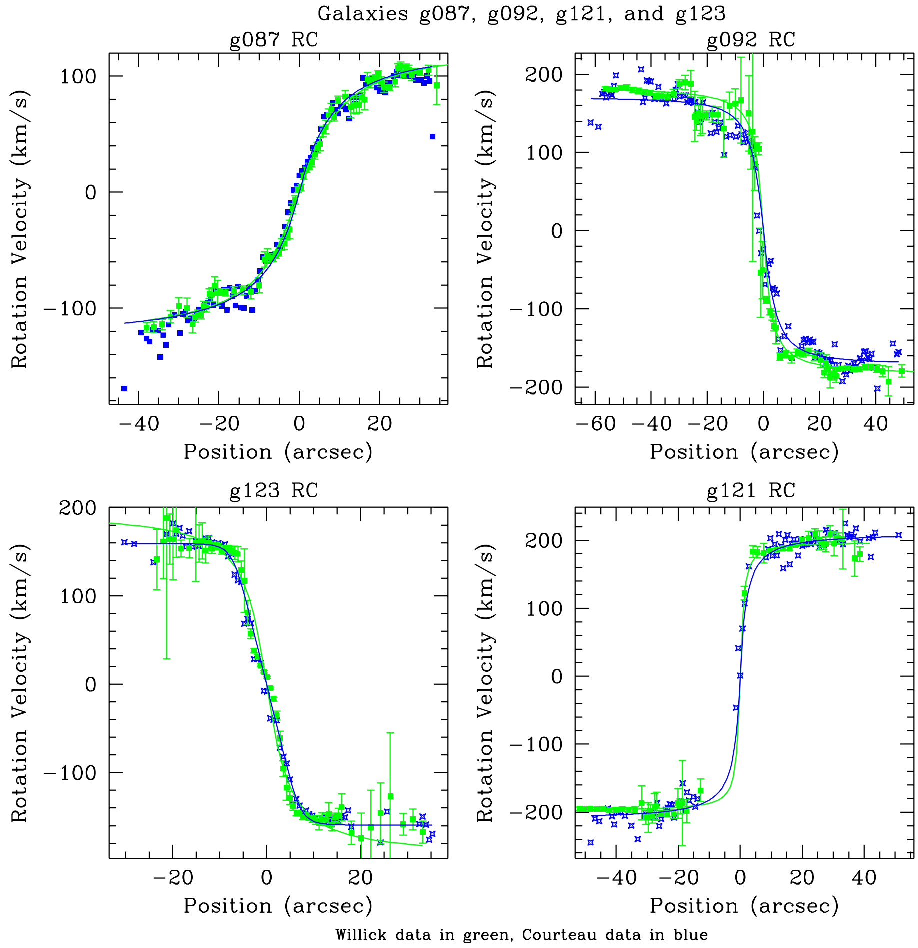

Figure C.34: Rotation curves from Mar 97 Kitt Peak run - 3/4

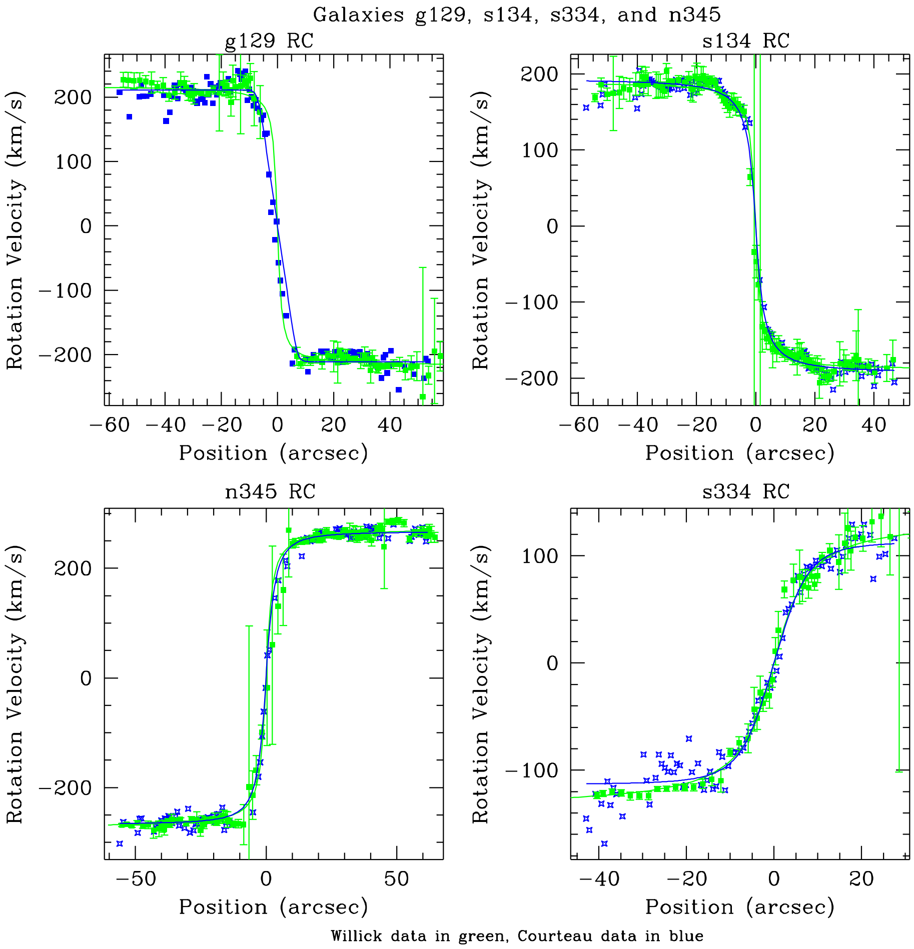

Figure C.35: Rotation curves from Mar 97 Kitt Peak run - 3/4 Note: s334 is called n334 on the observing log

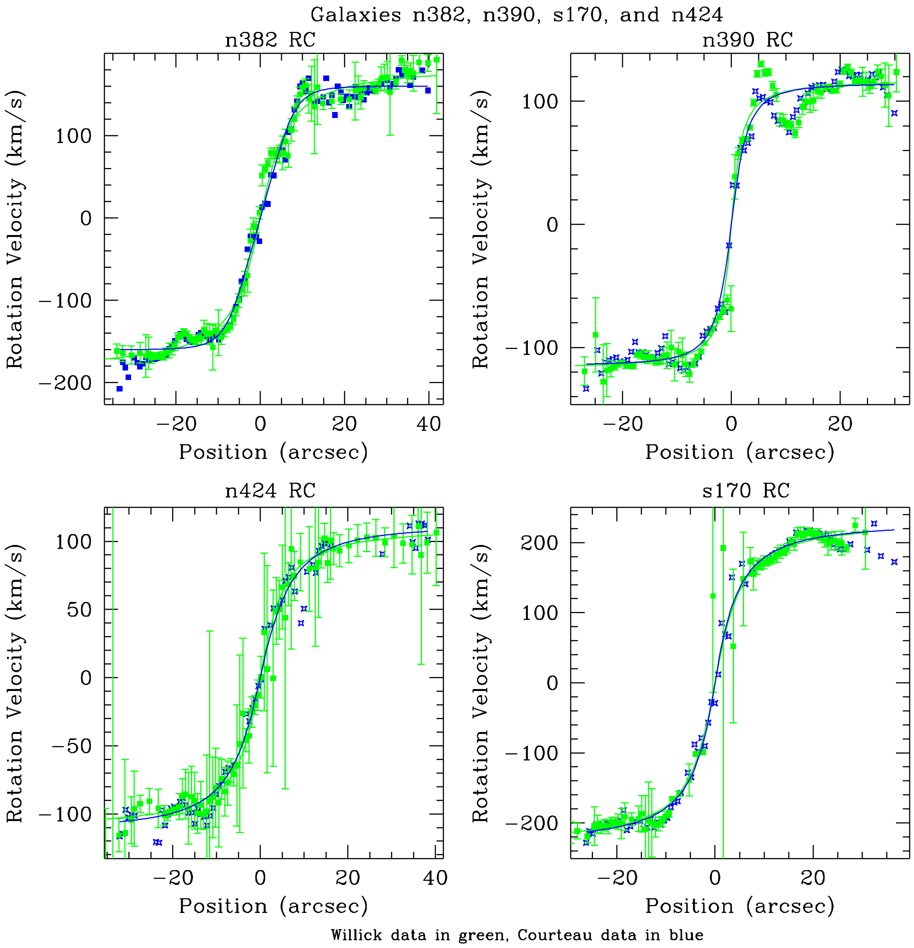

Figure C.36: Rotation curves from Mar 97 Kitt Peak run - 3/4

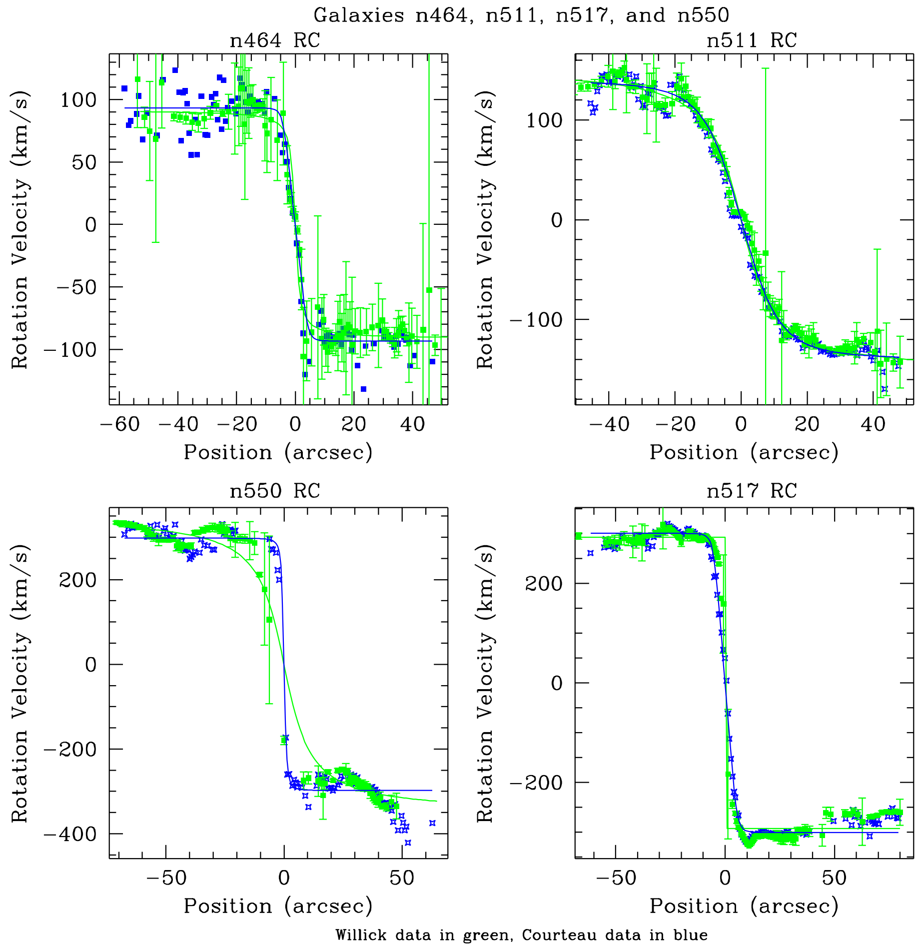

Figure C.37: Rotation curves from Mar 97 Kitt Peak run - 3/4

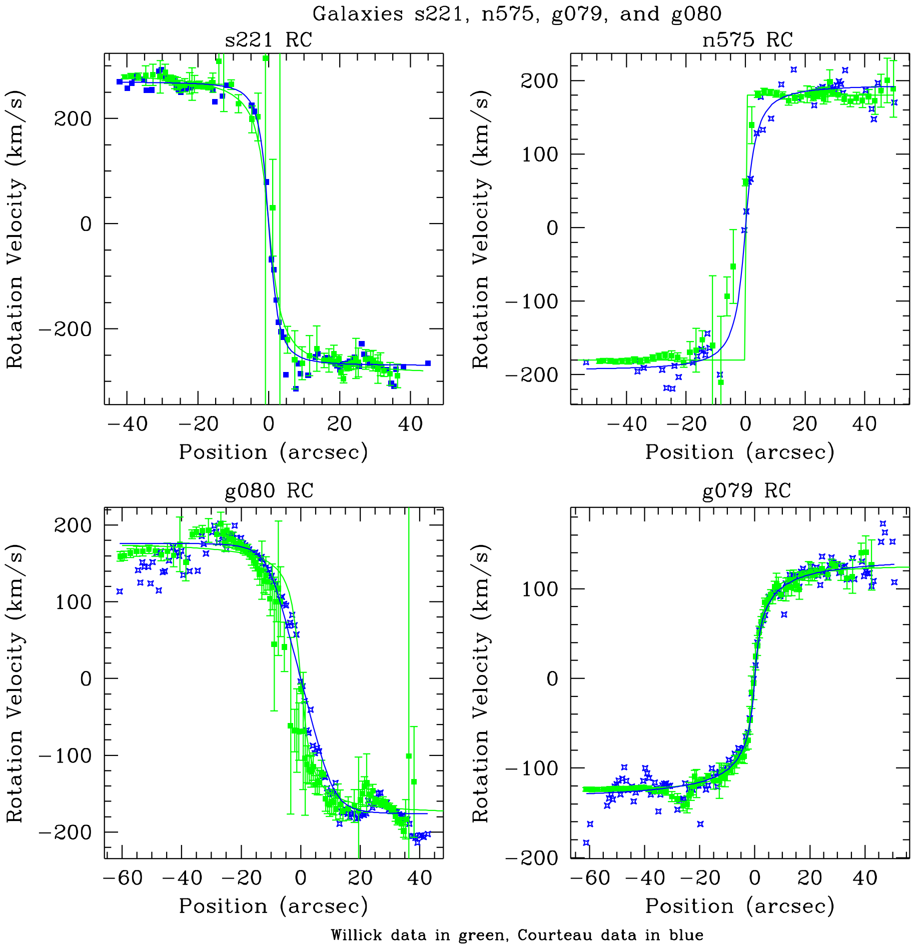

Figure C.38: Rotation curves from Mar 97 Kitt Peak run - 3/4-5

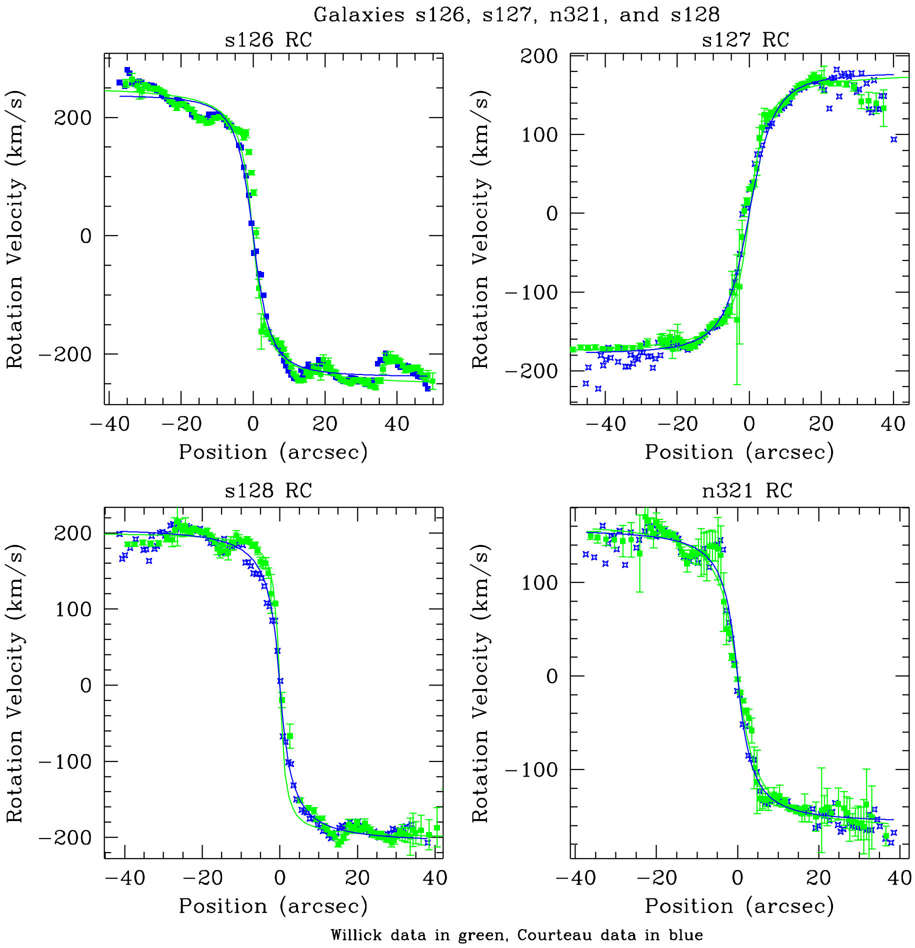

Figure C.39: Rotation curves from Mar 97 Kitt Peak run - 3/5

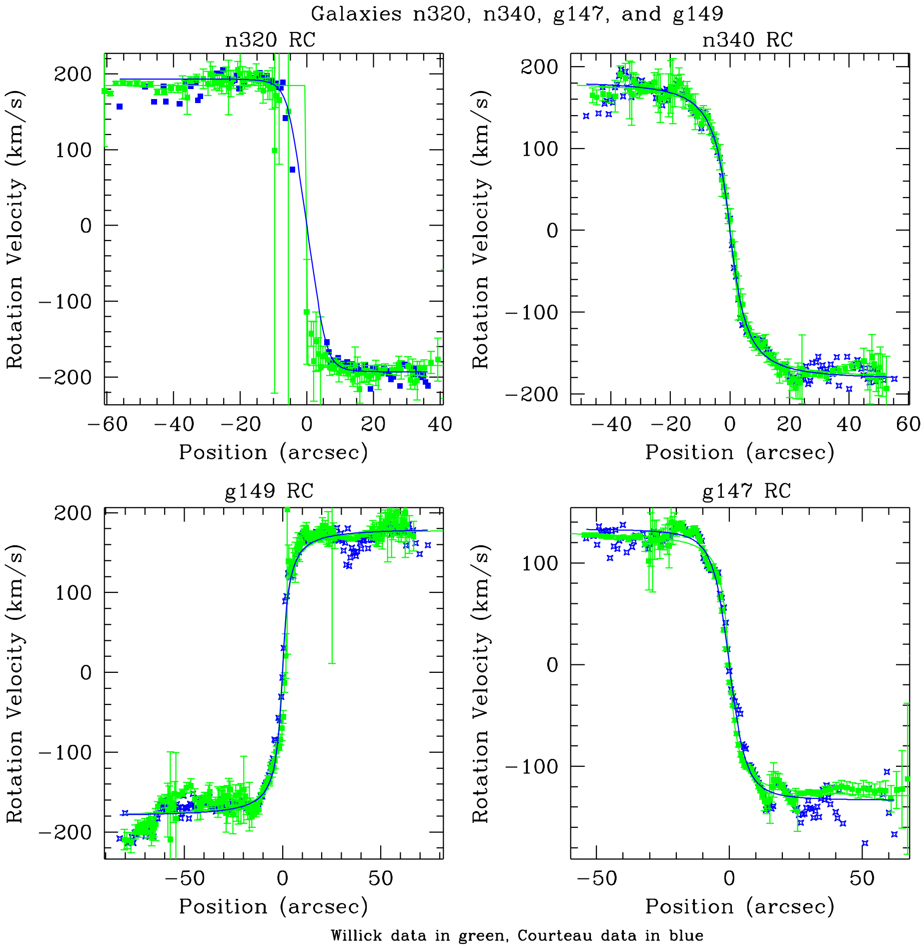

Figure C.40: Rotation curves from Mar 97 Kitt Peak run - 3/5

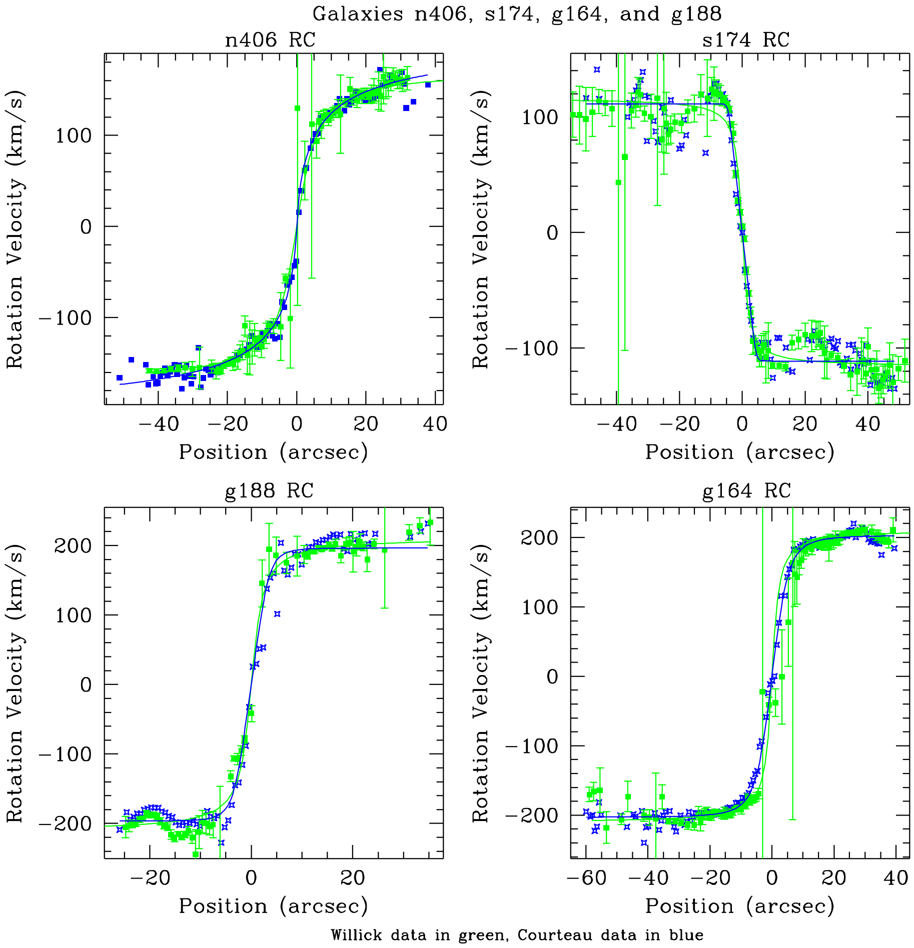

Figure C.41: Rotation curves from Mar 97 Kitt Peak run - 3/5

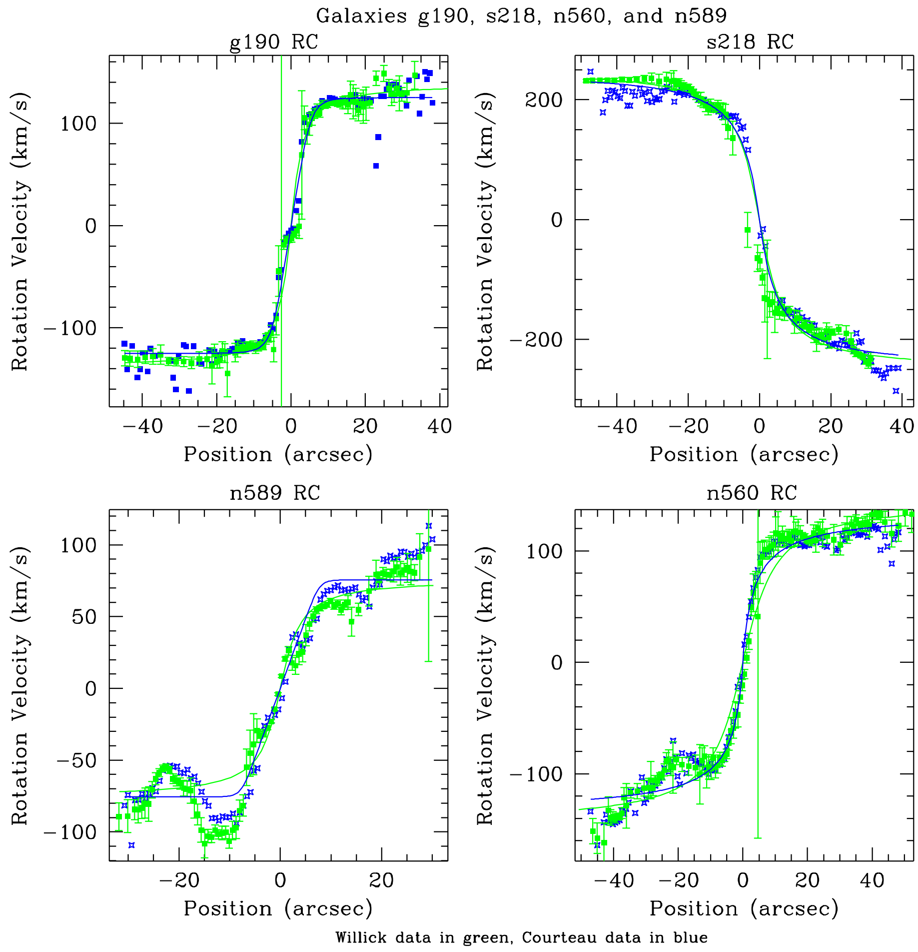

Figure C.42: Rotation curves from Mar 97 Kitt Peak run - 3/5

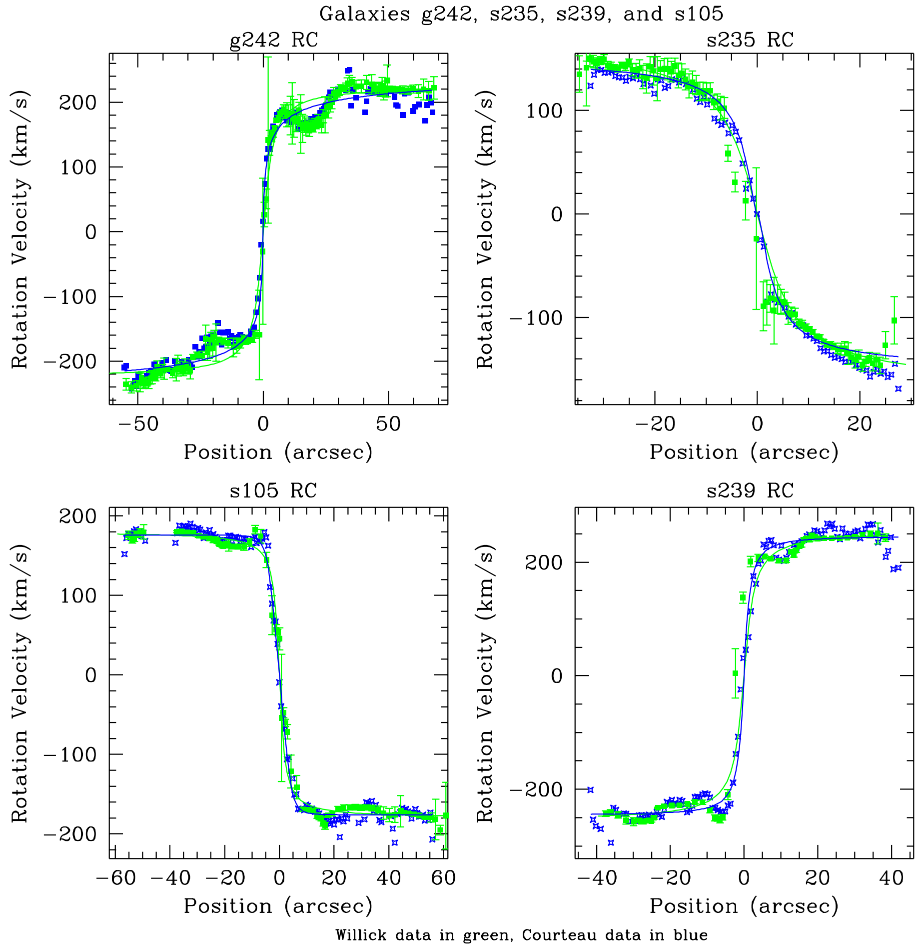

Figure C.43: Rotation curves from Mar 97 Kitt Peak run - 3/5-6

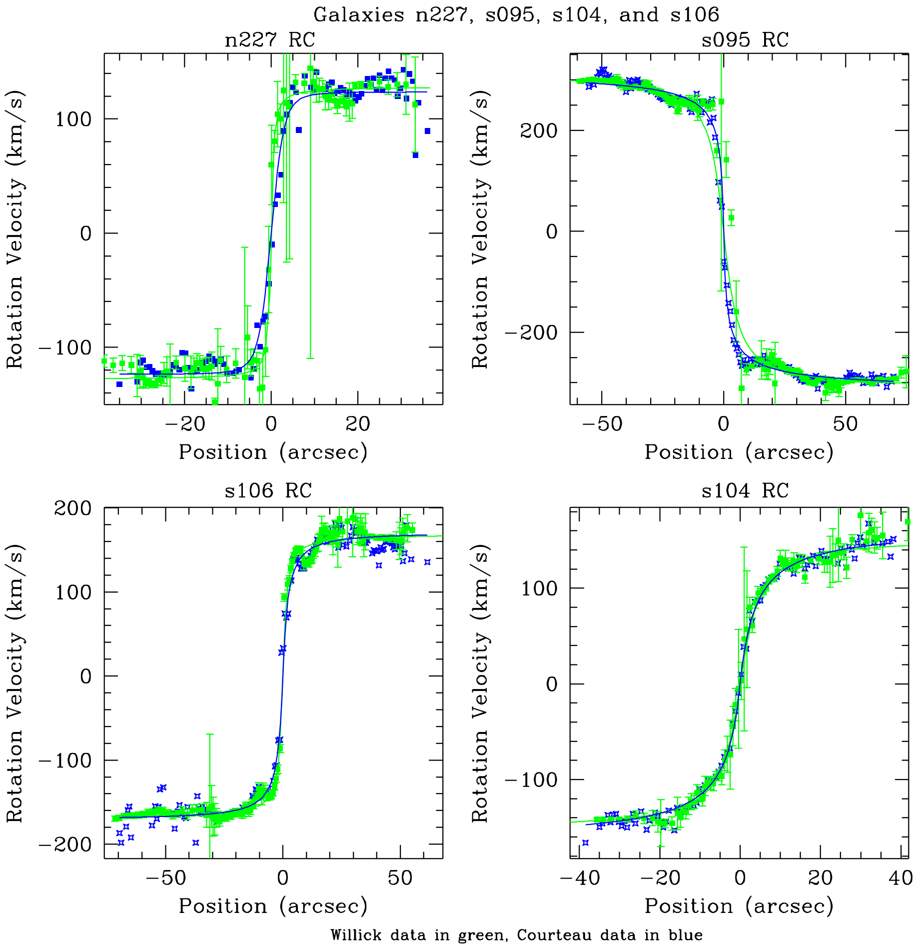

Figure C.44: Rotation curves from Mar 97 Kitt Peak run - 3/6

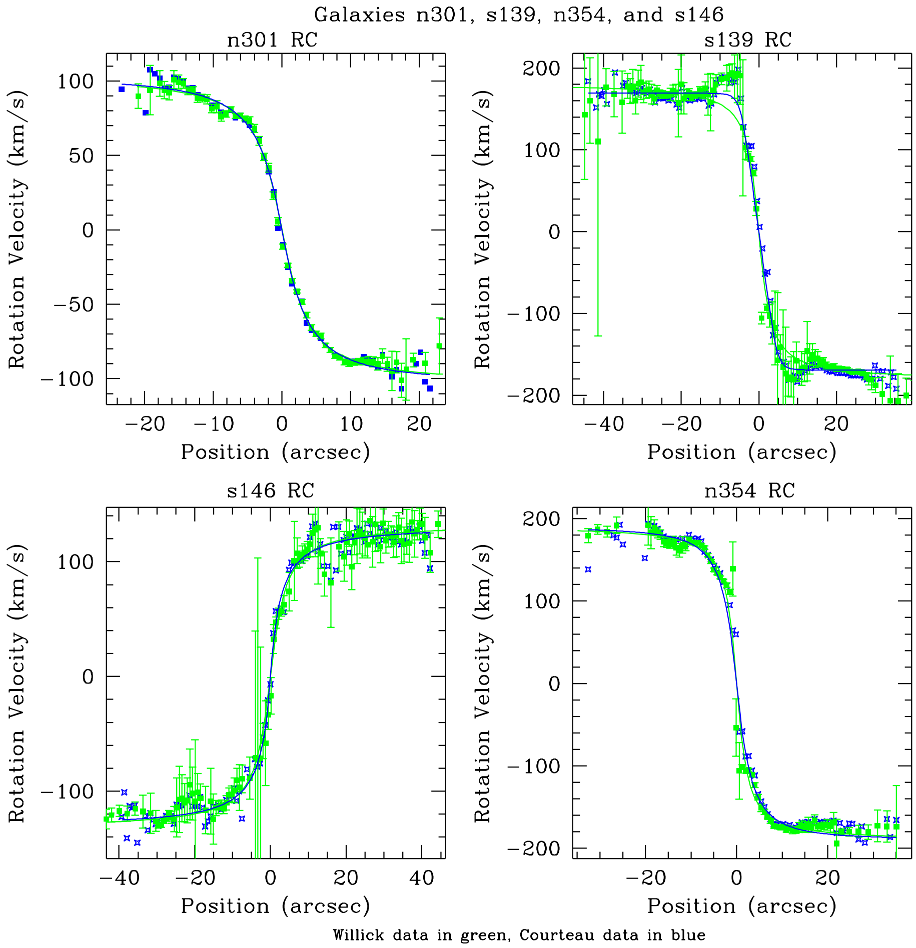

Figure C.45: Rotation curves from Mar 97 Kitt Peak run - 3/6

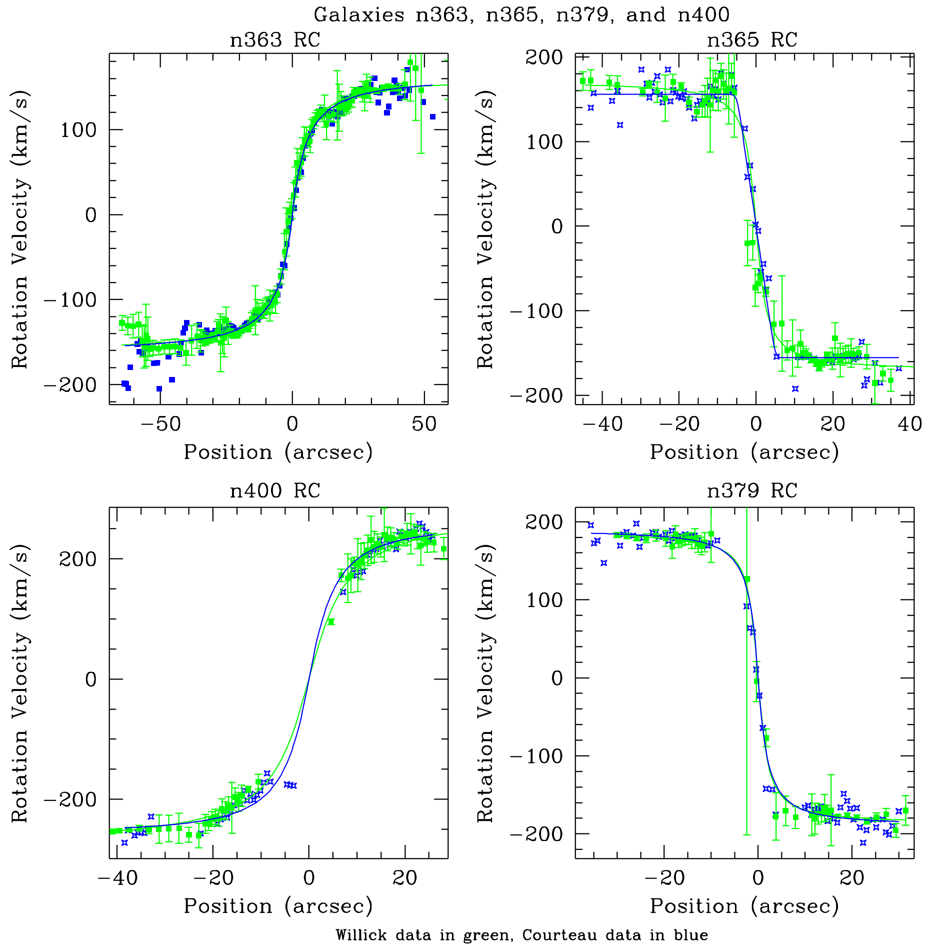

Figure C.46: Rotation curves from Mar 97 Kitt Peak run - 3/6

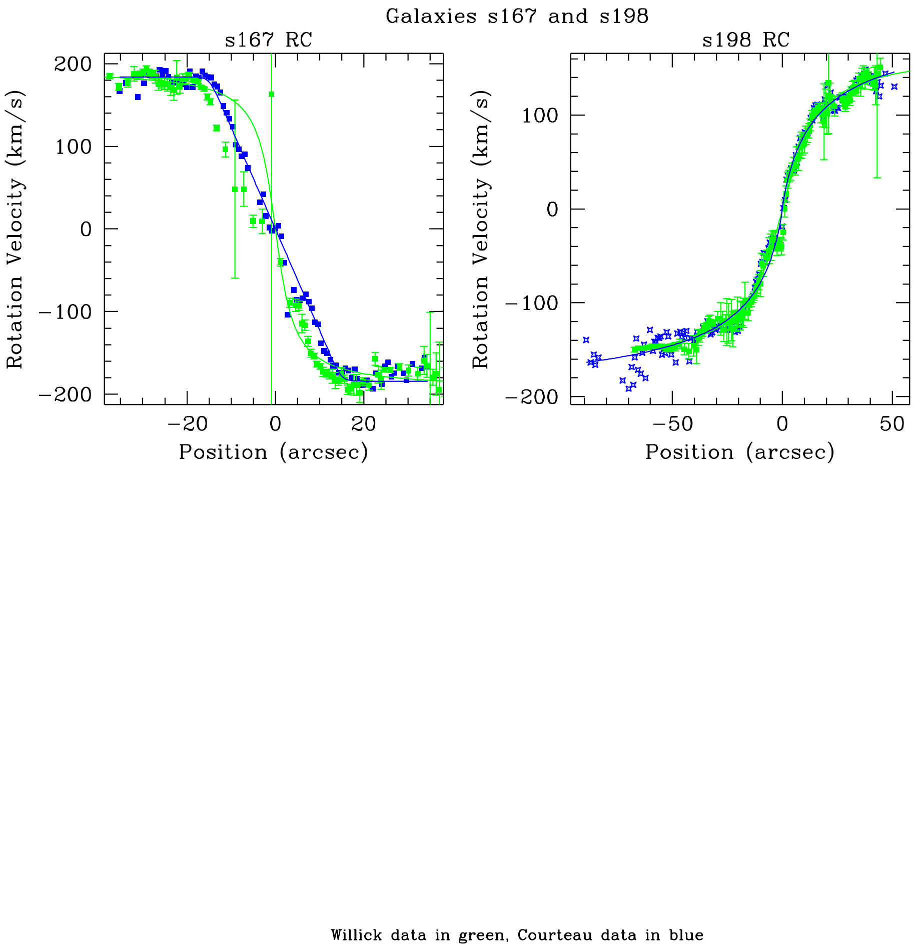

Figure C.47: Rotation curves from Mar 97 Kitt Peak run - 3/6

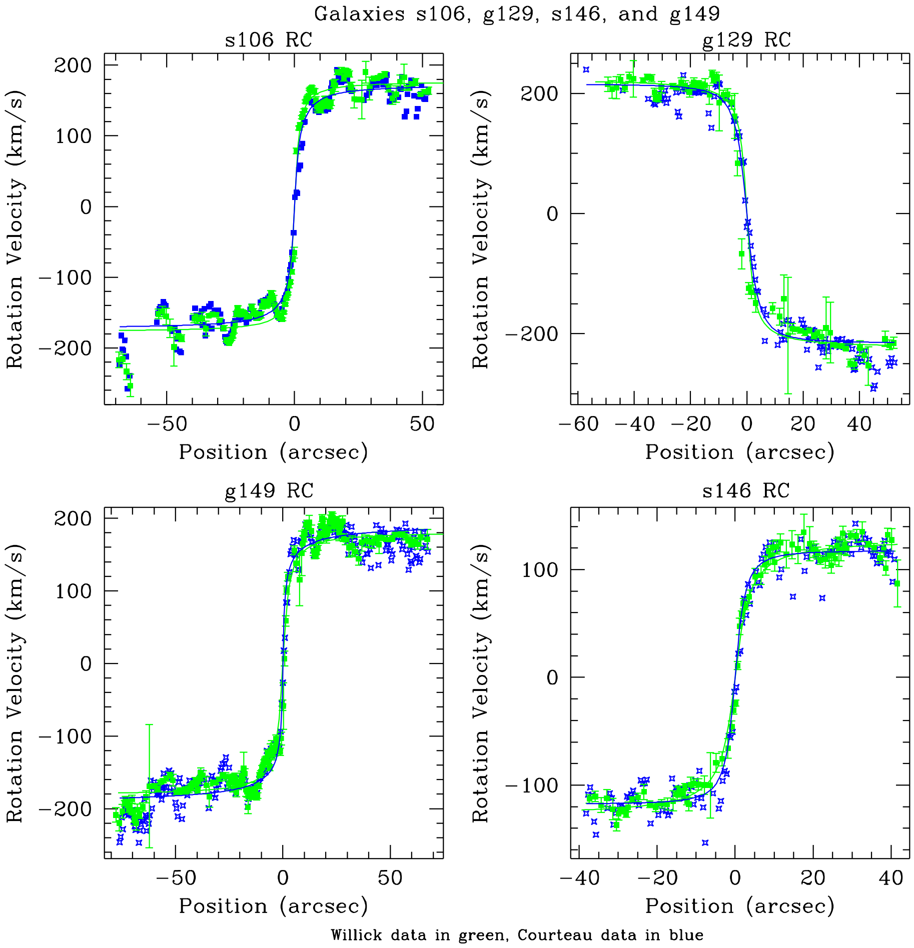

Figure C.48: Rotation curves from Apr 97 CTIO run - 4/5

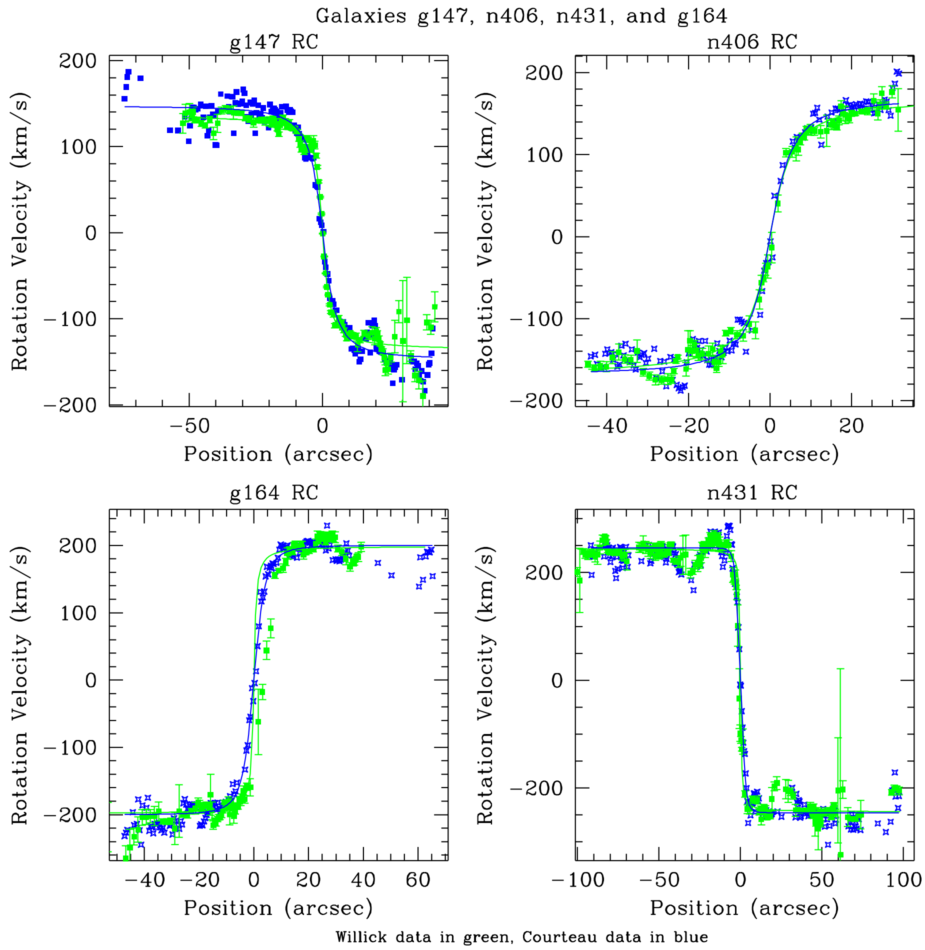

Figure C.49: Rotation curves from Apr 97 CTIO run - 4/5

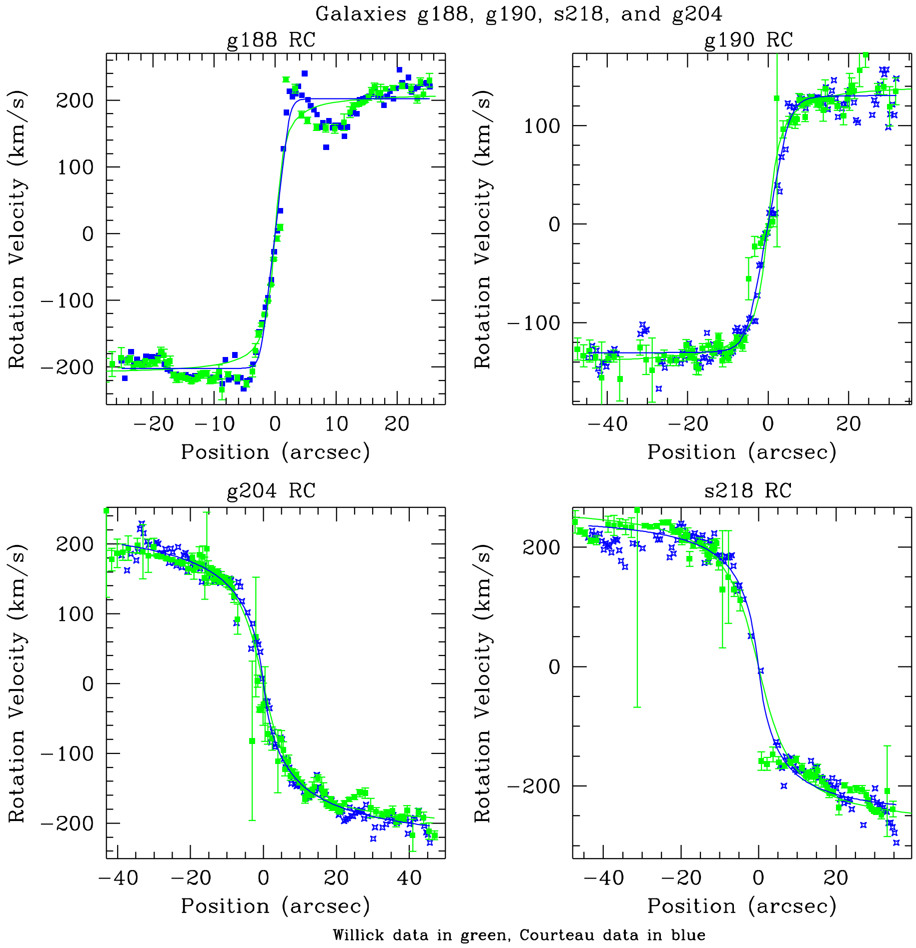

Figure C.50: Rotation curves from Apr 97 CTIO run - 4/5

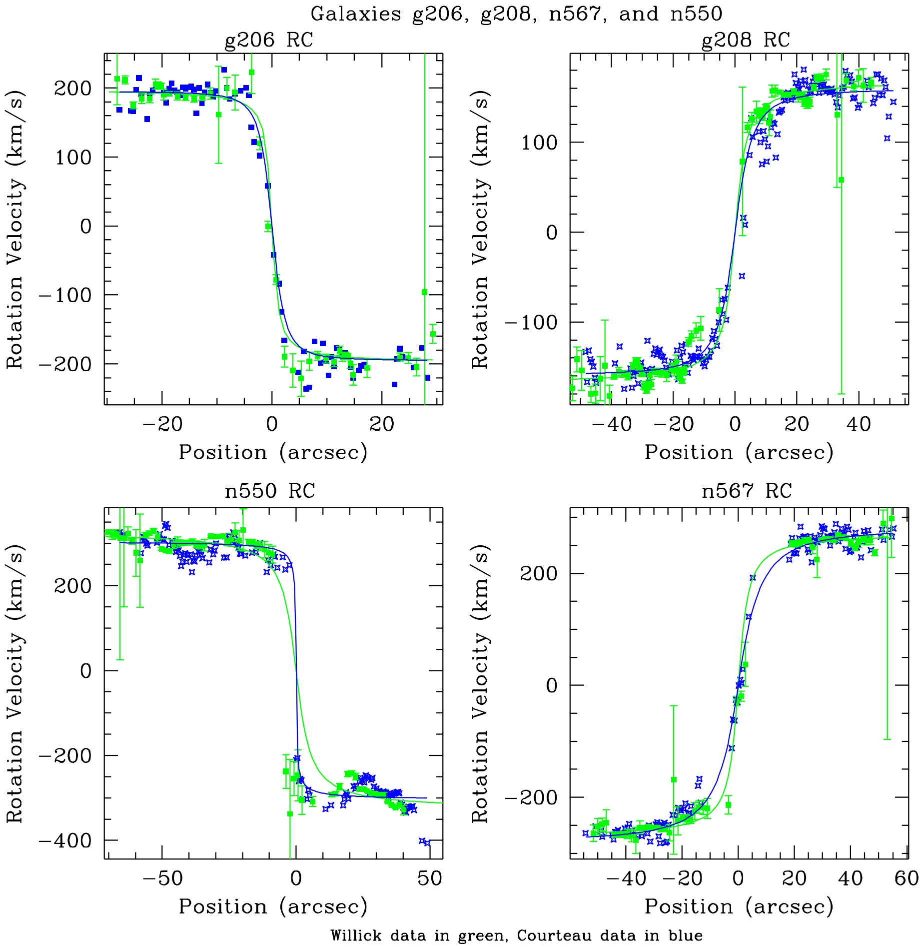

Figure C.51: Rotation curves from Apr 97 CTIO run - 4/5

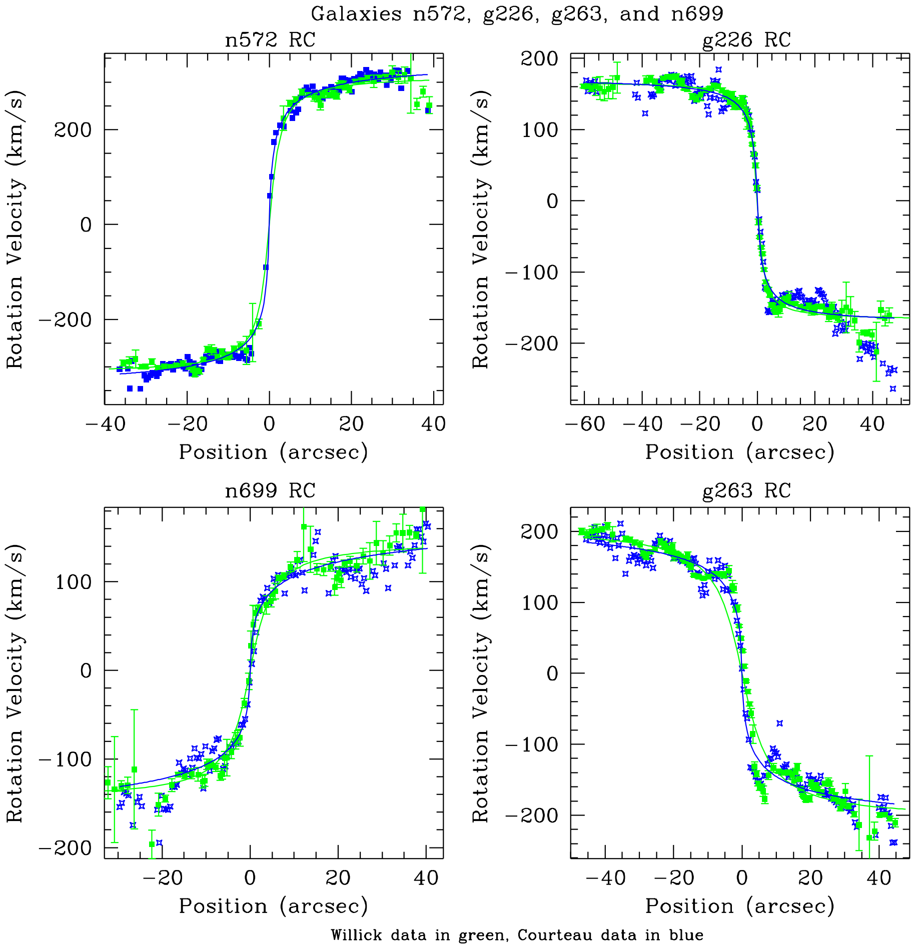

Figure C.52: Rotation curves from Apr 97 CTIO run - 4/5

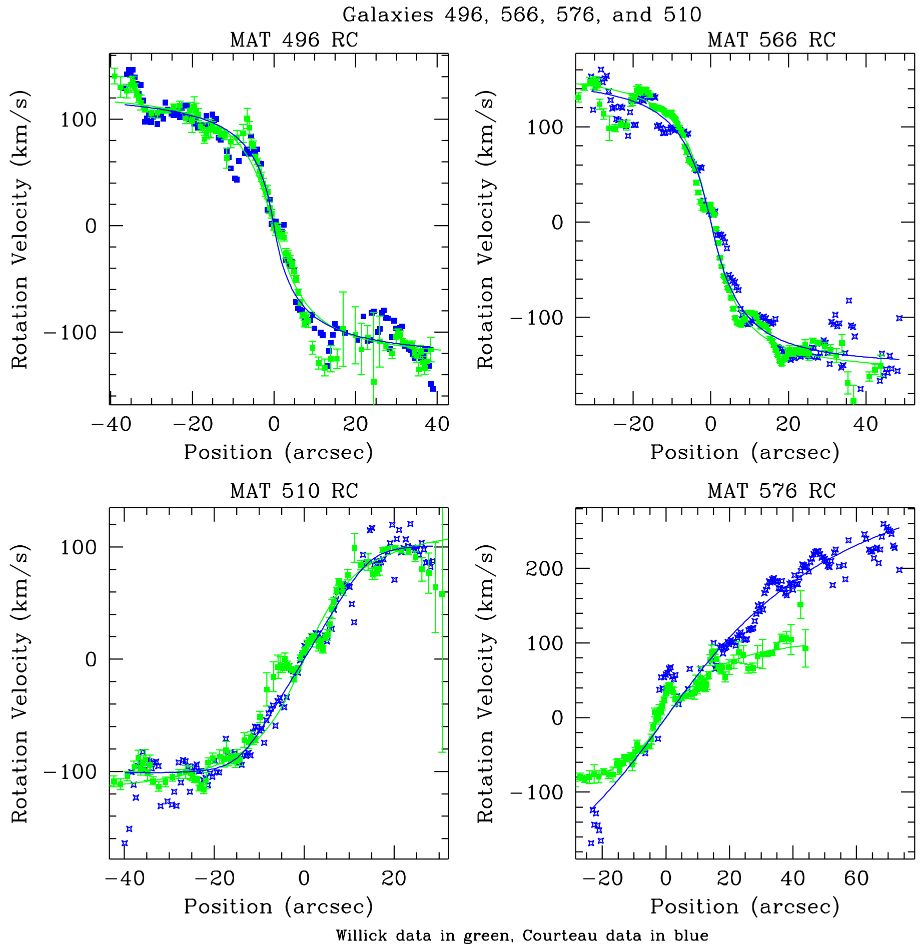

Figure C.53: Rotation curves from Apr 97 CTIO run (Mathewson galaxies) - 4/6

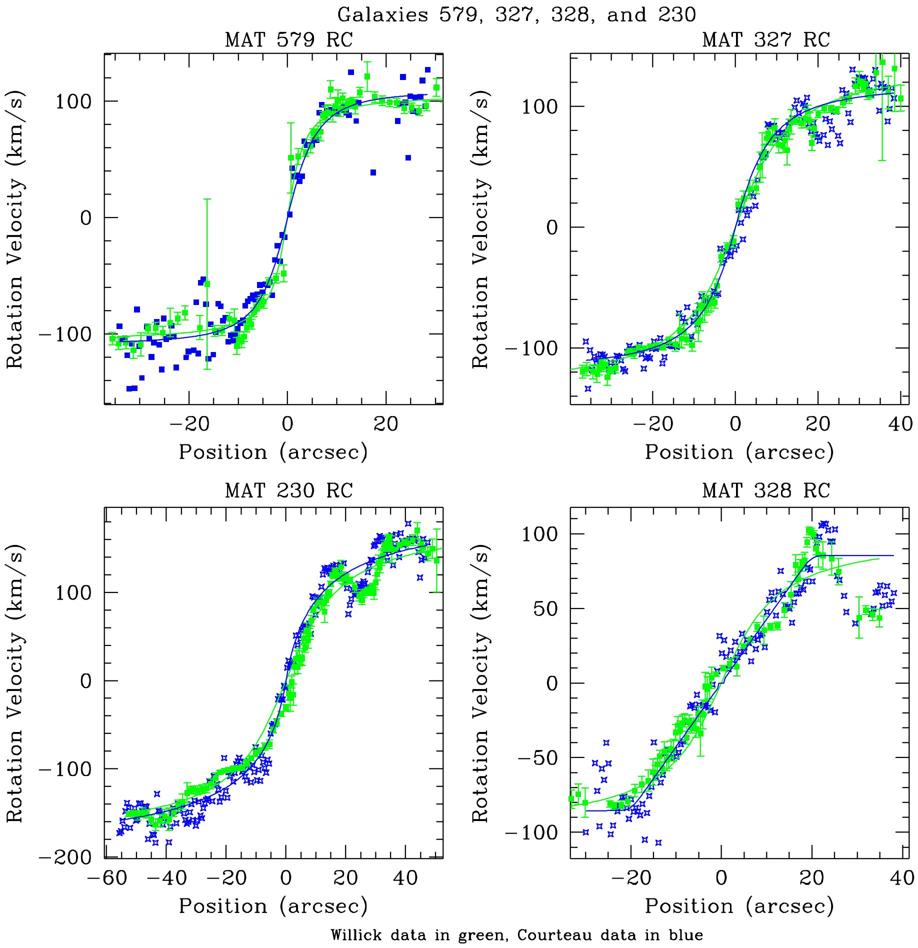

Figure C.54: Rotation curves from Apr 97 CTIO run (Mathewson galaxies) - 4/6

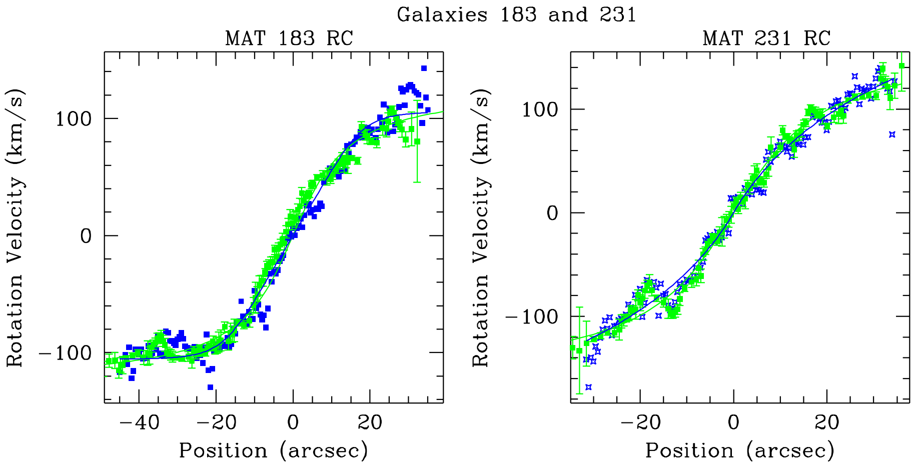

Willick data in green, Courteau data in blue

Figure C.55: Rotation curves from Apr 97 CTIO run (Mathewson galaxies) - 4/6